

Use of X-Ray Diffraction to Identify and Quantify Soil Swelling Potential

by

Zachery Shafer

A Thesis Presented in Partial Fulfillment  
of the Requirements for the Degree  
Master of Science

Approved May 2014 by the  
Graduate Supervisory Committee:

Claudia E. Zapata, Chair  
Edward Kavazanjian, Jr.  
Sandra L. Houston

ARIZONA STATE UNIVERSITY

May 2014

## ABSTRACT

Expansive soils impose challenges on the design, maintenance and long-term stability of many engineered infrastructure. These soils are composed of different clay minerals that are susceptible to changes in moisture content. Expansive clay soils wreak havoc due to their volume change property and, in many cases, exhibit extreme swelling and shrinking potentials. Understanding what type of minerals and clays react in the presence of water would allow for a more robust design and a better way to mitigate undesirable soil volume change. The relatively quick and widely used method of X-ray Diffraction (XRD) allows identifying the type of minerals present in the soil. As part of this study, three different clays from Colorado, San Antonio Texas, and Anthem Arizona were examined using XRD techniques. Oedometer-type testing was simultaneously performed in the laboratory to benchmark the behavior of these soils. This analysis allowed performing comparative studies to determining if the XRD technique and interpretation methods currently available could serve as quantitative tools for estimating swell potential through mineral identification. The soils were analyzed using two different software protocols after being subjected to different treatment techniques. Important observations include the formation of Ettringite and Thaumasite, the effect of mixed-layer clays in the interpretation of the data, and the soils being subject to Gypsification. The swelling data obtained from the oedometer-type laboratory testing was compared with predictive swelling functions available from literature. A correlation analysis was attempted in order to find what index properties and mineralogy parameters were most significant to the swelling behavior of the soils. The analysis demonstrated that Gypsification is as important to the swelling potential of the soil as the presence of

expansive clays; and it should be considered in the design and construction of structures in expansive soils. Also, the formation of Ettringite and Thaumasite observed during the treatment process validates the evidence of Delayed Ettringite Formation (DEF) reported in the literature. When comparing the measured results with a proposed method from the University of Texas at Arlington (UTA), it was found that the results were somewhat indicative of swell potential but did not explain all causes for expansivity. Finally, it was found that single index properties are not sufficient to estimate the free swell or the swell pressure of expansive soils. In order to have a significant correlation, two or more index properties should be combined when estimating the swell potential. When properties related to the soil mineralogy were correlated with swell potential parameters, the amount of Gypsum present in the soil seems to be as significant to the swell behavior of the soil as the amount of Smectite found.

## DECICATION

I would like to express my love and gratitude to my father, Thomas L. Shafer, for never letting me drop out of school during the early times in my academic career. Also, I would like to thank my wife, Mrs. Rachel J. Shafer, for the sacrifices she made to allow me to continue my education.

## ACKNOWLEDGEMENTS

I am indebted to my supervisor, Dr. Claudia E. Zapata of Arizona State University, for her invaluable guidance, patience and kindness throughout the research program. I also wish to express my thanks to Dr. Zapata for providing me an enthusiastic interest in the subject of study. The care she provided for me and my wife is greatly appreciated.

Special thanks go to my committee members, Dr. Edward Kavazanjian, Jr. and Dr. Sandra Houston, both of Arizona State University, for their advice, criticism and helpful comments on my research program and course work.

I would like to give special thanks to Dr. Emmanuel Soignard, David Wright and The LeRoy Eyring Center for Solid State Science for their invaluable assistance in the usage of their lab space and equipment.

Also, I would like to give credit to Peter Goguen and Kenny Witczak for their responsiveness to the needs of the project and general help with laboratory efficiency.

I would also like to thank my colleagues, Dr. Daniel Rosenbalm, Dr. Elham Hashem, and Dr. Aravind Pedarla of the University of Texas, Arlington for their assistance in laboratory testing and obtaining various soil properties. As well as Berenice Barranco for the gathering of the data used in the wPI and Group Index evaluations.

A special thanks to Lynda Williams for the use of her laboratory and the assistance of one of her graduate students, Keith Morrison.

Finally, I would like to thank the National Science Foundation for the financial support given to this work through the grant #1031238: Collaborative Research: SWCC Based Models for Realistic Simulation of Swell Behavior of Expansive Soils.

# TABLE OF CONTENTS

	Page
LIST OF TABLES.....	ix
LIST OF FIGURES .....	xi
CHAPTER	
1 INTRODUCTION.....	1
1.1 Importance of the Study .....	1
1.2 Objectives and scopes .....	3
1.3 Thesis outline.....	4
2 LITERATURE REVIEW.....	7
2.1 Introduction.....	7
2.2 Mechanisms of Swelling Clays.....	8
2.2.1 Formation of Clay Minerals .....	8
2.2.2 Properties of the Clay Mineral Structure .....	15
2.3 Traditional Swelling Test on Soil .....	29
2.4 X-ray Diffraction Test on Soil .....	32
3 LABORATORY CHARACTERIZATION OF SOIL MATERIALS .....	37
3.1 Soil Selection.....	37
3.2 Testing Information Used to Determine Soil Properties.....	37
3.3 Soil Properties.....	40
3.3.1 Anthem Soil Properties .....	41
3.3.2 Colorado Soil Properties .....	44
3.3.3 San Antonio Soil Properties .....	47

CHAPTER	Page
3.4 Conclusion and Summary .....	50
4 CHARACTERIZATION OF EXPANSIVE SOILS USING X-RAY DIFFRACTION	51
4.1 Introduction.....	51
4.2 Collection of data and Bragg’s Law .....	51
4.3 Procedure Followed to Obtain Mineral Information .....	54
4.4 Minerals Selected for Analysis .....	63
4.4.1 Qualification and Quantification of Anthem Soils.....	64
4.4.2 Qualification and Quantification of Colorado Soil .....	73
4.4.3 Qualification and Quantification of San Antonio Soil .....	83
4.5 Summary and Conclusions.....	92
5 COMPARATIVE ANALYSIS OF DATA .....	94
5.1 Introduction.....	94
5.2 Comparison of Results from Tests subjected to Different Treatments.....	94
5.2.1 Results Showing Gypsification.....	94
5.2.2 Results Showing Mixed-Layer Identification and Smectite Identification .....	99
5.2.3 Results Showing Ettringite and Thaumasite Formation .....	103
5.3 Comparison of Tests Performed on Wet Soil Conditions.....	106
5.4 Quantification of Minerals by Correlations with Other Properties.....	111
5.5 Summary and Conclusions.....	113
6 ANALYSIS OF THE EFFECT OF CLAY MINERALS AND SALT CONTENT IN THE ESTIMATION OF SWELLING POTENTIAL.....	116

CHAPTER	Page
6.1 Introduction.....	116
6.2 Swelling Correlations Comparison.....	116
6.3 Correlations Matrix .....	118
6.3.1 Parameters that Correlate with Free Swell .....	122
6.3.2 Parameters that Correlate with Swell Pressure.....	126
6.4 A closer look at properties that have a strong correlation with free swell..	129
6.4.1 Correlation of wPI and Free Swell.....	130
6.4.2 Correlation of GI and Free Swell.....	131
6.4.3 The correlation of D-spacing .....	132
6.5 Summary and Conclusion .....	133
7 CONCLUSIONS AND RECOMMENDATIONS FOR FUTURE RESEARCH....	135
7.1 Introduction.....	135
7.2 Conclusions of study .....	135
7.2.1 Objective 1 .....	135
7.2.2 Objective 2.....	136
7.2.3 Objective 3.....	138
7.2.4 Objective 4.....	139
7.2.5 Objective 5.....	140
7.3 Future research recommendations .....	142
REFERENCES .....	144
APPENDIX A .....	148
1: RockJock Analysis for Anthem Soil.....	149



CHAPTER	Page
2: RockJock Analysis for Colorado Soil .....	152
3: RockJock Analysis for San Antonio .....	155
APPENDIX B .....	160

## LIST OF TABLES

TABLE	Page
2.1: Typical values of cation exchange capacity of different minerals (Mitchell & Soga, 2005).....	22
2.2: Volume increase of selected mineral transformations (Mitchell & Soga, 2005).....	26
2.3: Typical values of the expansion index and potential parameter (ASTM D 4829-11). .....	31
3.2: Anthem soil index properties.....	42
3.3: Colorado soil index properties.....	45
3.4: San Antonio index properties .....	48
4.1: Minerals selected for analysis.....	64
4.2: Summary of Anthem Clay+Silt fraction mineral quantification .....	69
4.3: Summary of Anthem Clay fraction quantification .....	73
4.4: Summary of Colorado Clay+Silt fraction mineral quantification .....	79
4.5: Summary of Colorado Clay fraction mineral quantification .....	83
4.6: Summary of San Antonio Clay+Silt fraction mineral quantification .....	88
4.7: Summary of San Antonio Clay fraction mineral quantification .....	92
5.1: Volume increase of selected mineral transformations (Mitchell & Soga, 2005).....	95
5.2: Anthem soil wet analysis mineral quantification.....	107
5.3: Colorado soil wet analysis mineral quantification.....	109
5.4: San Antonio soil wet analysis mineral quantification .....	109
5.5: Mineral percentages obtained with UTA method.....	112
5.6: Comparison of mineral quantifications of Anthem soil from UTA and ASU.....	112

TABLE	Page
5.7: Comparison of mineral quantification of San Antonio soil from UTA and ASU ...	112
5.8: Comparison of mineral quantification of Colorado soil from UTA and ASU .....	113
6.1: Predictive equations for the swell potential of soils from different authors .....	117
6.2: Measured free swell data for Anthem, Colorado, and San Antonio soils and Results obtained with predictive equations .....	118
6.3: Data from the correlation matrix the free swell and pressure data .....	119
6.4: Summary of parameters that have high correlation values .....	122
6.5: Summary of regressions for parameters with free swell .....	123
6.6: Summary of regressions for parameters with swell pressure .....	127
6.7: Anthem soil $2\theta$ , d-spacing, and $\Delta d$ -spacing data obtained from the different treatments shown .....	132
6.8: San Antonio soil $2\theta$ , d-spacing, and $\Delta d$ -spacing data obtained from the different treatments shown .....	132
6.9: Colorado soil $2\theta$ , d-spacing, and $\Delta d$ -spacing data obtained from the different treatments shown .....	133
A-1: Mineral percentages from ASU using the RockJock method .....	159

## LIST OF FIGURES

FIGURE	Page
2.1: Figure explaining amorphous material formation. ....	10
2.2: (a) Single silica tetrahedron, (b) tetrahedron sheet .....	11
2.3: Typical usage of tetrahedron symbol.....	12
2.4: Top view of a tetrahedron sheet.....	12
2.5: (a) Single silica octahedral, (b) octahedral sheet .....	13
2.6: Typical usage of octahedral symbol .....	13
2.7: Synthesis pattern for the clay minerals and how they are stacked.....	14
2.8: Scanning electron microscope picture of Montmorillonite .....	16
2.9: Scanning electron microscope picture of Kaolinite.....	17
2.10: Broken edges trying to become electrically via the cations in solution.....	19
2.11: Kaolinite having interspacing bonds and has a balanced outer charge.....	19
2.12: (a) Water molecule (b) a tetrahedron configuration .....	20
2.13: Indicating the polarity with the positive charge on the hydrogen.....	20
2.14: Illustration of cation exchange (Brady & Weil, 2007) .....	22
2.15: Illustration describing the DLVO theory .....	23
2.16: Illustration of how anhydrite increases its volume when hydrated (Rauh, Spaun, & Thuro, 2006).....	27
2.17: Environmental chamber for measuring swell under different conditions (Deu, Romero, & Berdugo, 2013).....	28
2.18: Correlation between (a) Activity vs. Percent of clay and (b) Atterberg Limits alluding to swelling .....	32

FIGURE	Page
2.19: Bravais space lattices chart .....	34
2.20: Categorized six crystal systems .....	35
2.21: Analogy to specular reflection.....	36
3.2: Grain size distribution of Anthem Soil.....	43
3.3: USCS classification for Anthem Soil .....	43
3.4: Grain size distribution of Colorado Soil.....	46
3.5: USCS classification for Colorado Soil .....	46
3.6: Grain size distribution for San Antonio Soil .....	49
3.7: USCS classification for San Antonio Soil.....	49
4.1: Schematic of X-ray diffraction process .....	52
4.2: Typical diffractometer .....	52
4.3: Analogy to specular reflection (Jürgens, 2013).....	53
4.4: Tools needed for preferred orientation samples .....	56
4.5: Slurry of soil and sodium hexametaphosphate solution .....	56
4.6: Sample being filtered on a Millipore filter .....	57
4.7: Sample after filtration .....	57
4.8: Filter paper placed on glass beaker.....	58
4.9: Sample "rolled" on to quartz slide .....	58
4.10: Sample in adsorption treatment of Ethylene Glycol.....	59
4.11: Muffle furnace used for heat treatments .....	60
4.12: Centrifuge used for particle separation.....	62
4.13: Separation of clay fraction from silt fraction.....	63

FIGURE	Page
4.14: Treatment scans for the Anthem’s Clay+Silt fraction .....	65
4.15: Mineral quantification of Clay+Silt fraction of Anthem soil for untreated specimen .....	65
4.16: Mineral quantification of Clay+Silt fraction of Anthem soil for Glycol treated specimen .....	66
4.17: Mineral quantification of Clay+Silt fraction of Anthem soil for 400°C treated specimen .....	66
4.18: Mineral quantification of Clay+Silt fraction of Anthem soil for 550°C treated specimen .....	67
4.19: Mineral quantification of Clay+Silt fraction of Anthem soil for wetted short term specimen .....	67
4.20: Mineral quantification of Clay+Silt fraction of Anthem soil for wetted long term specimen .....	68
4.21: Completed signal quantification with labeled peaks .....	68
4.22: Treatment scans for the Anthem’s clay fraction .....	70
4.23: Mineral quantification of Clay fraction of Anthem soil for untreated specimen.....	70
4.24: Mineral quantification of Clay fraction of Anthem soil for Glycol treated specimen .....	71
4.25: Mineral quantification of Clay fraction of Anthem soil for 400°C treated specimen .....	71
4.26: Mineral quantification of Clay fraction of Anthem soil for 550°C treated specimen .....	72

FIGURE	Page
4.27: Completed signal quantification with labeled peaks .....	72
4.28: Treatment scans for the Colorado's clay+silt fraction.....	74
4.29: Mineral quantification of Clay+Silt fraction of Colorado soil for untreated specimen .....	75
4.30: Mineral quantification of Clay+Silt fraction of Colorado soil for Glycol treated specimen.....	75
4.31: Mineral quantification of Clay+Silt fraction of Colorado soil for 400°C treated specimen.....	76
4.32: Mineral quantification of Clay+Silt fraction of Colorado soil for 550°C treated specimen.....	76
4.33: Mineral quantification of Clay+Silt fraction of Colorado soil for wetted short term specimen.....	77
4.34: Mineral quantification of Clay+Silt fraction of Colorado soil for wetted long term specimen.....	77
4.35: Completed signal quantification with labeled peaks .....	78
4.36: Treatment scans for the Colorado's clay fraction.....	80
4.37: Mineral quantification of Clay fraction of Colorado soil for untreated specimen...	80
4.38: Mineral quantification of Clay fraction of Colorado soil for Glycol treated specimen .....	81
4.39: Mineral quantification of Clay fraction of Colorado soil for 400°C treated specimen .....	81

4.40: Mineral quantification of Clay fraction of Colorado soil for 500°C treated specimen .....	82
4.41: Completed signal quantification with labeled peaks .....	82
4.42: Treatment scans for the San Antonio’s Clay+Silt fraction .....	84
4.43: Mineral quantification of Clay+Silt fraction of San Antonio soil for untreated specimen .....	84
4.44: Mineral quantification of Clay+Silt fraction of San Antonio soil for Glycol treated specimen .....	85
4.45: Mineral quantification of Clay+Silt Fraction of San Antonio soil for 400°C treated specimen .....	85
4.46: Mineral quantification of Clay+Silt fraction of San Antonio soil for 550°C treated specimen .....	86
4.47: Mineral quantification of Clay+Silt fraction of San Antonio soil for wetted short term specimen.....	86
4.48: Mineral quantification of Clay+Silt fraction of San Antonio soil for wetted long term specimen.....	87
4.49: Completed signal quantification with labeled peaks .....	87
4.50: Treatment scans for the San Antonio’s clay fraction.....	89
4.51: Mineral quantification of Clay fraction of San Antonio soil for untreated specimen .....	89
4.52: Mineral quantification of Clay fraction of San Antonio soil for Glycol treated specimen .....	90



FIGURE	Page
4.53: Mineral quantification of Clay fraction of San Antonio soil for 400°C treated specimen.....	90
4.54: Mineral quantification of Clay fraction of San Antonio soil for 550°C treated specimen.....	91
4.55: Completed signal quantification with labeled peaks .....	91
5.1: Anthem’s Clay+Silt fraction of possible Calcite transformation into Gypsum.....	96
5.2: San Antonio Clay+Silt fraction of possible Calcite transformation into Gypsum and vice versa.....	97
5.3: Amounts of Gypsum observed in the Colorado Clay+Silt fraction.....	98
5.4: Smectite percentages of the Clay+Silt fraction for the three soils.....	99
5.5: Illite percentages of the Clay+Silt fraction of the three soils .....	100
5.6: Mixed-layer visual identification in diffractograms (a) Anthem, (b) San Antonio, (c) Colorado .....	101
5.7: Spectate identification on the Clay fraction of the studied soils.....	102
5.8: Illite identification on the Clay fraction of the soils in this study.....	103
5.9: Formation of Ettringite in Clay+Silt fraction at high temperatures.....	104
5.10: Thaumasite formation of the Clay+Silt fraction in this study .....	105
5.11: Time scale indicating Calcites transformation into Gypsum in Anthem soil.....	107
5.12: Time scale indicating Calcite transformation into Gypsum in San Antonio soil ..	110
6.1: Change in $2\theta$ between an air-dried and glycol sample, focusing on the primary Montmorillonite peak.....	126

FIGURE	Page
6.2: Linear regression of Free Swell vs. Weighted Plasticity Index with this study's data in red.....	130
6.3: Linear regression of Swell Pressure vs. Group Index with this study's data in red.	131
A-1: Residual analysis of Anthem .....	150
A-2: RockJock quantification of Clay and Non-clay for Anthem soil .....	150
A-3: RockJock quantification of non-clay minerals found in Anthem soil .....	151
A-4: RockJock quantification of clay minerals found in Anthem soil .....	152
A-5: Residual analysis of Colorado .....	153
A-6: RockJock quantification of Clay and Non-clay minerals for Colorado soil.....	153
A-7: RockJock quantification of non-clay minerals found in Colorado soil .....	154
A-8: RockJock quantification of clay minerals found in Colorado soil .....	155
A-9: Residual analysis of San Antonio.....	156
A-10: RockJock quantification for Clay and Non-clay minerals for San Antonio soil..	157
A-11: RockJock quantification of Non-Clay minerals in San Antonio .....	157
A-12: RockJock quantification of clay minerals in San Antonio .....	158

## CHAPTER 1

### INTRODUCTION

#### 1.1 Importance of the Study

An expansive soil is prone to large volume changes that are directly related to the changes in water content. The main contributors to this volume change behavior are the make-up of the clay minerals and their moisture retaining capabilities. Expansive soils are present in many areas of the world, particularly in semi-arid regions. The mitigation of the effects of expansive soil behavior on infrastructure has become a major challenge for geotechnical engineers.

Much of the world infrastructure is designed and constructed on soil as opposed to rock material. Soils will behave differently depending on their heterogeneous composition and fabric arrangement. Clays, for example, might have the most complicated composition due to their microscopic particle size and expansive potential. Expansive clay is prone to high volume change which can, in turn, lead to brittle failure of structures, such as foundations and road systems, built on such soils. This can be quite a challenge to the designer of an infrastructure upon the clay. The estimated annual cost of the damage due to the expansive soils is estimated to be \$1 billion in the USA, £150 million in the UK, and many billions of pounds worldwide (Das, 2009). Das also indicated that much of the damage related to expansive soils is not due to the lack of appropriate engineering solutions but to the failure to identify the existence and magnitude of expansion of these soils early in land use and project planning. Knowing the mineral composition of the soil allows the possibility of estimating the expansive behavior of that soil. As stated by (Mitchell & Soga, 2005), for soil pore water contents

typically encountered in practice only about one-third of the soil solids need be composed of clay in order to dominate the behavior of the soil by preventing direct interparticle contact of the granular particles (Mitchell & Soga, 2005).

In the current state of the art, two general approaches can be recognized when considering studies on the swell potential of soil: the macro-scale and the micro-scale approaches. Traditionally, macro-scale test consists of direct and indirect measurements of swell potential. Direct methods are widely used in several different forms. The most common swell tests are the Free Swell (FS) test, the Load-Back (LB) test, and the Constant Volume (CV) test. Typically, an oedometer type device is used to measure the swelling properties of a soil, although other devices such as triaxial or modified pressure-plate devices have been used. Despite the variety of swell pressure measurement techniques and equipment, it is still believed by most geotechnical engineers that the one-dimensional consolidometer test is the most practical and applicable test for evaluating soil swelling pressure (Attom & Barakat, 2000). On the other hand, the indirect methods make use of index properties and other variables of the soil in correlations that yield the swelling properties of such soil.

Traditionally, swelling behavior is assessed by using macro-scale testing, rather than focusing on the micro-scale level. However, when one evaluates a soil on the micro-scale level, a better understanding of the swell potential can be expected, especially when dealing with clay mineralogy. There are numerous studies in which observations have been made on micro-scale parameters, such as specific surface area and cation exchange capacity for the benefit of quantification of clay minerals. In general, this gives a better understanding of the composition of the soils. Other tests make use of powder X-ray

diffraction to obtain a semi-quantitative analysis of the soil. These aforementioned methods provide insight to the quantification and identification of clay minerals present in the tested soil, but offer little guidance to the potential volume change of the minerals.

Identifying expansive soils and quantifying their potential expansivity is a crucial concern in geotechnical site investigations. The presence of expansive soils can often be overlooked. Additionally, if their presence is noticed, their potential expansiveness can often be underestimated. Therefore, it is important to design a cost effective investigation technique that can support conventional geotechnical investigation and testing (Yitagesu, 2009). With this information the expansiveness will be better understood for design, maintenance, and long-term stability of infrastructures.

## **1.2 Objectives and scopes**

The intent of this research study is to investigate the behavior of expansive soils via X-ray technologies and being able to compare the results obtained with the swell properties that are usually measured in the laboratory. The study focus on possible mechanisms associated with volume change in clay bearing soils. The objectives of this research study are as follows:

1. To investigate and compare methods currently used to quantify clay minerals present in the soils.
2. To identify clay minerals that can cause volume change when hydrated and contribute to swell potential. The soils will be subject to different treatments.
3. To identify additional geochemical reactions and processes that contributes to soil swelling.

4. To compare the results obtained with predicting models available in the literature.
5. Identify the most significant parameters associates with swell potential.

The findings of this research work will contribute to the geotechnical profession by providing insight as to what other conditions besides the presence of clay minerals need to be monitored when dealing with construction of expansive soils. A better ingof the composition and nature of the soil would allow for better engineering judgment.

### **1.3 Thesis outline**

This thesis is organized into seven different chapters. Chapter 1, “Introduction”, presents the need for the research study, the objectives, the scope of the research study, and the outline of the thesis.

Chapter 2, “Literature Review”, is comprised of four parts. The first part presents a brief review of the importance of soil mineralogy, volume change, and expansive soils in geotechnical engineering. The second part reviews the traditional methods currently used by engineers to currently determine the swelling potential of clay soils. The third section reviews X-ray diffraction methods used in previous studies. The fourth part summarizes the geochemical reactions related to soil swell behavior.

Chapter 3, “Laboratory Characterization of Soil Materials”, presents the results of the characterization of the soils used in the study and the methods followed to obtain the required soils properties.

Chapter 4, “Characterization of Expansive Soils using X-ray Diffraction” is comprised of three parts. The first part presents a background on X-ray diffraction and the data it gathers. Second, it presents the X-ray diffraction procedure PANalytical X’Pert

Pro MRD powder, used by LeRoy Eyring Center for Solid State Science at Arizona State University to test and analyze powder samples, is explained along with the sample preparation procedure. This method looks at two different soil portions of the soil: clay+silt portion and the clay portion. The third part presents the mineral quantification of the three soils used in this study.

Chapter 5, “Comparative Analysis of Data”, contains three parts. The first part will compare the results of the two software packages, PANalytical and RockJock. The second part explains the results of the wetting test. Finally, data is given for the quantification of minerals that correlate with other properties. This includes the joint collaboration of Arizona State University and University of Texas, Arlington’s quantification comparison of the same soils.

Chapter 6, “Analysis of the Effect of Clay Minerals and Salt in the Estimation of Swell Potential”, will contain four parts. First the chapter will look at existing predictive equation for the free swell of soils using different properties and evaluate those with the free swell data obtained in this study. Next, a correlation matrix was constructed using the different parameters found in the study. Where a table of 1:1 ratios regarding the selected parameters correlating with the free swell and swell pressure of the soils. The chapter was structured as the correlations for free swell and swell pressure in one part. Finally, specific parameters had yielded strong correlations to the swelling of the soils, therefore these parameters were observed more closely to imply better conclusions about these specific parameters.

Chapter 7, “Conclusions and Recommendations for Future Research”, contains two parts. First the chapter revisits the data already presented to formulate conclusions

from the data. Second, are recommendations for the future use of this study as a base for a more in-depth analysis. With these recommendations, including testing ideas and methods of testing, it will to light in some detail a more complete picture of expansive soils.



## CHAPTER 2

### LITERATURE REVIEW

#### **2.1 Introduction**

Clay is an abundant raw material which has an amazing variety of uses and properties that are largely dependent on their mineral structure and composition (Murray, 2007). Within these abundant raw materials, mineral structures are arrangements that react with water and cause the soil to be expansive.

Expansive soil, the type of clayey soil that experiences volumetric swelling or shrinkage with adsorption or desorption of water, covers a quarter of the United States and causes more than nine billion dollars in loss every year (Lin & Cerato, 2012). The most complicated types of soils are those, which consist of clay minerals in a solid phase. Clay minerals influence the swelling behavior and strength of soils, through chemical, physical, or mechanical effects. Justified by (Mitchell & Soga, 2005), he states that for water contents typically encountered in practice, around 15 to 40 percent, only about one-third of the soil solids need be clay in order to dominate the behavior by preventing direct interparticle contact of the granular particles.

It is therefore, important to establish simple and inexpensive test procedures that can be used to determine both clay mineralogy and the dominating clay mineral in a soil (Chittoori & Puppala, 2011). The methods that are used to establish the expansive nature of the soil would be the use of traditional methods and a technique of X-ray Diffraction (XRD). Though the traditional methods give the swelling potential of the soil on a macro-scale, this method does not consider the micro-scale, the mineralogical composition of the soil. In the coming sections of this chapter I will give a brief background on the

causes of swelling and the types of testing. The review will go into as much detail as will be required to provide an understanding of the clays mineralogical make-up and to make aware of the possible mechanisms that create the need for swelling test on soils. This will conclude with traditional testing and a XRD technique, while observing its role in the use of determining swelling minerals and swelling potential.

## **2.2 Mechanisms of Swelling Clays**

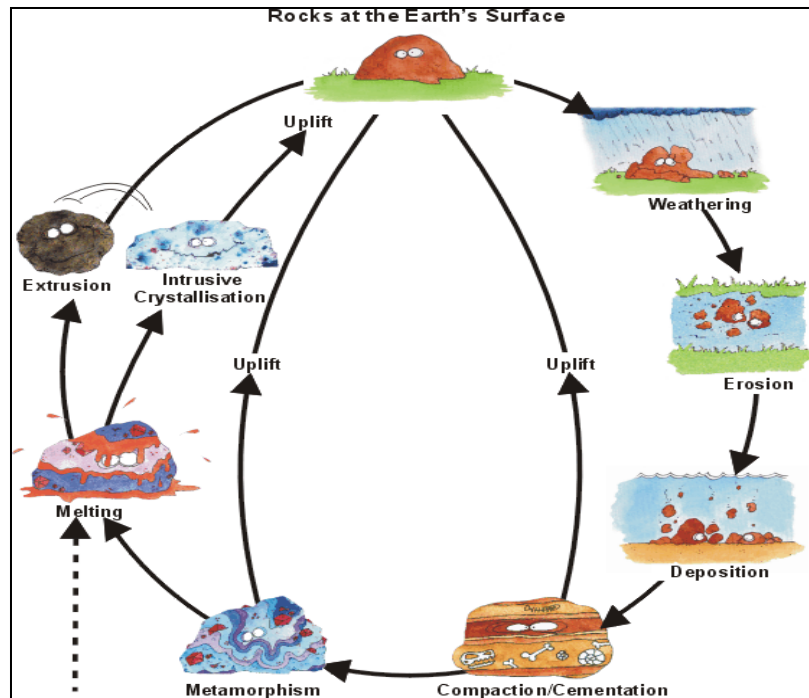
Certain types of clayey soils expand when they are wetted and shrink when dried (Coduto, 1999). Swelling is a somewhat more complex process than shrinkage (Holtz & Kovacs, 1981). The problem of expansive soils was not recognized by soil engineers until the latter part of 1930 (Chen, 1975). The amount of swelling and the magnitude of swelling pressure depend on the clay minerals present in the soil, the soil structure and fabric, and several physico-chemical aspects of the soil such as the cation valance, salt concentration, cementation, and presence of organic matter (Holtz & Kovacs, 1981).

### **2.2.1 Formation of Clay Minerals**

To understand how the clay minerals affect the swelling of the soil, one would need to consider the actual mineral its self. With mineralogy being the primary factor controlling the size, shape, and properties of the soil we will need to start with the structure and make-up of individual clay particles. First, is the definition of a clay or fine-grained particle. A particle smaller then a 200 mesh sieve size (0.074 mm), is the boundary between the sand and fine-grained particles, which include clay. Mitchell et al (2005) stated that, clay can refer both to size and to a class of minerals. As a size term, it refers to all constituents of a soil smaller than a particular size, usually 0.002 mm (2  $\mu\text{m}$ ) in engineering classification. As a mineral term, it refers to specific clay minerals that

distinguished by (1) small particle size; (2) a net negative electrical charge; (3) plasticity when mixed with water; and (4) high weathering resistance. For use in this report, the latter of the two definitions will be considered, because size alone does not portray the behavior of clay particles.

Now that parameters have been defined, the next area to look at is the actual structure, or what clay minerals are made of. Clay minerals are very tiny crystalline substances evolved primarily from chemical weathering of certain rock-forming minerals (Holtz & Kovacs, 1981). A crystal is a homogenous body bounded by smooth plane surfaces that are the external expression of an orderly internal atomic arrangement (Mitchell & Soga, 2005). The atoms in a crystal are arranged in a definite orderly manner to form a three dimensional network termed a lattice. A deeper look in to the three dimensional network of the crystalline structure of clay will be undertaken in a later Chapter 2. Weathering of rocks and soils is a destructive process whereby debris of various sizes, compositions, and shapes are formed. The new compositions are usually more stable than the old and involve a decrease in the internal energy of the materials (Mitchell & Soga, 2005). There are three general mechanisms of clay formation by weathering (Eberl, 1984): (1) inheritance; (2) neoformation; and (3) transformation. Inheritance means that a clay mineral originated from reactions that occurred in another area during a previous stage in the rock cycle and that the clay is stable enough to remain in its present environment. Origin by neoformation means that the clay has precipitated from solution or formed from reactions of amorphous materials (Figure 2.1).



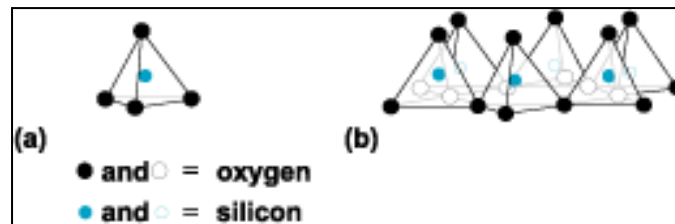
**Figure 2.1: Figure explaining amorphous material formation.**

Transformation genesis requires that the clay has kept some of its inherited structure while undergoing chemical reactions. These reactions are typically characterized by ion exchange, explained later in this chapter, with the surrounding environment and/or layer transformation in which the structure of octahedral, tetrahedral, or fixed interlayer cations is modified (Mitchell & Soga, 2005).

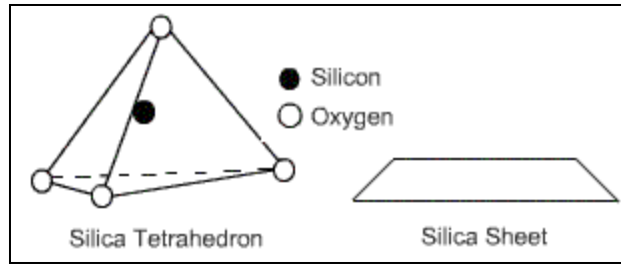
Once the weathering on the parent material and a more stable product has emerged, clay mineral formation can take place. Clay minerals in soils belong to the mineral family termed phyllosilicates, which contains other layer silicates such as serpentine, pyrophyllite, talc, mica, and chlorite (Mitchell & Soga, 2005). Chemically, they are hydrous aluminosilicates plus other metallic ions (Holtz & Kovacs, 1981). There are considerable variations in chemical and physical properties within this family of minerals (Moore & Reynolds, 1997). All clay minerals are very small, colloidal-sized

crystals, and they can only be seen with an electron microscope. In fact, there are only two fundamental crystal sheets, the tetrahedral (or silica) and the octahedral or alumina, sheets (Holtz & Kovacs, 1981).

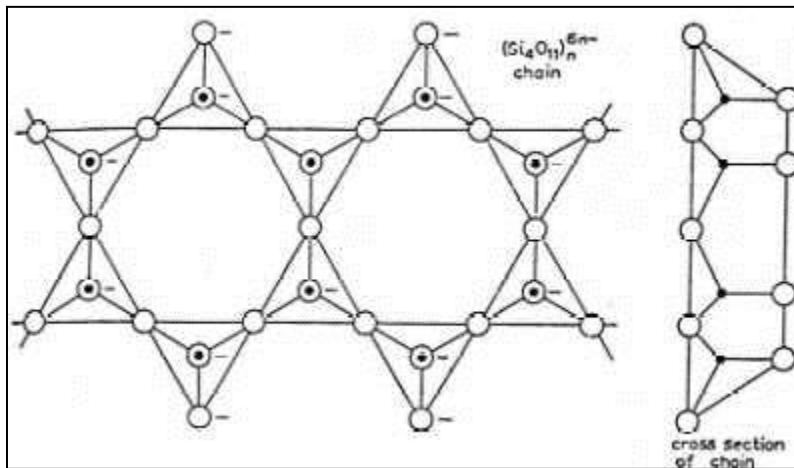
In most clay minerals structures, the silica tetrahedral are interconnected in a sheet structure (Mitchell & Soga, 2005). The tetrahedral sheet is a combination of silica tetrahedral units which consist of four oxygen atoms at the corners, surrounding a single silicon atom. Figure 2.2 shows a single silica tetrahedron Figure 2.2 also shows how the oxygen atoms at the bases of each tetrahedron are combined to form a sheet structure. The oxygen atoms at the bases of each tetrahedron are in one plane, and the un-joined oxygen corners all point in the same direction (Holtz & Kovacs, 1981). The structure has a composition  $(\text{Si}_4\text{O}_{10})^{4-}$  and can repeat indefinitely. Electrical neutrality can be obtained by replacement of four oxygens by hydroxyls or by the union with a sheet of different composition that is positively charged (Mitchell & Soga, 2005). A common schematic representation of the tetrahedral sheet which is used later is shown in Figure 2.3. A top view of the silica sheet showing how oxygen atoms at the base of each tetrahedron belong to two tetrahedrons and how adjacent silicon atoms are bonded is shown in Figure 2.4. Note the hexagonal “holes” in the sheet (Holtz & Kovacs, 1981).



**Figure 2.2: (a) Single silica tetrahedron, (b) tetrahedron sheet**



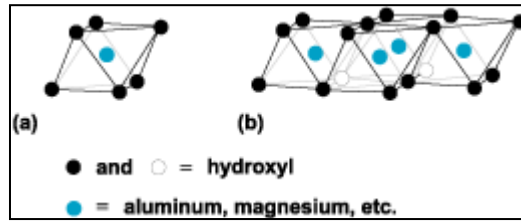
**Figure 2.3: Typical usage of tetrahedron symbol**



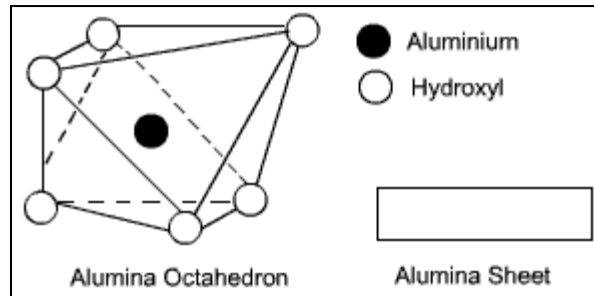
**Figure 2.4: Top view of a tetrahedron sheet**

The other sheet that which forms a clay mineral is an octahedral sheet. The octahedral sheet is a combination of octahedral units consisting of six oxygen or hydroxyls enclosing an aluminum, magnesium, iron, or other atoms (Holtz & Kovacs, 1981). The octahedral sheet can be thought of as two planes of closest-packed oxygen ions with cations occupying the resulting octahedral sites between the two planes. When we connect the centers of the six oxygen ions packed around an octahedral cation site, we have an octahedron (Moore & Reynolds, 1997). A single octahedron is shown in Figure 2.5, while Figure 2.5 also shows how the octahedrons combine to form a sheet structure.

The rows of oxygen or hydroxyls in the sheet are in two planes. Figure 2.6 is a schematic representation of the octahedral sheet which we use later.



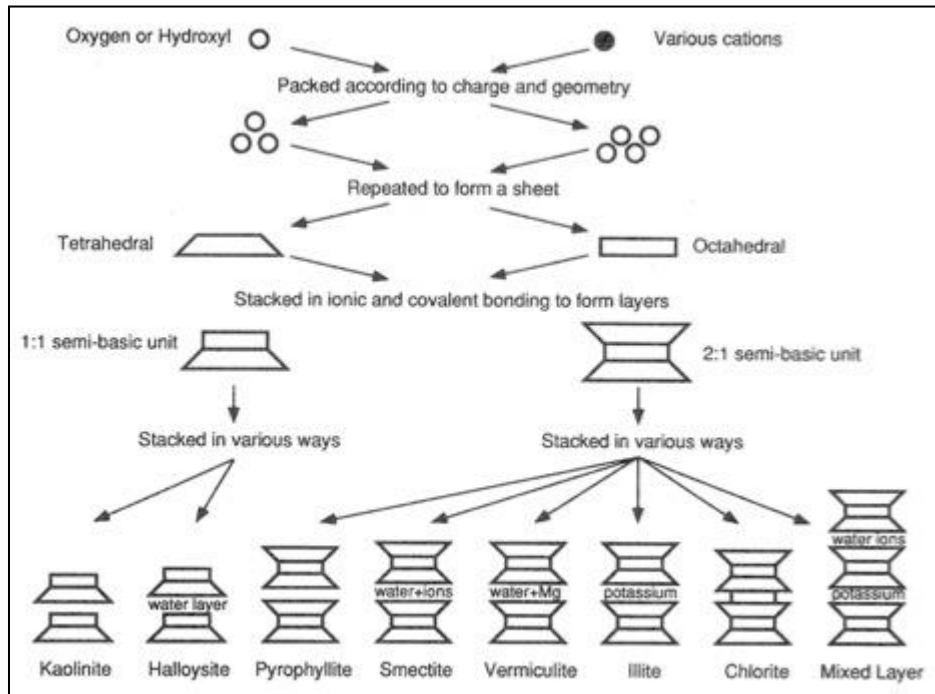
**Figure 2.5: (a) Single silica octahedral, (b) octahedral sheet**



**Figure 2.6: Typical usage of octahedral symbol**

The cations that can be surrounded by the six oxygen's can vary. The cations are usually  $\text{Al}^{3+}$ ,  $\text{Mg}^{2+}$ ,  $\text{Fe}^{2+}$ , or  $\text{Fe}^{3+}$ , but all the other transition elements and Li have been identified in the cation sites of the octahedral sheet (Moore & Reynolds, 1997). Though aluminum and magnesium are the two most commonly found, each has their own specific characterization. If all the anions of the octahedral sheet are hydroxyls and two-thirds of the cation positions are filled with aluminum, the mineral is called Gibbsite. If magnesium is substituted for the aluminum in the sheet and it fills all the cations positions, then the mineral is called Brucite (Holtz & Kovacs, 1981). Grouping the clay minerals according to crystal structure and stacking sequence of the layers is conventional since members of the same group have generally similar engineering

properties'. The minerals have unit cells consisting of two, three, or four sheets. The two-sheet minerals are made up of a silica sheet and an octahedral sheet. The unit layer within a three-sheet mineral is composed of either a dioctahedral or trioctahedral sheet sandwiched between two silica sheets (Mitchell & Soga, 2005). Figure 2.7 shows the synthesis pattern for the clay minerals and how they are stacked. The particular way these sheets are stacked, together with different bonding and different metallic ions in the crystal lattice, constitute the different clay minerals (Holtz & Kovacs, 1981). The structures shown are idealized; in actual minerals, irregular substitutions and interlayering or mixed-layer structures are common (Mitchell & Soga, 2005). For engineering purposes it is usually sufficient to describe only a few of the more common clay minerals which are found in clay soils.



**Figure 2.7: Synthesis pattern for the clay minerals and how they are stacked**



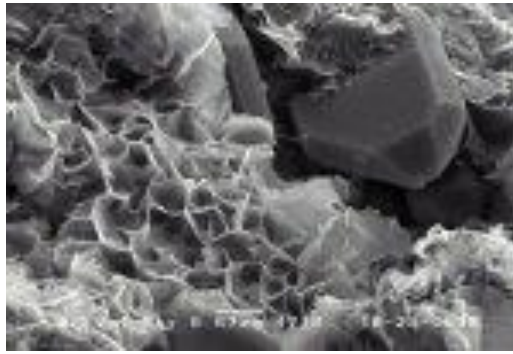
Figure 2.7 above indicate that there are two primary semi-basic units of how clay minerals are stacked. Unit layers may be stacked closely together or water layers may intervene (Mitchell & Soga, 2005). The intrusion of water or polar molecules practically takes place in the 2:1 unit layer of the clay minerals. This interaction with water is the catalysis that leads to the expansion potential of clay minerals and will be discussed further in the following section.

### **2.2.2 Properties of the Clay Mineral Structure**

In geotechnical engineering practice, the structure of a soil is taken to mean both the geometric arrangement of the particles or mineral grains as well as the interparticle forces which may act between them (Holtz & Kovacs, 1981). From herein, the term structure will refer to the latter of the two explanations given by Holtz & Kovacs. The properties of minerals are directly or indirectly related to their primary property, their structure. Clay minerals are no exception. In what follows, however, we will be concerned with properties that result from the interaction of clay minerals with other substances, mainly water (Moore & Reynolds, 1997). The structure of clay soils and thus their engineering properties ultimately depend on the nature of this adsorbed water layer (Holtz & Kovacs, 1981). Therefore, this requires an understanding of the properties of clay mineral particles. The properties of great importance here are the specific surface area for clay minerals, layer and surface charge, the electrical double layer, exchangeable ions, the nature of water when it is adsorbed on edges or in the interlayer space, and Sulfate interaction with clay minerals.

Engineering behavior for majority of the fine-grained soils is predominantly influenced by their specific surface area. Hence, these soils exhibit extremely or

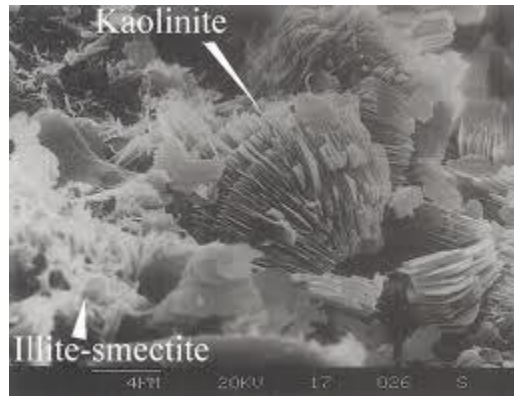
relatively high swelling and shrinkage characteristics (Arnepalli, 2008). Clays contribute the greatest amount of surface area of any of the mineral constituents of soil, but may also differ a great deal in specific surface area. For example, swelling clays such as Montmorillonites have specific surface areas up to 810 ( $\text{m}^2/\text{g}$ ) (Cerato, 2002). Montmorillonite may occur as equidimensional flakes that are so thin as to appear more like films, as shown in Figure 2.8.



**Figure 2.8: Scanning electron microscope picture of Montmorillonite**

(<http://www.carmodymcknight.com/more-information/13/>)

Particles range in thickness from 1-*nm* unit layers upward to about 1/100 of the width of the thickness. Nonexpanding soils such as Kaolinites typically have specific surface areas ranging from 10 to 40 ( $\text{m}^2/\text{g}$ ). Well-crystallized particles, shown in Figure 2.9, occur as well-formed six-sided plates. The lateral dimensions of these plates range from about 0.1 to 4  $\mu\text{m}$ , and their thickness can range from roughly 0.05 to 2  $\mu\text{m}$  (Mitchell & Soga, 2005).



**Figure 2.9: Scanning electron microscope picture of Kaolinite**

([http://pubs.usgs.gov/dds/dds-033/USGS\\_3D/ssx\\_txt/figur27.htm](http://pubs.usgs.gov/dds/dds-033/USGS_3D/ssx_txt/figur27.htm))

For many materials when particle size is reduced to 1 or 2  $\mu\text{m}$  or less the surface forces begin to exert a distinct influence on the behavior (Mitchell & Soga, 2005). Since the surface area of a soil is controlled by the grain-size distribution and clay mineralogy, it can be considered an “inherent” soil property. Consequently, the type of clay mineral present in soil is of significant importance when determining the effect of specific surface area on soil properties (Cerato, 2002).

Understanding the layer and surface charge of the clay mineral structure is of great importance in how the mineral is going to react to its environment. Clay minerals and clay-sized minerals have charges on their surfaces. These determine ion-exchange capacities; the dispersion/flocculation behaviors; the transport and fate of solutes; and governs the rate of chemical weathering and the erodibility of the land surface (Moore & Reynolds, 1997). There are two sources that create a charge on the clay surface, as stated by Holtz & Kovacs (1981). Isomorphous substitution was introduced earlier in connection with tetrahedral and octahedral sheets, practically in reference to the formation of Gibbsite and Brucite minerals. Isomorphous substitution in all of the clay

minerals, with the possible exception of those in the Kaolinite group, gives clay particles a net negative charge (Mitchell & Soga, 2005). The other charge is at the edges of the mineral particle, the boundaries where structural patterns end as broken bonds. Here, the chemical composition and structure cannot be maintained without additional ions, usually  $H^+$  or  $OH^-$ , to satisfy the unsatisfied bonds (Moore & Reynolds, 1997). Broken edges contribute greatly to unsatisfied valance charges at the edges of the crystal. Since the crystal holds a natural preference to be electrically neutral, cations in the water may be strongly attracted to the clay, depending on the amount of negative charge present (Holtz & Kovacs, 1981). This can be observed in Figure 2.10, where the illustration displays how the broken edges are trying to become electrically neutral through the cations in the water. It also show the phenomenon of cation-exchange, which will be addressed shortly. While Figure 2.11 demonstrates how a 1:1 mineral, such as Kaolinite, bonds and has a balanced charge, presumably. The clay particles having unbalanced charges at the broken edges and the ability to construct an isomorphous substitution, this creates a spring board for the clay mineral to change its distance between individual particles to accommodate a multitude of structural variation, i.e. volume change.

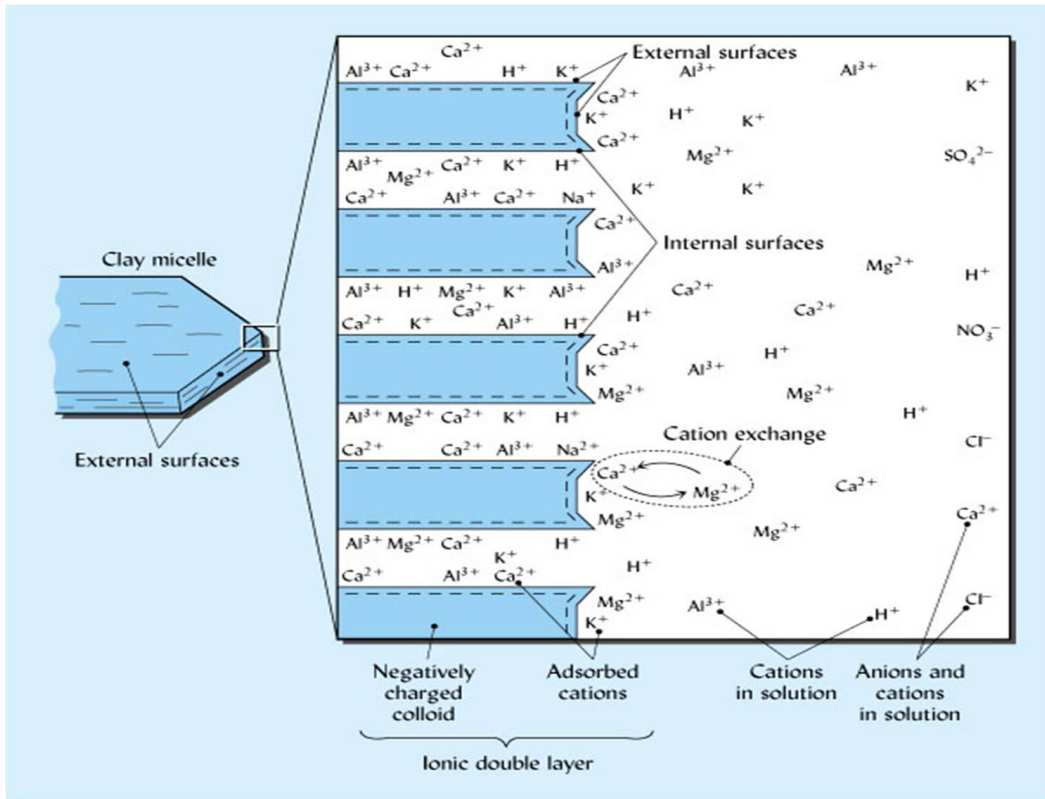


Figure 2.10: Broken edges trying to become electrically via the cations in solution

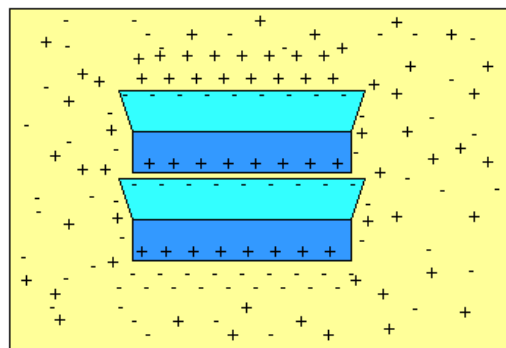
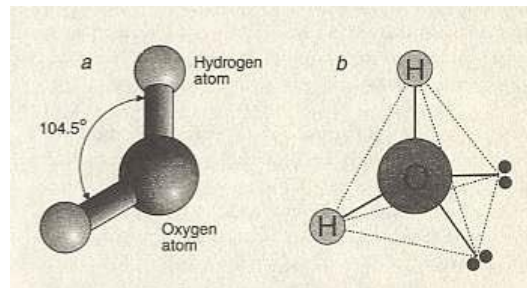


Figure 2.11: Kaolinite having interspacing bonds and has a balanced outer charge

(<http://clay.uga.edu/courses/8550/CM19.html>)

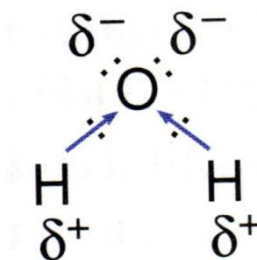
Being that water is the prime catalyst for the swelling of clay minerals, it is only right to examine the water itself. Understanding here will help relate how water is adsorbed and invades the interlayer of the clay minerals and hydrates. The water

molecule ( $\text{H}_2\text{O}$ ) is composed of a V-shaped arrangement of H and O atomic nuclei. The outer shell electronic charges, six from the oxygen and one from each hydrogen, are distributed in the form of four electrical pairs per molecule. The resulting configuration is tetrahedral, with two positive corners that are the sites of the hydrogen protons and two negative corners that are located above and below the plane of the atomic nuclei (Mitchell & Soga, 2005). The V-shape can be observed in Figure 2.12, while Figure 2.12 also illustrates the resulting configuration of the tetrahedral. Figure 2.13 shows the location of the dipole created by water. Even though water is electrically neutral, it has two separate centers of charge, one positive and one negative. Thus the water molecule is electrostatically attracted to the surface of the clay crystal (Holtz & Kovacs, 1981).



**Figure 2.12: (a) Water molecule (b) a tetrahedron configuration**

(<http://www.nivoland.net/ItCalore.htm>)

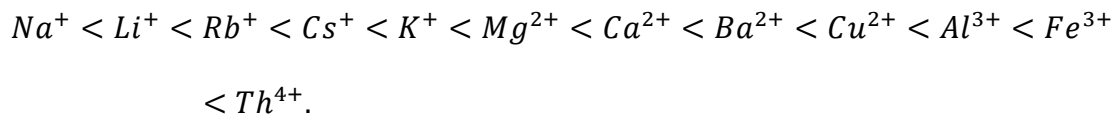


**Figure 2.13: Indicating the polarity with the positive charge on the hydrogen**

(<http://witcombe.sbc.edu/water/chemistrystructure.html>)

Because of the uneven charge distribution and dipolar character of water molecules, they are attracted to ions in solution, leading to ion hydration. Positive ions attract the negative corners of the water molecule, and vice versa (Mitchell & Soga, 2005). With water working to balance its own electrostatic potential with the cations and clay mineral platelets eager to equilibrate its deficiencies in charge, cations will migrate into the interlayers of the clay.

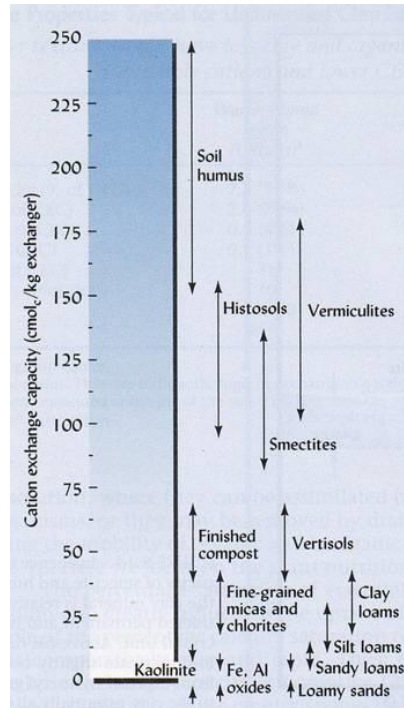
Under a given set of environmental conditions (temperature, pressure, pH, chemical and biological compositions of water), clays adsorb cations of specific types and amounts (Mitchell & Soga, 2005). Different clays have different charge deficiencies and thus have different tendencies to attract the exchangeable cations. They are called exchangeable since one cation can easily be exchanged with one of the same valence or by two of one-half the valence of the original cation (Holtz & Kovacs, 1981). A typical replacement series of cations in approximate order is;



With the multitude of contributing factors it is hard for any given clay to have a fixed single value of exchange capacity. This capacity is directly related to the surface charge density of the clay. The cation exchange capacity, that is, the number of exchangeable charges, is usually between 1 and 150 meq/100 g. Ranges of cation exchange capacity (CEC) for different clays are in Table 2.1 and an illustration of cation exchange can be seen in Figure 2.14. Although the exchange reactions do not ordinarily affect the structure of the clay particles themselves; important changes in the physical and physicochemical properties of the soil may result (Mitchell & Soga, 2005).

**Table 2.1: Typical values of cation exchange capacity of different minerals (Mitchell & Soga, 2005).**

Mineral	CEC (meq/100g)
Kaolinite	3 to 15
Illite	10 to 40
Smectite	80 to 150

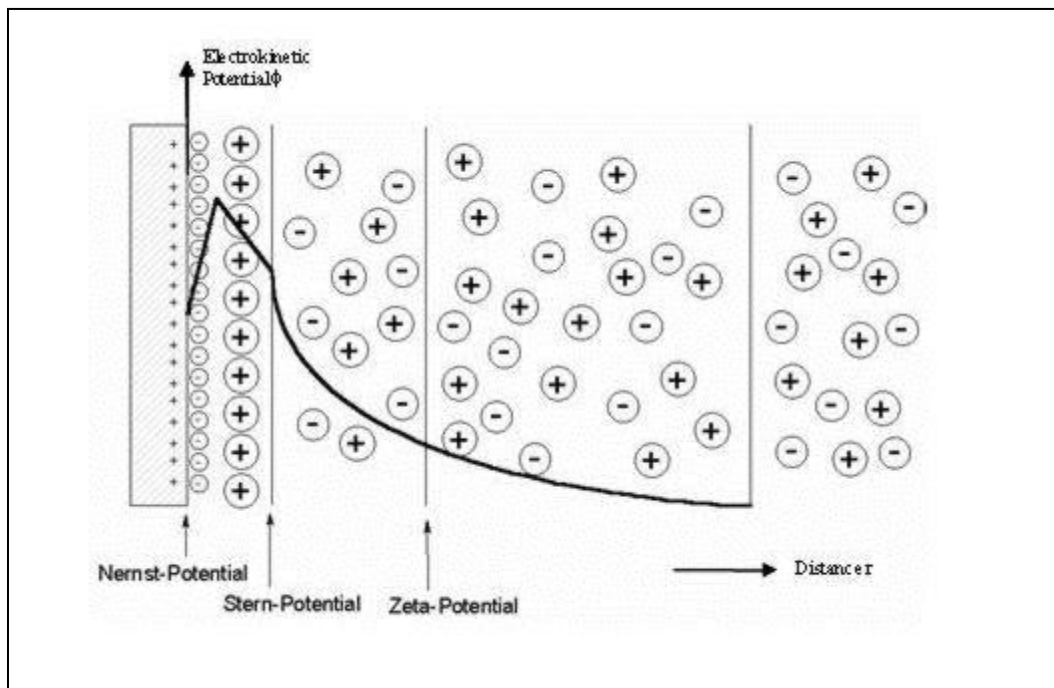


**Figure 2.14: Illustration of cation exchange (Brady & Weil, 2007)**

It has been shown that the clay lattice carries a net negative charge as a result of isomorphous substitution of certain electropositive elements by elements of a lower valence. The net negative lattice charge is compensated by cations which are located on the unit-layer surfaces. In the presence of water, these compensating cations have a tendency to diffuse away from the layer surface since their concentration will be smaller than the bulk solution (van Olphen, 1963). This mechanism of diffusion away from the clay surface is related to the negative electrical field orientating in the particle surface and



ion-surface interactions. The charged surface and the distributed charge in the adjacent phase are together termed the diffuse double layer (Mitchell & Soga, 2005). The theory is now referred to as the DLVO theory. The DLVO theory, based on the Gouy-Chapman model, gives reasonable predictions for freely swelling clay systems of very fine clay particles with monovalent ions, such as Na and Li Montmorillonite (Mitchell & Soga, 2005). Clay particles can repulse each other electrostatically, but the process depends on the ion concentration, interparticle spacing, and other factors. Similarly, there can be attraction of the individual particles due to the tendency for hydrogen bonding, van der Waals' forces, and other types of chemical and organic bonds (Holtz & Kovacs, 1981). An illustration of the described theory is shown in Figure 2.15.



**Figure 2.15: Illustration describing the DLVO theory**

The theory of the diffuse double layer provides useful insight into ionic distributions adjacent to clay particles, which, in turn, allows for reasonable predictions

of processes such as flocculation-deflocculation, swelling, and the effects of pore fluid compositional changes under idealized conditions. discrepancies between predictions of this theory and the behavior of most other types of clay, both in suspension and in more condensed forms, has focused attention on other theories (Mitchell & Soga, 2005). Another popular theory is that of osmotic pressure. Osmosis is the movement of a solvent through a semi-permeable membrane into a solution of higher solute concentration that tends to equalize the concentrations of solute on the two sides of the membrane (Merriam-Webster, 2013). It is well recognized that osmotic pressure can be expected to take place in the soil-water system. Assuming that the double-layer system exists in the soil lattice, the concentration of ions being held by the attractive force prevents the ions from moving away from the double layer. However, water is able to move in and dilute the concentration, and, consequently, a semi-permeable membrane effect is achieved (Chen, 1975). In a study conducted by (Bolt, 1956), he concluded that the swelling of both Illitic clays and Montmorillonite clays is caused by the excess osmotic pressure in the adsorbed layers of ions. Bolt (1956) claimed that the osmotic pressure of the system might reach a value of 50 to 100 tons per square foot. It is therefore, not surprising that the swelling pressure of expansive clays sometimes reaches more than 25 tons per square foot (Chen, 1975).

In soils in which swelling is dominated by the clay content, Smectite or Vermiculite, are relatively straight-forward. Details of structure and the presence of interlayer materials may have significant effects on the swelling properties of these minerals. In addition, the presence of certain other minerals in soils, such as Pyrite and

Gypsum, as well as geochemical and microbiological factors, may lead to significant amounts of swelling and heave (Mitchell & Soga, 2005).

Swelling in Sulfate argillaceous rocks is a complex phenomenon in which key factors are not deeply defined. Sulfate mineral crystal growth in open discontinuities due to the evaporation of groundwater can contribute to large displacements and high swelling pressures recorded in both field observations and laboratory tests (Deu, Romero, & Berdugo, 2013). Sulfate crystals develop in the capillary zone and tend to localize along discontinuities due to reduced stress regions. The increase in volume resulting for the growth of Sulfate minerals along bedding planes is a dominant factor in the vertical heave that occurs in sedimentary rocks and other materials that have sub-horizontal fissility (Mitchell & Soga, 2005). Degradation and swelling of clayey rocks bearing calcium Sulfate produces considerable damage to civil engineering works. This behavior has undergone extensive study in the past, in relation to tunnel and foundation engineering. Different possible mechanisms were suggested for explaining the typically observed degradation and swelling behavior, namely, Gypsification, i.e., transformation of Anhydrite into Gypsum, dissolution of Anhydrite and re-crystallization of Gypsum influenced by the presence of clay minerals, precipitation of Gypsum due to preferential flow of Sulfate-rich water through fissures opened by mechanical stress relief, precipitation of Gypsum from supersaturated pore water induced by evaporation (Oldecop & Alonso, 2012). The production of Sulfates by Pyrite oxidation also increases the potential for further deleterious reactions, such as the formation of Gypsum and expansive Sulfate materials (e.g. Ettringite) (Mitchell & Soga, 2005). Gypsum forms when Sulfate ions react with Calcium in the presence of water, resulting in very large

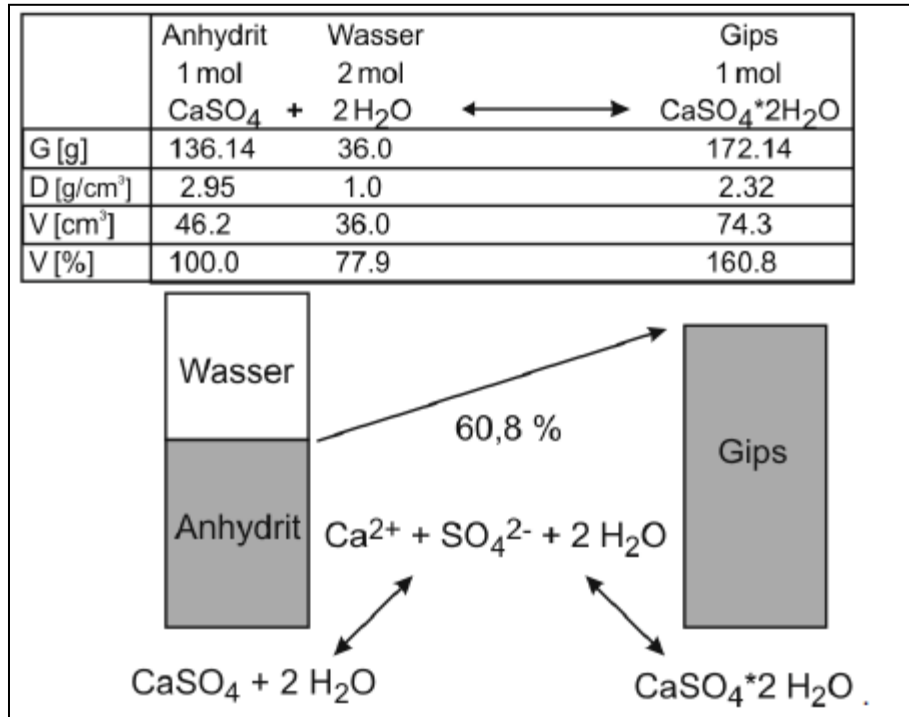
volume increases (Mitchell & Soga, 2005). This process of Gypsification refers to the addition of water of crystallization to the mineral and is associated with a volume increase of up to 62% (Blatt, Middleton, & Murray, 1980). Volume increase associated with several Sulfidic chemical weathering reactions are given in Table 2.2.

**Table 2.2: Volume increase of selected mineral transformations (Mitchell & Soga, 2005).**

Mineral Transformation		Volume Increase of Crystalline Solids (%)
Original Mineral	New Mineral	
Illite	Alunite	8
Illite	Jarosite	10
Calcite	Gypsum	60
Pyrite	Jarosite	115
Pyrite	Anhydrous ferrous sulfate	350
Pyrite	Melanterite	536

Gypsification in anhydrous Calcium Sulfate bearing soils can cause serious engineering problems for various structures and pavements. The presence of hydrating Anhydrite layers in soils can create swell pressure and floor heave in tunnels and massive rock uplift in dams (Azam & Abduljawwad, 2000). This phenomenon was investigated in the construction of the Lilla tunnel of the AVE Madrid-Barcelona high speed railway line. The floor of the Lilla tunnel experienced serious damage due to swelling of rock, during the months following the completion of the concrete lining. The extent and magnitude of the damage was unexpectedly large, since the floor slab heaved up to 80 cm in the term of a year and a half after completion of the concrete (Oldecop & Alonso, 2012). Rauh et al. (2006) explained in great detail how swelling could occur in tunnel construction and along with a test to determine the potential of swelling Gypsification,

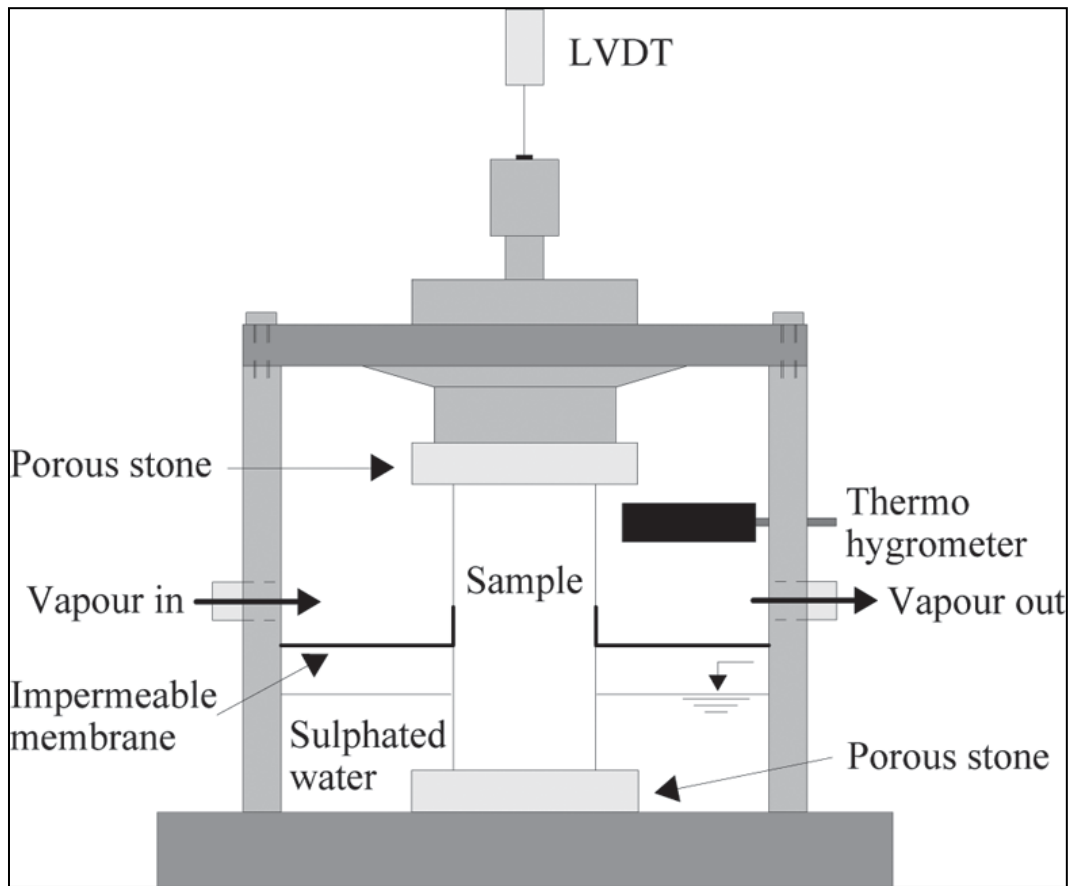
which was concluded to be 60%. This chemical change is shown in Figure 2.16. Looking closer, this equation is quite simple, since the reaction involves a solution and a crystallization process (Rauh, Spaun, & Thuro, 2006).



**Figure 2.16: Illustration of how anhydrite increases its volume when hydrated (Rauh, Spaun, & Thuro, 2006).**

The interpretation of swelling phenomena in sulfate argillaceous rocks implies a great complexity, involving variables related to mineralogy and tectonic history of samples, as well as chemical composition of groundwater and environmental conditions (Deu, Romero, & Berdugo, 2013). Deu et al. (2013) conducted a highly complex study to control some of the complexities. Using the Lilla claystone from the same area as the high speed rail tunnel in Spain, a test was created where the control of the hydraulic/environmental conditions was conducted. A new swelling chamber was developed and is shown in Figure 2.17. Using different environmental conditions, via

relative humidity and temperature, in the upper part of the chamber controlled by a constant vapor flow associated with a saturated hygroscopic solution.



**Figure 2.17: Environmental chamber for measuring swell under different conditions (Deu, Romero, & Berdugo, 2013).**

Controlling the environmental conditions in the top of the chamber allows for suction to be created, pulling the Sulfated water in the bottom of the chamber up through the sample. After 160 days of test, an axial swelling strain of roughly 13% was measured. Growth of Gypsum crystals due to the evaporation of soaked water and supersaturation in hydrated Calcium Sulfate were clearly observed in discontinuities. The precipitation of Sulfate crystals in open discontinuities allows the generation of new fissures where neo-formations of crystals are able to precipitate, causing swelling. Following this

interpretation some factors must be taken into account in order to study the swelling phenomenon: saturation conditions of groundwater regarding Gypsum, environmental conditions that may induce vapor and water flow, mineralogical properties of argillaceous rocks and the presence of open discontinuities in the rock, usually related to fissures and slickenside surfaces.

Sulfate argillaceous rocks manifest high mechanical competences in undisturbed state. Though, when subjected to unload processes or when exposed to atmospheric agents often exhibit important degradation and large swelling pressures that occur during a large period of time without signs of attenuation (Deu, Romero, & Berdugo, 2013).

In observing the a fore-mentioned properties, from the formations of clay minerals to its interaction with water and interlayer surfaces, it is observed that Holtz (1981) was correct to state that the amount of swelling and the magnitude of swelling pressure depends on the clay minerals present in the soil, the soil structure and fabric, and several physico-chemical aspects of the soil such as the cation valance, salt concentration, cementation, and presence of organic matter. In summary, the structure of clay and the engineering behavior of this structure are strongly influenced by its make-up and interaction with the surrounding environment.

### **2.3 Traditional Swelling Test on Soil**

Now that there has been sufficient information given in the structure of clay minerals and some of the mechanisms that influence the swelling of clay, a look at how the swelling pressure for clay soils can be obtained. There are numerous tests that would provide the swell pressure or percent swell of the soil in question. To name a few, there is

the Load Swell test (One-Dimensional Swell), Expansive Index (EI) test, and correlations from extensive studies are used quite frequently for practice and research.

The most supported and convenient method of determining the swelling potential and swelling pressure of an expansive clay is by direct measurement. Direct measurement of expansive soils can be achieved by the use of the conventional one-dimensional consolidometer (Chen, 1975). The test is thoroughly explained in the Standard Test Methods for One-Dimensional Swell or Settlement Potential of Cohesive Soils ASTM D 4546-08. These test methods cover three alternative laboratory methods for determining the magnitude of the swell or settlement of relatively undisturbed or compacted cohesive soil. The test methods can be used to determine (a) the magnitude of swell or settlement under known vertical (axial) pressure, or (b) the magnitude of vertical pressure needed to maintain no volume change of laterally constrained, axially loaded specimens. Estimates of the swell and settlement of soil determined by these test methods are often of key importance in the design of floor slabs on grade and the evaluation of their performance. However, when using these estimates it is recognized that swell parameters determined from these test methods for the purpose of estimating in situ heave of foundations and compacted soils may not be representative of many field conditions because lateral swell and lateral confining pressure are not simulated. This standard was followed to complete the swelling test needed in this study.

Another test that is used is the Standard Test Method for Expansion Index of Soils ASTM D 4829-11. This test method allows for determination of expansion potential of compacted soils when inundated with distilled water. This test method provides a simple yet sensitive method for determination of the expansion potential of compacted soils for

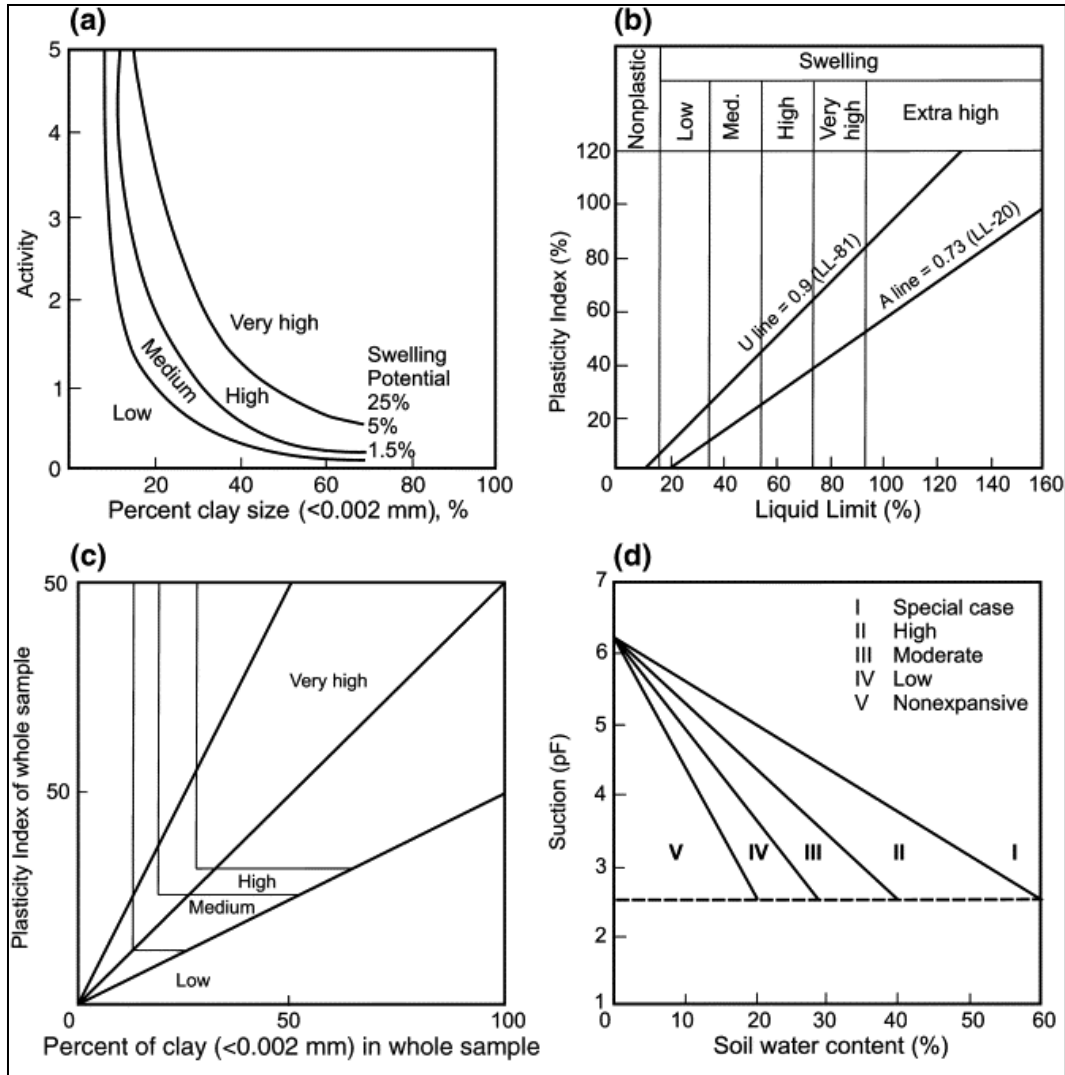


practical engineering applications using an index parameter. The index parameter for the potential expansion is indicated in Table 2.3. This test was used through the research presented here and the results will be explored later in Chapter 5.

**Table 2.3: Typical values of the expansion index and potential parameter (ASTM D 4829-11).**

Expansion Index	EI Potential Expansion
0-20	Very Low
21-50	Low
51-90	Medium
91-130	High
>130	Very High

The final test, which is not really a test, is the use of correlations to provide light to the swelling potential of clay soils. This has been studied extensively with no clear agreement. Seed et al. (1962) identified a correlation using the percent clay verses the activity of the soil. Activity can be defined as the ratio of the plasticity index to the clay fraction. This relationship can be observed in Figure 2.18. Another correlation that was created by Casagrande (1948) uses Atterberg limits. By locating the LL-PI on a plasticity chart, as shown in Figure 2.18, relationships of the swelling characteristics and mineral content are given. If a given sample has Atterberg limits that plot high above the A-line near the U-line, this indicates a strong likelihood that there exist a great deal of active clay minerals such as Montmorillonite (Holtz & Kovacs, 1981). Many more correlations could be discussed here however they would be nothing more than just that, another correlation. Though if correlations were the “be all end all”, the understanding of expansive soils would not be such a difficult process.



**Figure 2.18: Correlation between (a) Activity vs. Percent of clay and (b) Atterberg Limits alluding to swelling**

## 2.4 X-ray Diffraction Test on Soil

When using X-ray diffractions to determine the composition of minerals in clay soil one should consider how the X-ray is used to gather a signal. Once the composition is understood inferences can then be made in relation to the swell potential of clay minerals.

To start, the characteristics of crystals need to be revisited specifically the structure of the crystal. The atoms in a crystal are arranged in a definite orderly manner to form a three-dimensional network termed *lattice*. Positions within the lattice where atoms or atomic groups are located are termed *lattice points* (Moore & Reynolds, 1997). Only 14 different arrangements of lattice points in space are possible these are the *Bravais space lattices*, and are illustrated in Figure 2.19. These can be categorized into six crystal systems show in Figure 2.20. To describe the plane orientation and directions in crystal system miller indices can be used. This information, along with the distances that separate parallel planes is important for the identification and classification of different minerals (Moore & Reynolds, 1997). The indices are always enclosed within parentheses and indicated in the order *abc* without commas. The general indices (*hkl*) are used to refer to any plane that cuts all three axes. The (001) planes of soil minerals are of particular interest because they are indicative of specific clay mineral types (Moore & Reynolds, 1997).








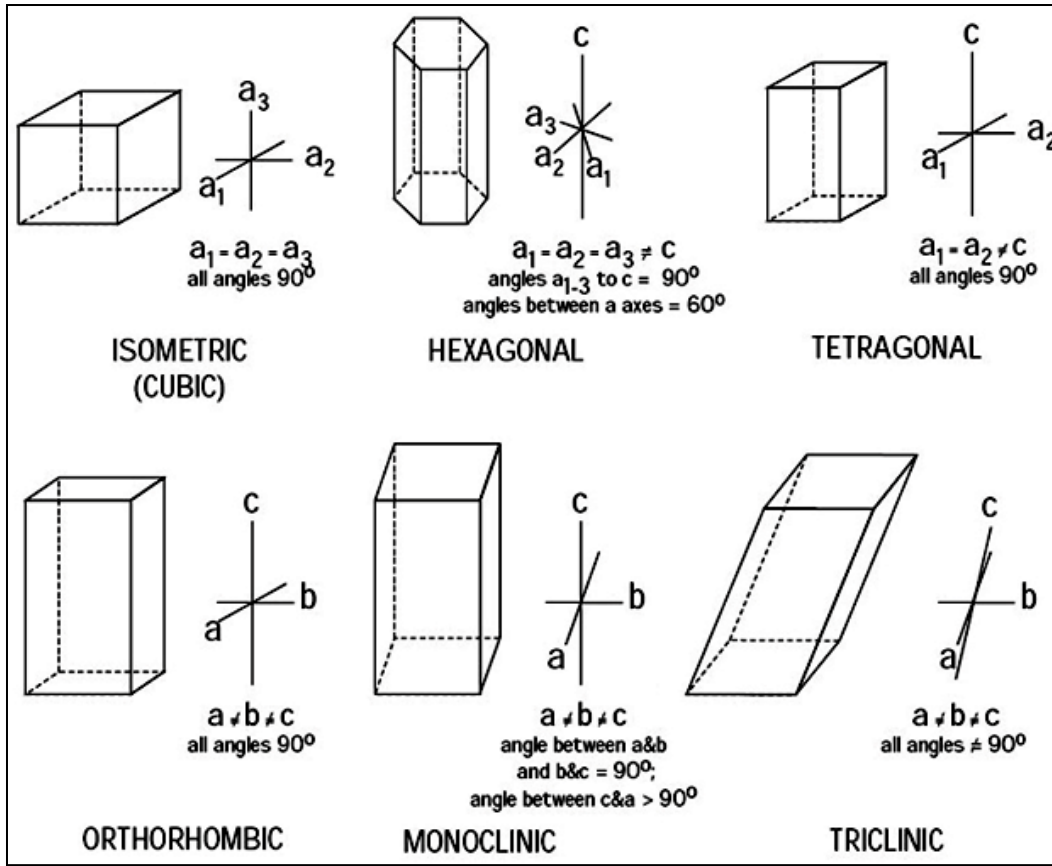
Bravais lattice cells	Axes and interaxial angles
 <p>Cubic P    Cubic I    Cubic F</p>	<p>Three axes at right angles; all equal: <math>a = b = c; \alpha = \beta = \gamma = 90^\circ</math></p>
 <p>Tetragonal P    Tetragonal I</p>	<p>Three axes at right angles; two equal: <math>a = b \neq c; \alpha = \beta = \gamma = 90^\circ</math></p>
 <p>Orthorhombic</p>	<p>Three axes at right angles; all unequal: <math>a \neq b \neq c; \alpha = \beta = \gamma = 90^\circ</math></p>
 <p>Monoclinic P    Monoclinic C</p>	<p>Three axes, one pair not at right angles, of any lengths: <math>a \neq b \neq c; \alpha = \gamma = 90^\circ \neq \beta</math></p>
 <p>Triclinic P</p>	<p>Three axes not at right angles, of any lengths: <math>a \neq b \neq c; \alpha \neq \beta \neq \gamma \neq 90^\circ</math></p>
 <p>Trigonal R (rhombohedral)</p>	<p>Rhombohedral: three axes equally inclined, not at right angles; all equal: <math>a = b = c; \alpha = \beta = \gamma \neq 90^\circ</math></p>
 <p>Trigonal and hexagonal C (or P)</p>	<p>Hexagonal: three equal axes coplanar at <math>120^\circ</math>, fourth axis at right angles to these: <math>a_1 = a_2 = a_3 \neq c;</math> <math>\alpha = \beta = 90^\circ, \gamma = 120^\circ</math></p>

Figure 2.19: Bravais space lattices chart

(<http://www.answers.com/topic/crystallography>)

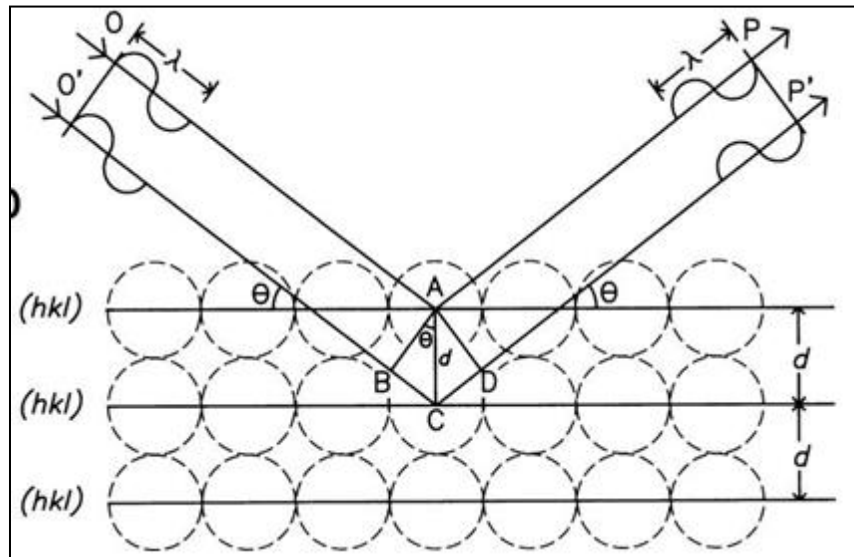


**Figure 2.20: Categorized six crystal systems**

(<http://academic.emporia.edu/abersusa/go324/mineral.htm>)

As indicated, clay minerals are extremely small. They are on the order of angstroms ( $\text{\AA}$ ) which is  $1.0 \times 10^{-10}$  meters ( $m$ ). The spacing between them is no different. Because wavelengths of about  $1\text{\AA}$  are of the same order as the spacing of atomic planes in crystalline materials, X-rays are useful for the analysis of crystal structures (Mitchell & Soga, 2005). At each atomic plane a minute portion of the beam is absorbed by individual atoms that then oscillate as dipoles and radiate waves in all directions. Radiated waves in certain directions will be in phase and can be interpreted in simplistic fashion as a wave resulting from a reflection of the incident beam. In-phase radiations emerge as a coherent beam that can be detected on film by a radiation counting device (Figure 2.21). The

orientation of parallel atomic planes, relative to the direction of the incident beam, at which radiations are in phase depends on the wave length of the X-rays and the spacing between atomic planes (Mitchell & Soga, 2005). The relationship among the wavelength of the radiation  $\lambda$ , the angle  $\theta$  between the incident beam of radiation and the parallel planes of atoms causing the diffraction, and the spacing  $d$  between these planes is called *Bragg's Law* and is developed in Chapter 4 (Moore & Reynolds, 1997).



**Figure 2.21: Analogy to specular reflection**

Soil particles come in a great variety of sizes, shapes, and compositions. The possible particle arrangements (fabric) and stabilities of these arrangements (structure) are many; therefore, any single soil can exist in many different states, each of which can be viewed as a somewhat different material (Mitchell & Soga, 2005). One might think that the subject of water interacting with clay mineral surfaces, water in the interlayer space, would be pretty straightforward. Ha! In spite of having thrown almost all the technology of modern instrumentation at the problem, there remains confusion and disagreement about the number of details (Moore & Reynolds, 1997).

## CHAPTER 3

### LABORATORY CHARACTERIZATION OF SOIL MATERIALS

#### **3.1 Soil Selection**

In this study, the soils were selected based on their moderate to high expansive potential. The three soils that were selected were soils that ranged from sandy clay to high plastic clay based on the presumed swell potential of the soil types. The swell potential wanted for the study needed to be moderate to high, to very high to insure that the soils contained the necessary clay minerals to qualify for the study. The three soils selected were collected for the following areas: Anthem (Arizona), Denver (Colorado), and San Antonio (Texas). The Anthem (Arizona), Denver (Colorado), San Antonio (Texas) soils will be referenced as Anthem, Colorado, and San Antonio, respectively, herein.

#### **3.2 Testing Information Used to Determine Soil Properties**

To determine the basic index properties, the soils were subjected to common standardized index test procedures. The index property testing was conducted collectively by a group of graduate students working as part of the National Science Foundation project *Collaborative Research: SWCC Based Models for Realistic Simulation of Swell Behavior of Expansive Soils, Award #1031238*. Table 3.1 presents a list of the tests that were completed on Anthem, Colorado, and San Antonio clays, along with the standard procedure used to obtain the results. Most of the tests in Table 3.1 were completed by Daniel Rosenbalm a group members with assistance from the group. As for the specific surface area and cation exchange capacity testing, a procedure followed from papers written by Cerato (2002) and Derkowski & Bristow (2012), respectively, were used to determine these quantities. The method to estimate the specific surface area involves

saturation prepared soil samples with EGME (ethylene glycol monoethyl ether), equilibrating them in vacuum over a CaCl<sub>2</sub>-EGME solvate, and weighing to find the point when equilibrium is reached. This process allows the infiltration into the mineral structure between the interlayers and thereby gives the total surface area. The specific surface area test was performed at Arizona State University while the cation exchange capacity test was performed at University of Texas, Arlington.

**Table 3.1: ASTM test complete on selected soils**

Soil Test	ASTM Designation
Atterberg Limits	D4318 Standard Test Methods for Liquid Limit, Plastic Limit and Plasticity Index of Soils
Hydrometer and Sieve Analysis	D422 Standard Test Method for Particle Size Analysis of Soils
Shrinkage Limit	D4943 Standard Test Method For Shrinkage Factors of Soils by Wax Method
Specific Gravity	D854 Standard test methods for specific gravity of soil solids by water Pycnometer
Swell Potential	D4546 Standard Test Method for One-Dimensional Swell or Collapse on Cohesive Soils
USCS Soil Classification	D2487 Standard Practice for Classification of Soils for Engineering Purposes (Unified Soil Classification System)
Salt Test	ADOT Arizona 733

Other tests that were performed outside the laboratory at Arizona State University were the salt content test, which was performed at IAS laboratories in Phoenix, Arizona. In cases where the tests could not be completed, correlations with other index properties were used to obtain the value. For instance, when the shrinkage was not measured for the soil; it was estimated from Equation 3.1. Of the three soils, Anthem and Colorado were measured directly while; San Antonio was inferred using equation 3.1.

$$SL = 20 \pm \Delta p_i \dots\dots\dots (3.1)$$



Where:

*SL* is the shrinkage limit

$\Delta p_i$  is the vertical distance for the A-Line

The vertical distance from the A-Line can be determined by the following equation:

$$\Delta p_i = PI - 0.73(LL - 20) \dots \dots \dots (3.2)$$

Where:

*PI* is the plasticity index,

*LL* is the Liquid Limit.

Other properties were determined based on their intrinsic relationships with soil.

The *wPI* of the soil was determined by the following equation:

$$wPI = \% Pass\ 200 * PI / 100 \dots \dots \dots (3.3)$$

Where:

*wPI* is the weighted plasticity index,

*% Pass 200* is the percentage passing the #200 sieve.

The Group Index (*GI*) of the soil was determined by the following equation:

$$GI = (\% Pass\ 200 - 35) * (0.2 + 0.005 * (LL - 40)) + 0.01 * (\% Pass\ 200 - 15) * (PI - 10) \dots \dots \dots (3.4)$$

Where:

*GI* is the group index of the soil.

The Activity of the soil was determined by the following equation:

$$Activity\ (A) = \frac{PI}{\% < 0.002\ mm} \dots \dots \dots (3.5)$$

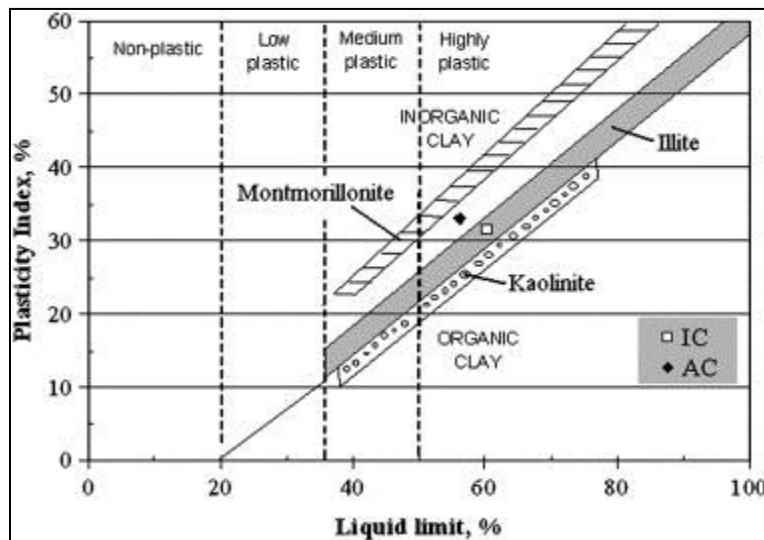
Where:

$A$  is the activity,

$PI$  is the plasticity index,

$\% < 0.002 \text{ mm}$  is the clay content of the soil.

The activity can be used to predict the dominant clay type present in the soil. The typical range for clay is between 0.75 and 1.25. If the activity is greater than 1.25, it is considered active. The free swell test were prepared in one-dimensional rings and re-compacted to optimum moisture content and at 95% maximum dry density. The Atterberg Limits also can be used to also get an idea of the dominant clay mineral present in the soil. This was shown in the Casagrande plasticity chart in Figure 3.1.



**Figure 3.1: Casagrande plasticity chart related to the mineralogy of the soil (Celik, 2010)**

### 3.3 Soil Properties

The soil index properties measured on the three different soils, using the ASTM testing indicated in Table 3.1 are presented in the following subsections. The

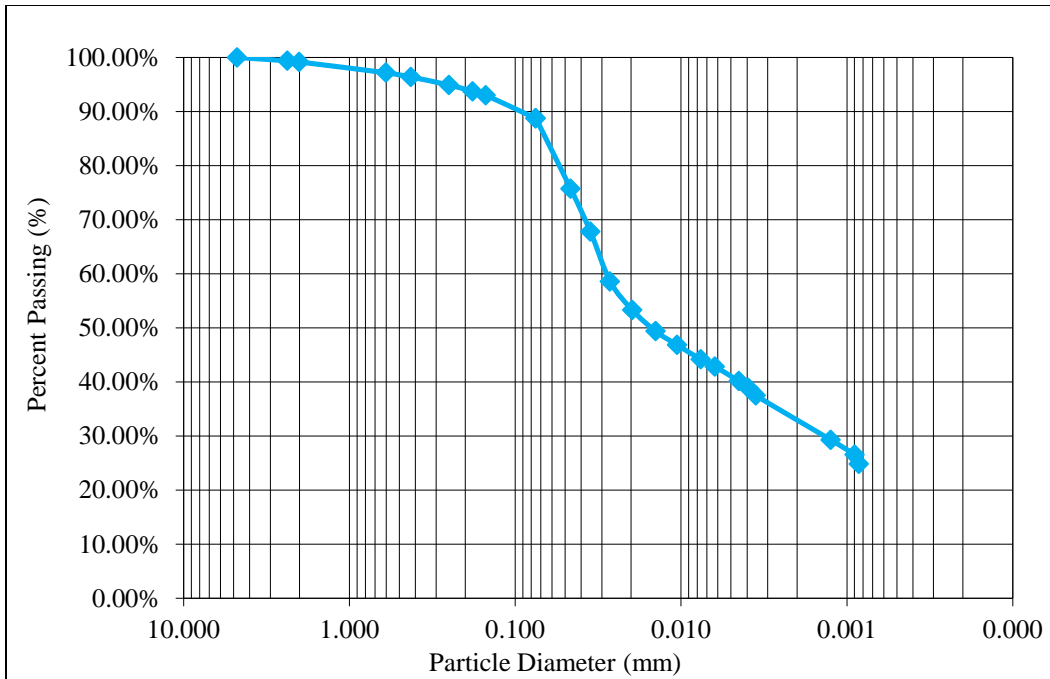
interpolation of the data along with the mineral composition will be revisited in Chapter 6 “Analysis of Mineralogy Used to Estimate Swelling Minerals”.

### **3.3.1 Anthem Soil Properties**

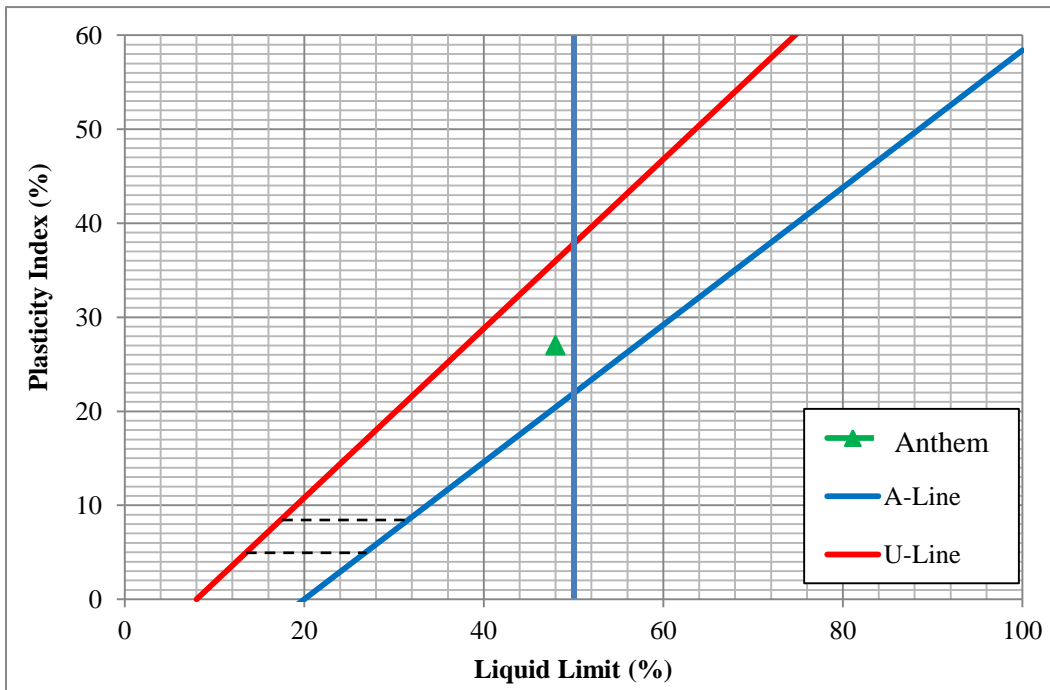
A summary of the basic index properties for the Anthem soil can be found in Table 3.2. The index properties were used in correlations, shown in equations 3.3, 3.4, and 3.5 above, to indicate some intrinsic properties, such as  $wPI$ , Group Index ( $GI$ ), and Activity ( $A$ ) of the Anthem soil. The Unified Soil Classification System (USCS) places the soil as a Lean Clay, which is due to the percent passing number 200 sieve and the Atterberg Limits. Figure 3.2 shows the grains size distribution, while the Casagrande chart indicating the USCS classification of Anthem soil is shown in Figure 3.3. Along with the soil index properties of the soil, the Specific Surface Area ( $SSA$ ) and Cation Exchange Capacity ( $CEC$ ) were included in the study. The values of these two properties are indicated in Table 3.2.

**Table 4: Anthem soil index properties**

Particle Size Analysis		
% Gravel		0.0
% Sand		11.3
% Silt		56.5
% Clay		32.2
Atterberg Limits/ Consistency Limits		
Liquid Limit (%)		48
Plastic Limit (%)		21
Plasticity Index (%)		27
Shrinkage Limit Measured (%)		15
Other Index Properties		
Activity		0.84
Weighted Plasticity Index		24
Group Index		25.42
Cation Exchange Capacity ( <i>meq/100g</i> )		71.78
Specific Surface Area ( $m^2/g$ )		168.74
Calcium ( <i>ppm</i> )		150
Sodium ( <i>ppm</i> )		850
Sulfur ( <i>ppm</i> )		610
Sulfate ( <i>ppm</i> )		1800
USCS Classification		CL
Free Swell Data		
# of Test	% Swell	Swell Pressure (kPa)
2	8.6%	96.2



**Figure 22: Grain size distribution of Anthem Soil**



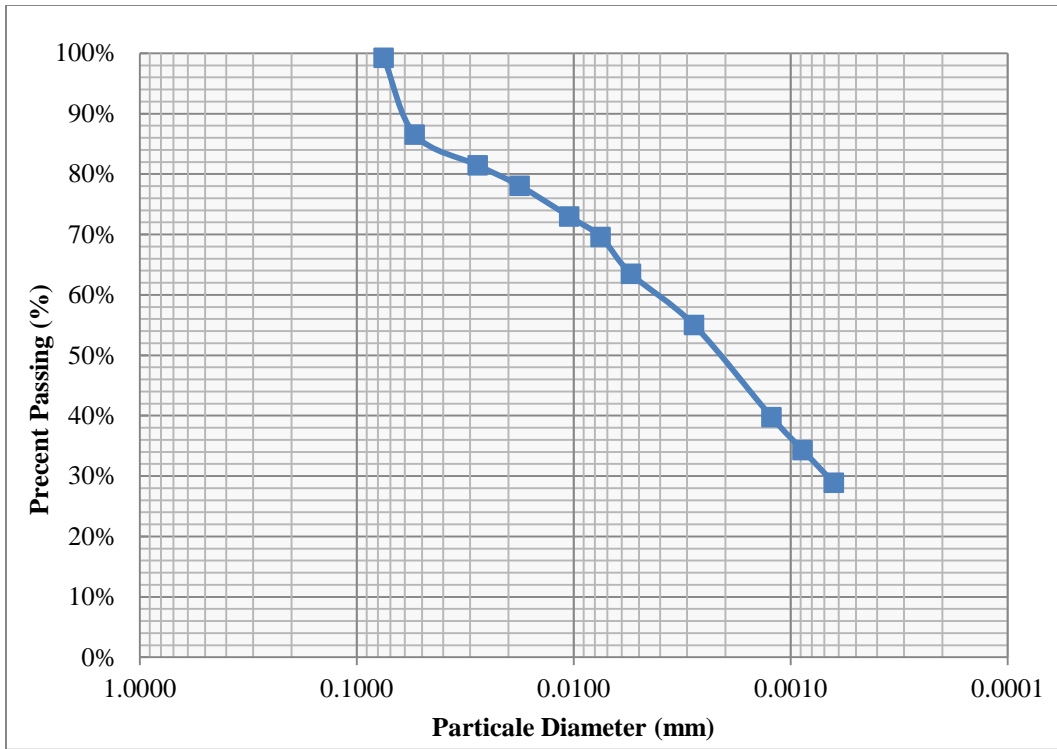
**Figure 23: USCS classification for Anthem Soil**

### **3.3.2 Colorado Soil Properties**

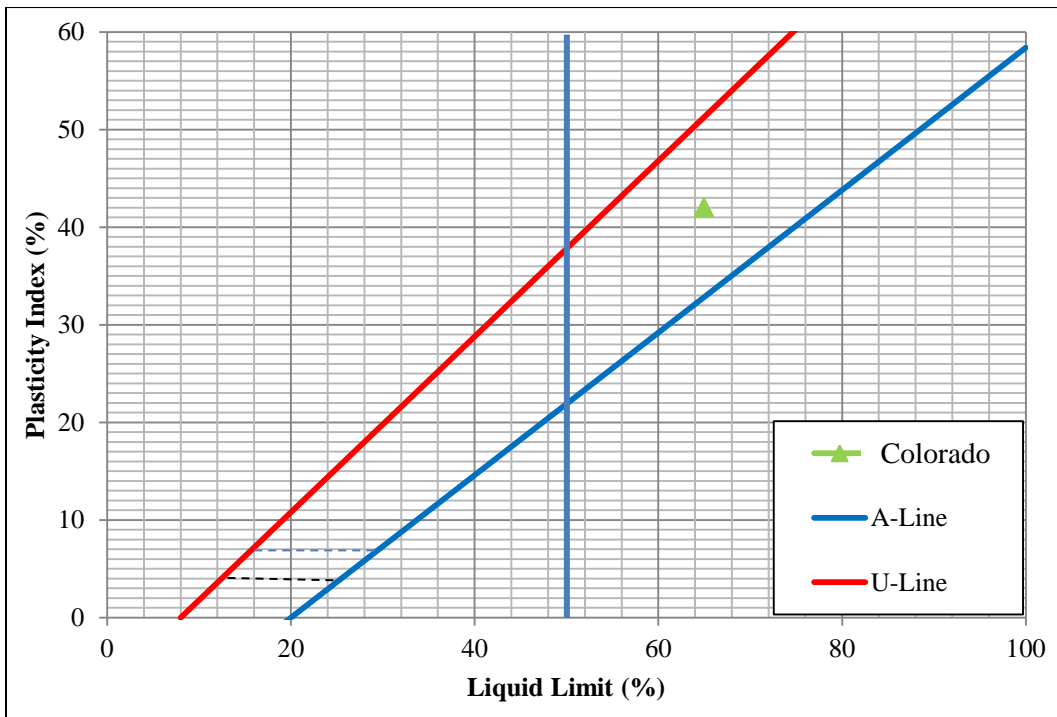
A summary of the basic index properties for the Colorado soil can be found in Table 3.3. The index properties were also used in correlations, shown in equation 3.3, 3.4, and 3.5 above, to indicate some intrinsic properties, such as  $wPI$ , Group Index ( $GI$ ), and Activity ( $A$ ) of the Colorado soil. The USCS classification for the soil is a Fat Clay, which is due to the percent passing a number 200 sieve and the Atterberg Limits. Figure 3.4 shows the grains size distribution and the Casagrande chart indicating the USCS classification of Colorado is shown in Figure 3.5. In determining all of these properties, it was felt that the Specific Surface Area ( $SSA$ ) and Cation Exchange Capacity ( $CEC$ ) be included with in this study. The values of said two properties are indicated in Table 3.3.

**Table 5: Colorado soil index properties**

Particle Size Analysis		
% Gravel		0.0
% Sand		0.9
% Silt		50.5
% Clay		48.6
Atterberg Limits/ Consistency Limits		
Liquid Limit (%)		65
Plastic Limit (%)		23
Plasticity Index (%)		42
Shrinkage Limit Measured (%)		12
Other Index Properties		
Activity		0.86
Weighted Plasticity Index		41
Group Index		47.74
Cation Exchange Capacity ( <i>meq/100g</i> )		91.6
Specific Surface Area ( <i>m<sup>2</sup>/g</i> )		271.69
Calcium ( <i>ppm</i> )		91
Sodium ( <i>ppm</i> )		140
Sulfur ( <i>ppm</i> )		80
Sulfate ( <i>ppm</i> )		240
USCS Classification		CH
Free Swell Data		
# of Test	% Swell	Swell Pressure (kPa)
3	18.7%	232.2



**Figure 24: Grain size distribution of Colorado Soil**



**Figure 25: USCS classification for Colorado Soil**

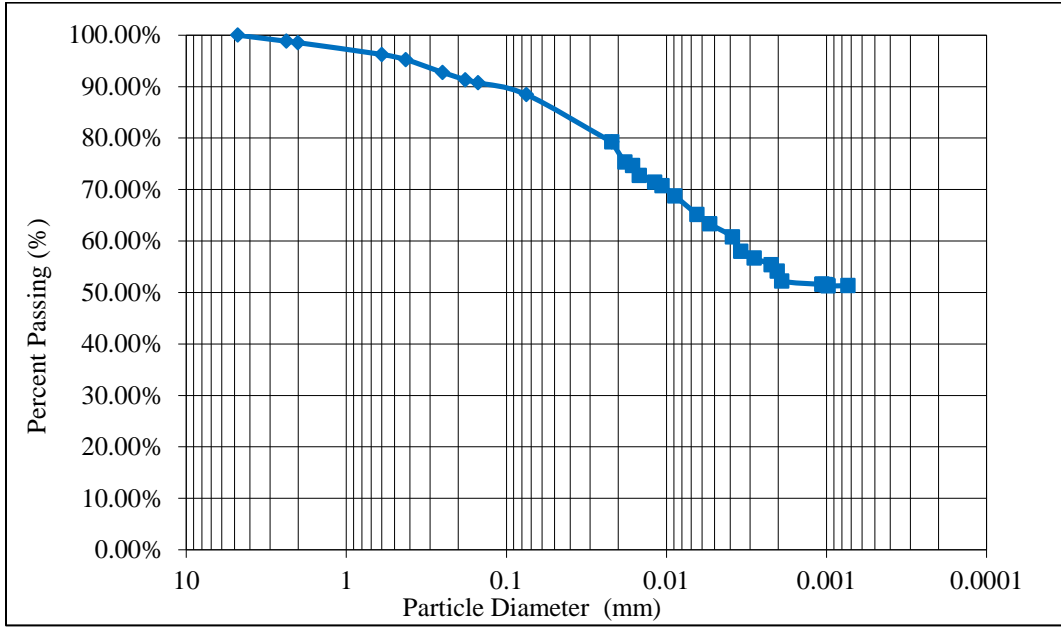


### 3.3.3 San Antonio Soil Properties

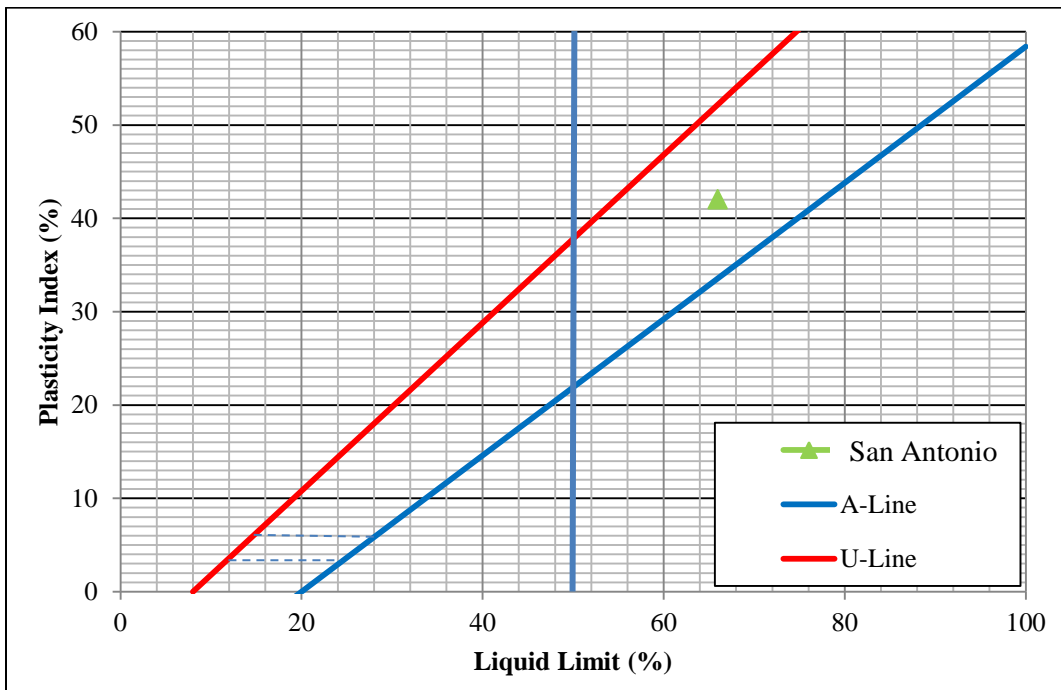
A summary of the basic index properties for the San Antonio soil can be found in Table 3.4. The index properties were also used in correlations, shown in equation 3.3, 3.4, and 3.5 above, to indicate some intrinsic properties, such as  $wPI$ , Group Index ( $GI$ ), and Activity ( $A$ ) of the San Antonio soil. The USCS classification for the soil is a Fat Clay, which is due to the percent passing number 200 sieve and the Atterberg Limits. Figure 3.6 shows the grain size distribution while the Casagrande chart indicating the USCS classification of San Antonio is shown in Figure 3.7. In addition, the Specific Surface Area (SSA) and Cation Exchange Capacity (CEC) are included in Table 3.4.

**Table 6: San Antonio index properties**

Particle Size Analysis		
% Gravel		0.0
% Sand		11.6
% Silt		34.7
% Clay		53.8
Atterberg Limits/ Consistency Limits		
Liquid Limit (%)		67
Plastic Limit (%)		24
Plasticity Index (%)		43
Shrinkage Limit Measured (%)		12
Other Index Properties		
Activity		0.80
Weighted Plasticity Index		38
Group Index		42.18
Cation Exchange Capacity ( <i>meq/100g</i> )		97.5
Specific Surface Area ( <i>m<sup>2</sup>/g</i> )		213.43
Calcium ( <i>ppm</i> )		1100
Sodium ( <i>ppm</i> )		810
Sulfur ( <i>ppm</i> )		1900
Sulfate ( <i>ppm</i> )		5700
USCS Classification		CH
Free Swell Data		
# of Test	% Swell	Swell Pressure (kPa)
2	14.1%	158.4



**Figure 26: Grain size distribution for San Antonio Soil**



**Figure 277: USCS classification for San Antonio Soil**

### **3.4 Conclusion and Summary**

This chapter showed the selection of the soils used for this study. Once the soils were selected testing the soils for their different properties was done. The data was then tabulated and presented in preceding sections. The completion of the general laboratory testing indication in Table 3.1 allows for the study to commence with X-raying of the selected soil. The X-raying of the soils will allow for qualification and quantification of the minerals in the three soils. This process and data will be presented in the next chapter.

## CHAPTER 4

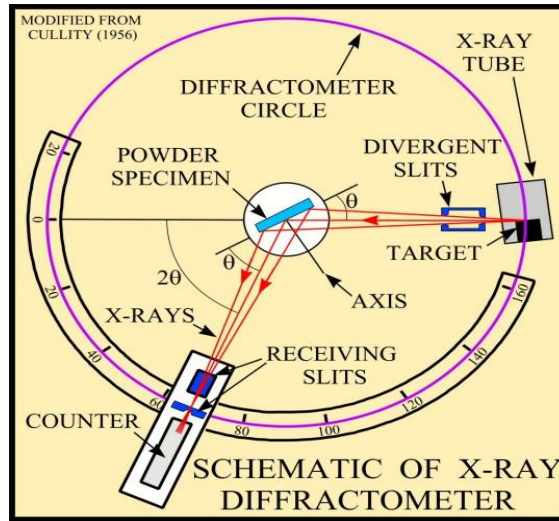
### CHARACTERIZATION OF EXPANSIVE SOILS USING X-RAY DIFFRACTION

#### 4.1 Introduction

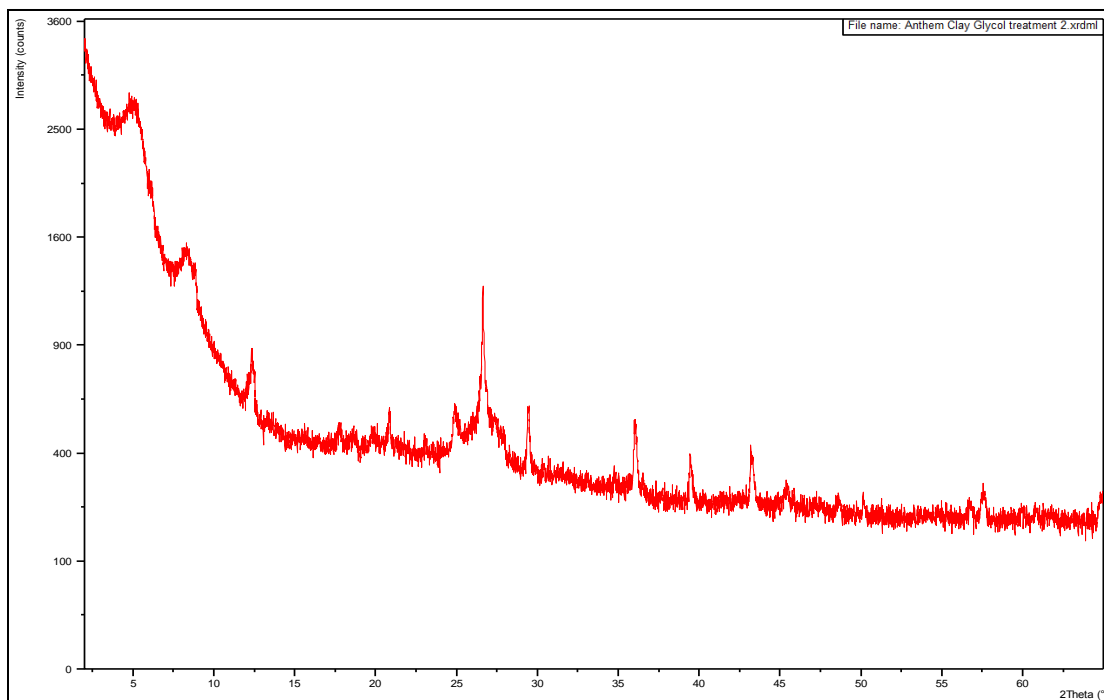
This chapter presents a brief overview of the X-ray diffraction technique. This will be helpful in understanding how the data is gathered and will help in the understanding of the data that will be explained in later sections. Also, with the understating of how X-ray diffraction is used in the detection of clay minerals, an explanation of how the specimens were prepared for quantification. After the samples are prepared, they are scanned and quantified using different tools. These different interpretation tools and the mineral quantification results are presented at the within of this chapter.

#### 4.2 Collection of data and Bragg's Law

To understand what is being gathered for analysis, some fundamental concepts need to be reviewed. It was explained in the previous chapter how the characteristics of an X-ray could penetrate into the structure of a clay mineral. What was collected from the diffracted X-rays is what was used to identify what clay minerals are present in the sample. The sample was set on the stage following the schematic shown in Figure 4.1. As the stage moves at a rate of one degree ( $\theta$ ) per minute, the collector will move at a rate that is twice what the stage moves; that is  $2(\theta)$  per minute. A program collects the intensity at which the beam is diffracted off the sample into the collector in conjunction with the position of the collector, represented by  $2(\theta)$ . As a result, the collection of data produces a diffractometer to be used for analysis, such as the one shown in Figure 4.2.



**Figure 28: Schematic of X-ray diffraction process**



**Figure 29: Typical diffractometer**

All prominent atomic planes in a crystal will produce a reflection when properly positioned with respect to the X-ray beam. Thus, each mineral will produce a characteristic set of reflections at values of theta corresponding to the interatomic

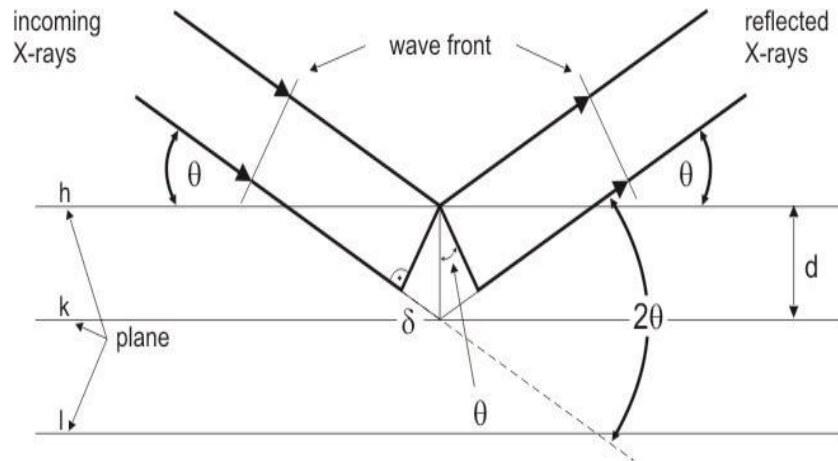
spacing's between the prominent planes (Mitchell & Soga, 2005). Peaks occur at specific two-theta angles, which can be converted to  $d$  spacing by using the Bragg's law. Bragg gave a simple geometrical interpretation of diffraction by a crystal grating. Using an analogy to specular reflection, he showed (Figure 4.3) that the conditions for “reflected” (diffracted) beam are given by the following relationship (Klug & Alexander, 1974):

$$n\lambda = 2d \sin \theta \dots\dots\dots (4.1)$$

Where:

- $n$ : is an integer that represents the “order of the reflection”,
- $\lambda$ : wavelength of the x-rays,
- $d$ : the interplanar spacing between successive atomic planes in the crystal,
- $\theta$ : the angle between the atomic plane and both the incident beam and reflected beams.

This fundamental relationship is known as the Bragg equation or Bragg's law.



**Figure 30: Analogy to specular reflection (Jürgens, 2013)**

Since no two minerals have the same spacing's of interatomic planes spacing in the three dimensions, the angles at which diffractions occur (and atomic spacing's

calculated from them) can be used for identification (Mitchell & Soga, 2005). The early work carried on by W.P. Davey, A.S., W.L. Fink, H.W. Pickett, A.J.C. Wilson and L.L. Wyman in the first half of the century started the creation of a database of two-theta values for a vast number of minerals (Smith, 2013). This population of data was very helpful for the identification of the minerals present in the specimen's samples in this study, but it does not allow for a straight quantification of the amount of minerals in multi-phase materials. Using this large database the identification of multiple minerals within soil samples can be found. This technology was used in this study. The next sections will explain how this technology was used and what information needs to be gathered.

#### **4.3 Procedure Followed to Obtain Mineral Information**

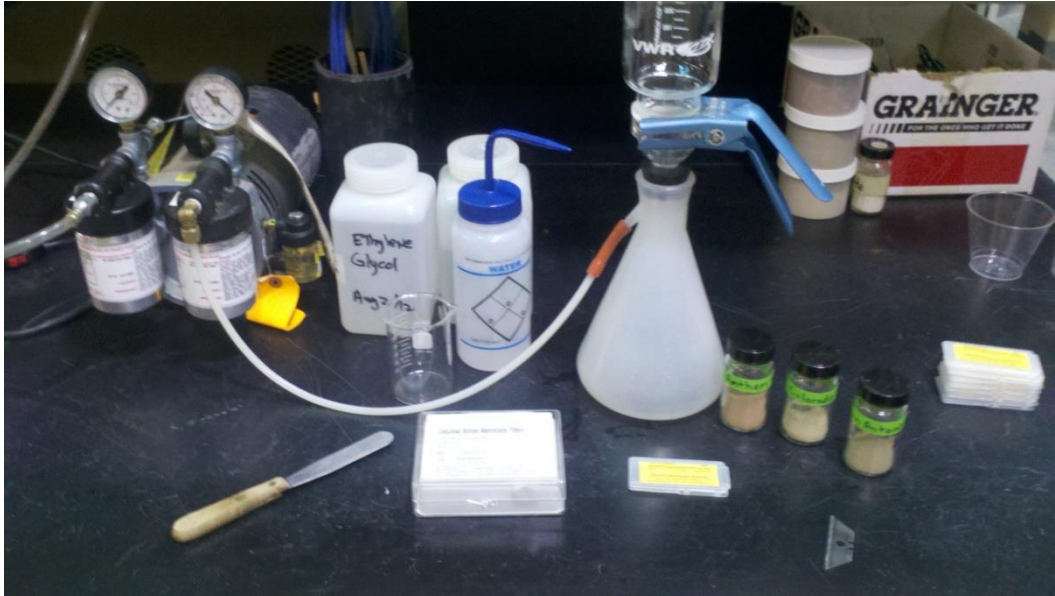
To gather the diffractometers needed for the analysis of the soils that were chosen, we looked outside of our department for interdisciplinary help. We gratefully acknowledge the use of the facilities within the LeRoy Eyring Center for Solid State Science at Arizona State University. The device used for the largest portion of the study was a PANalytical Xpert Pro MRD, while a Siemens D5000 was used for the RockJock portion of the data sampling. The PANalytical Xpert Pro MRD (PANalytical) was used to scan the untreated soils as well as the specimens subjected to Glycol, heat, and water treatments. Heat treatment is used to distinguish between Kaolinite and Chlorite (Carlton, 1978). These samples will have a preferred orientation to them, beside the water treatment, due to the process of how they are made. A preferred orientation is when all of the particles are laying down flat, like pieces of paper on top of each other. Also, specimens of a clay+silt fraction (passing a #200 sieve) and clay fractions are also to be



tested. How these specimens are prepared and tested is explained in the subsequent section in this chapter.

The first set of specimens was prepared with material passing the #200 US sieve. All three soils were prepared by following the procedure explained by the United States Geological Survey (USGS) manual (Poppe, 2002) for preparation of samples to be examined by X-Ray diffraction. Centrifuging the sample was not done due to the fact that we wanted to examine what was passing a #200 sieve. The three soil samples, 5g each, were inundated in de-ionized water with sodium hexametaphosphate (per ASTM D422) in a centrifuge tube to create a slurred mix. The slurry was mix very well by capping the centrifuge tube and shaking. The samples were placed in a Millipore filtration apparatus with a 45 $\mu$ m Whatman filter paper with a size according to the Millipore filtration apparatus. Once the sample was filtered onto the Whatman filter paper; both the filter paper and the sample still intact were placed on a beaker. A quartz slide was then used to “roll” the sample form the filter paper to the quartz slide.

These steps can be seen in Figures 4.4 to 4.9 below. Figure 4.4 presents the tools needed to prepare the preferred orientation specimens which included 45 $\mu$ m Whatman filter paper, Millipore filter, de-ionized water, soil, beaker and a vacuum pump. Figure 4.5 shows soil in a slurred mix. Figure 4.6 illiterates a sample being filtered through a Millipore filter. Figure 4.7 shows the sample in a preferred orientation on a Whatman filter paper. Figure 4.8 shows how the filter paper was placed on the beaker. Figure 4.9 demonstrates how the sample was “rolled” on to the quartz slide. After the samples were air-dried for 24 hours, they were taken to the PANalytical Xpert Pro MRD for scanning.



**Figure 31: Tools needed for preferred orientation samples**



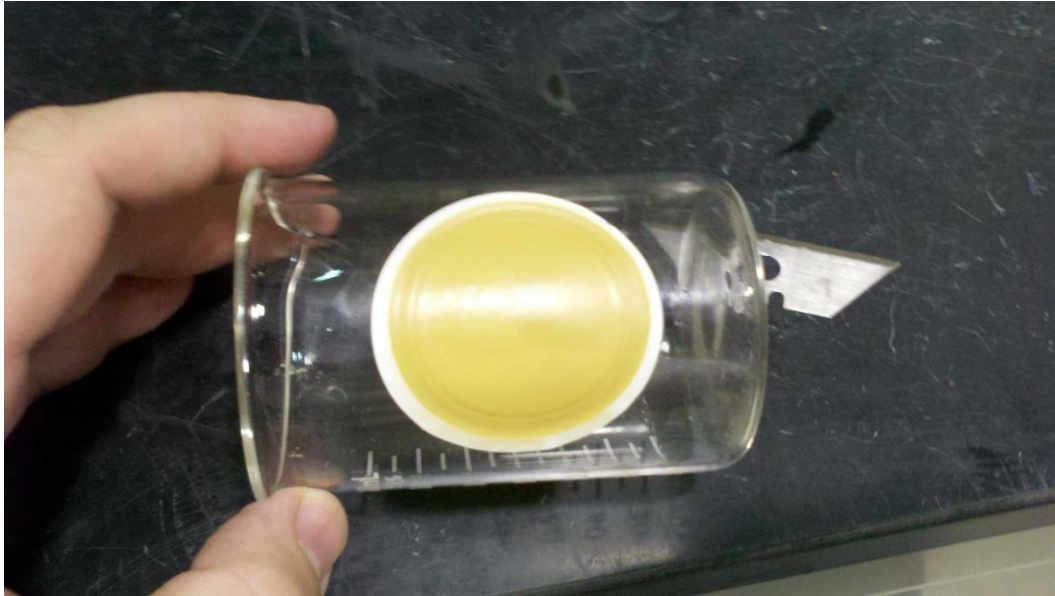
**Figure 32: Slurry of soil and sodium hexametaphosphate solution**



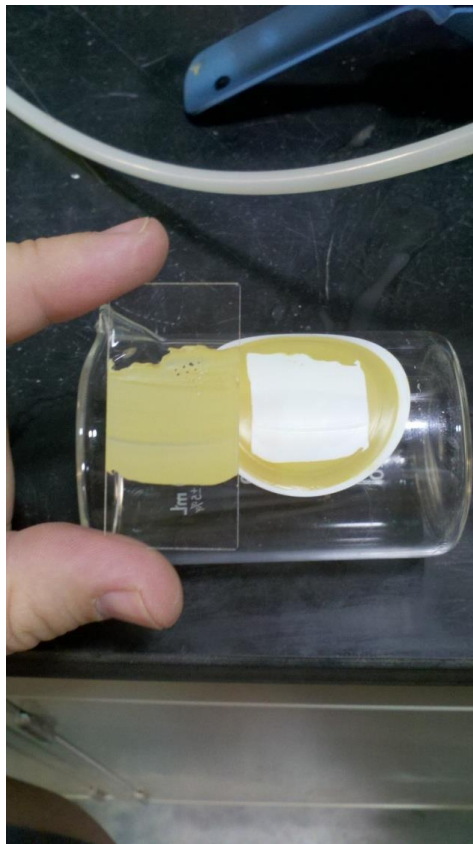
**Figure 33: Sample being filtered on a Millipore filter**



**Figure 34: Sample after filtration**



**Figure 35: Filter paper placed on glass beaker**



**Figure 36: Sample "rolled" on to quartz slide**

After the samples air-dried for 24 hours, the specimens were subjected to different treatment process: glycol treatment, a 400°C heat treatment and a 550°C heat treatment. These treatments are recommended to create different interparticle spacing in the clay particles (Poppe, 2002). A “no treatment” or untreated specimens were also tested. Once the sample dried on the quartz slide, it was ready to be scanned. Once the specimen was scanned untreated it was placed into a desiccator with a pint of Ethylene Glycol in the base, as shown in Figure 4.10. Since Ethylene Glycol has a greater polarity than water, clay particles were expected to exhibit greater separation once Glycol adsorption was achieved. The advantages of using ethylene glycol complexes, as compared with water complexes are: (1) increased intensities of second and higher order reflections; and (2) development, under room conditions, of relatively stable, two-layer complexes by all varieties of dioctahedral smectite if ethylene Glycol is used (Srodon, 1980). With the samples in place, the desiccator was placed in an oven for 16-18 hour at 60°C. This allowed adsorption by vapor within the sample. With the adsorption complete the sample was ready to be scanned.



**Figure 37: Sample in adsorption treatment of Ethylene Glycol**



Once the scan was completed the heat treatments were applied. A muffle furnace, as that shown in Figure 4.11, was used to achieve the needed temperatures to dry out the samples. During each temperature treatment, 400°C and 550°C, the specimens were heated for 24 hours, scanned, and placed back in the furnace for the next treatment. After that, the specimen was scanned again. Examples of these records will be shown in subsequent section, where the main features will be presented.



**Figure 38: Muffle furnace used for heat treatments**

Along with the three treatments mentioned above a fourth was also done with water. The treatment was called the wet treatment and it was performed as follows. First, a scan of the material passing a # 200 sieve was done. With the dry sample scanned, de-ionized water was added to the soil to reach +2% of the soil's liquid limit. The sample was mix very well and allowed to sit for approximately ten minutes to equilibrate. The wet sample was then applied again to a slide to be X-rayed. The specimen prepared as explained will be called "wet short-term" herein. The remaining soil mixed with water was placed into a Ziploc bag and sealed without air. That bag was placed into another Ziploc bag to insure no evaporation. After one year, the Ziploc bag was opened and a

small portion of the soil was placed on a zero background disk and scanned. This specimen is called “wet long-term” in subsequent sections.

Analysis of the prepared sample was done using a PANalytical X’Pert Pro MRD powder diffractometer with X’Celerator detector. Each individual diffractometer was then analyzed using the “Reference Pattern” function in the software. This is the step when the user can narrow down the search to the number of minerals that are of interest. The “Mineral” sub tab was selected to use the software’s database, for ICDD cards, to isolate reference peaks within the signal. Also, there was an option available to optimize the search by using the “Periodic Table” option. Using the empirical formulas in Table 4.1, shown later, those elements were used to narrow down the mineral search. Once the optimization was completed, the analysis of the scans was finalized. From the 500 minerals that were found, the minerals presented in Table 4.1 were isolated and selected to be quantified. Once the selected minerals were in “Phase”, each mineral crystalline structure was entered to the system. The minerals’ crystalline structure was referenced from the American Mineralogist Crystal Structure Database (Downs & Hall-Wallace, 2013). With the crystalline structure in place, the Rietveld Analysis was ready to commence. The crystalline phases of minerals present in the samples were identified using X’Pert HighScore plus software. The relative phase amounts (weight %) was estimated using the Rietveld analysis. A Rietveld Analysis compares the measured profile and calculated profiles. The variation of many parameters the difference between the two profiles is minimized. This analysis has the highest priority of quantification in this software. The quantification gives a percentage by crystalline weight of the mineral in phase and the mineral quantification and qualification is presented in the next section.

Samples were scanned at Cu K-alpha 1 radiation of  $1.54 \text{ \AA}$  using a Tension of 45 kV and a Current of 40 mA. The divergent slits for testing were  $1/4^\circ$  and  $1/8^\circ$  with a mask of 10 mm. There were no receiving slits used on the collector. The two-theta range of scanning was from  $2^\circ$  to  $65^\circ$ . The step size of the scan was set at  $0.0125^\circ$  with a scan time per step of 0.5085 sec., resulting in a scan speed of  $0.035305^\circ/\text{sec}$ .

As shown later, the diffractometers obtained for the soils passing the #200 sieve registered a lot of noise which “masked” some of the minerals of interest. Therefore, the complete procedure explained by the USGS manual (Poppe, 2002) was followed. This required the samples to follow the same procedure as explained earlier, but a centrifuge was used to separate the silt fraction from the clay fraction. This device is shown in Figure 4.12. The clay fraction solution was then removed from the overall sample solution before running the sample through the Millipore filter (Figure 4.13). The same scanning procedure described for the clay+silt samples was used to process the clay fraction. The mineral quantification and qualification is presented in the next chapter.



**Figure 39: Centrifuge used for particle separation**





**Figure 40: Separation of clay fraction from silt fraction**

In combination with the PANalytical Xpert Pro MRD analysis, a separate analysis using RockJock software was pursued in order to take another approach to the quantification of clay minerals and verify the two protocols. Due to the inconsistency in the quantification results when comparing both methods, this study relied heavily on the mineral quantification obtained with the PANalytical interpretation method. This could be due to the RockJock method of analysis not using the complete signal,  $20^{\circ} - 65^{\circ} 2\theta$ , thus missing the primary peaks of Illite and Montmorillonite. The RockJock procedure and mineral quantification based on this method can be found in Appendix A. The mineral quantification and qualification using the PANalytical method will be presented in the next section.

#### **4.4 Minerals Selected for Analysis**

Due to the abundant amount of data available for interpretation, the study focused on the amount and type of minerals that are known to exhibit swelling behavior. Table

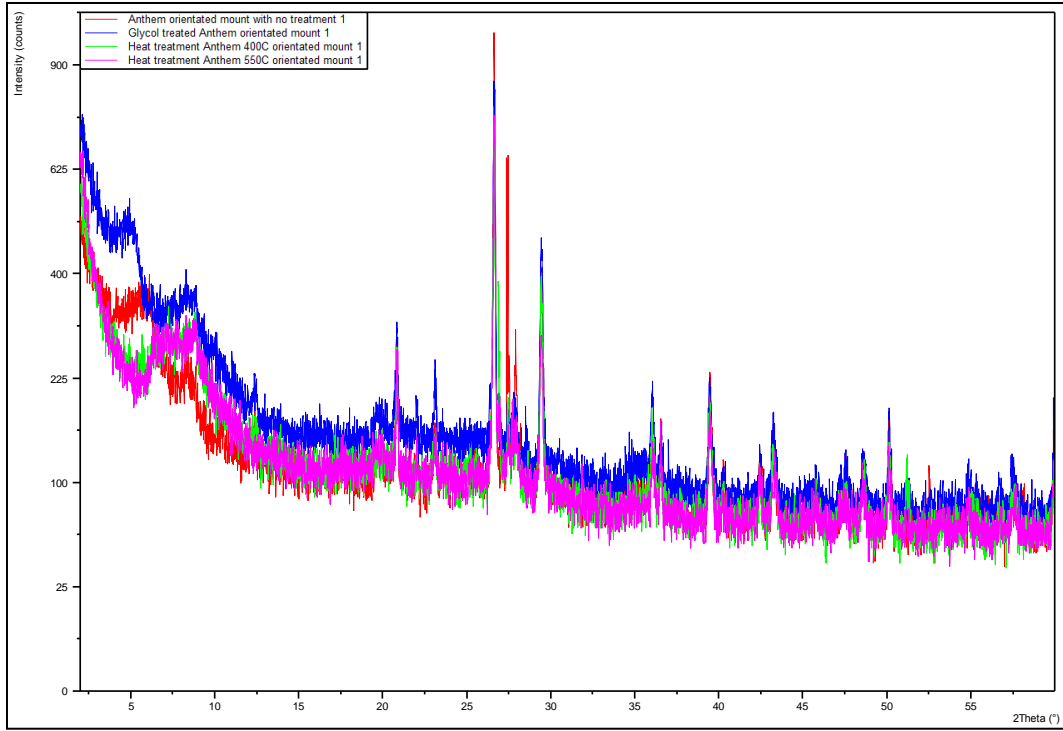
4.1 illustrates the minerals selected for analysis with the PANalytical method explained in the previous section.

**Table 7: Minerals selected for analysis**

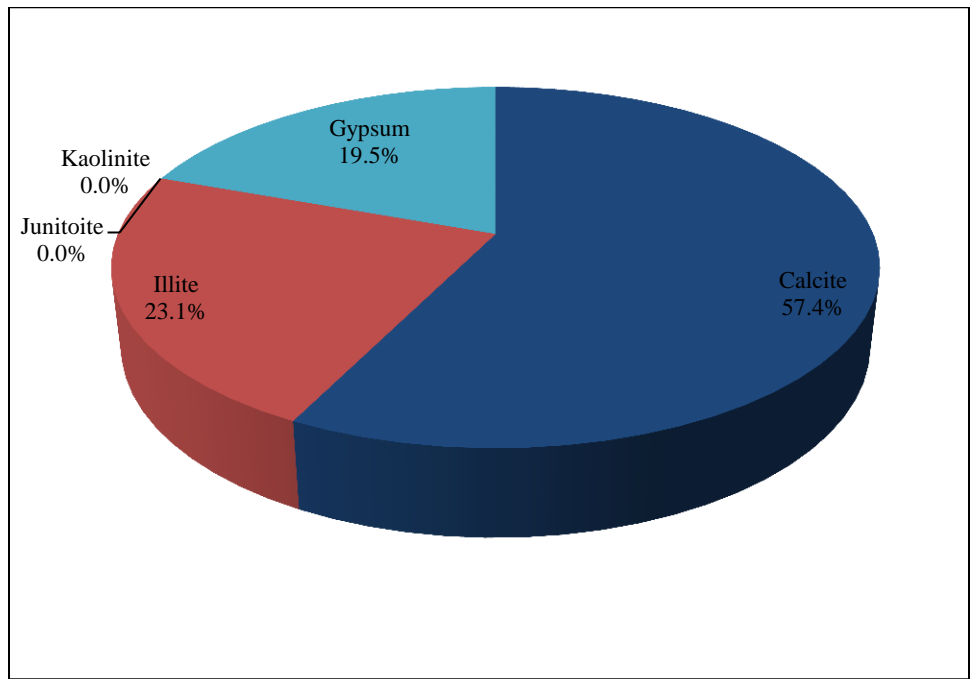
	Clay Minerals Investigated	Empirical Formula
Smectite	Beidellite	$\text{Na}_{0.5}\text{Al}_{2.5}\text{Si}_{3.5}\text{O}_{10}(\text{OH})_2 \cdot (\text{H}_2\text{O})$
	Hectorite	$\text{Na}_{0.4}\text{Mg}_{2.7}\text{Li}_{0.3}\text{Si}_4\text{O}_{10}(\text{OH})_2$
	Montmorillonite	$\text{Na}_{0.2}\text{Ca}_{0.1}\text{Al}_2\text{Si}_4\text{O}_{10}(\text{OH})_2(\text{H}_2\text{O})_{10}$
	Nontronite	$\text{Na}_{0.3}\text{Fe}^{3+}_2\text{Si}_3\text{AlO}_{10}(\text{OH})_2 \cdot 4(\text{H}_2\text{O})$
	Saponite	$\text{Ca}_{0.1}\text{Na}_{0.1}\text{Mg}_{2.25}\text{Fe}^{2+}_{0.75}\text{Si}_3\text{AlO}_{10}(\text{OH})_2 \cdot 4(\text{H}_2\text{O})$
	Sauconite	$\text{Na}_{0.3}\text{Zn}_3\text{Si}_3\text{AlO}_{10}(\text{OH})_2 \cdot 4(\text{H}_2\text{O})$
	Ettringite	$\text{Ca}_6\text{Al}_2(\text{SO}_4)_3(\text{OH})_{12} \cdot 26(\text{H}_2\text{O})$
	Thaumasite	$\text{Ca}_3\text{Si}(\text{CO}_3)(\text{SO}_4)(\text{OH})_6 \cdot 12(\text{H}_2\text{O})$
	Kaolinite	$\text{Al}_2\text{Si}_2\text{O}_5(\text{OH})_4$
Others	Illite	$\text{K}_{0.6}(\text{H}_3\text{O})_{0.4}\text{Al}_{1.3}\text{Mg}_{0.3}\text{Fe}^{2+}_{0.1}\text{Si}_{3.5}\text{O}_{10}(\text{OH})_2 \cdot (\text{HO})$
	Hydrated Halloysite	$\text{Al}_2\text{Si}_2\text{O}_5(\text{OH})_4 \cdot 2(\text{H}_2\text{O})$
	Calcite	$(\text{CO}_3)$

#### 4.4.1 Qualification and Quantification of Anthem Soils

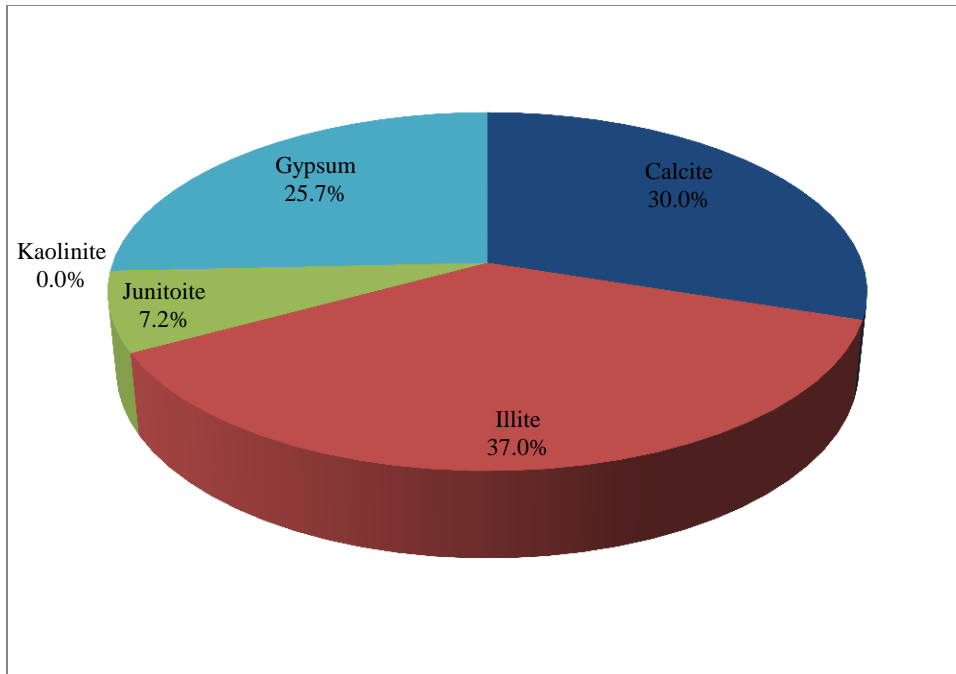
Once the scanning of all treated Anthem specimens was completed the data was analyzed using the software provided by HighScore Plus. Figure 4.14 presents the scan results for Anthem clay+silt fraction after all of the treatments were applied. Here you are able to see the “noise” mentioned in the previous section due to the scans being sloppy and undefined. The red line represents the untreated sample, the blue line is the glycol sample, the green line is the sample subjected to 400°C sample, and the purple line represents the results of the sample subjected to 550°C sample. The Anthem’s clay+silt quantifications for each treatment can be seen in Figures 4.15 to 4.20.



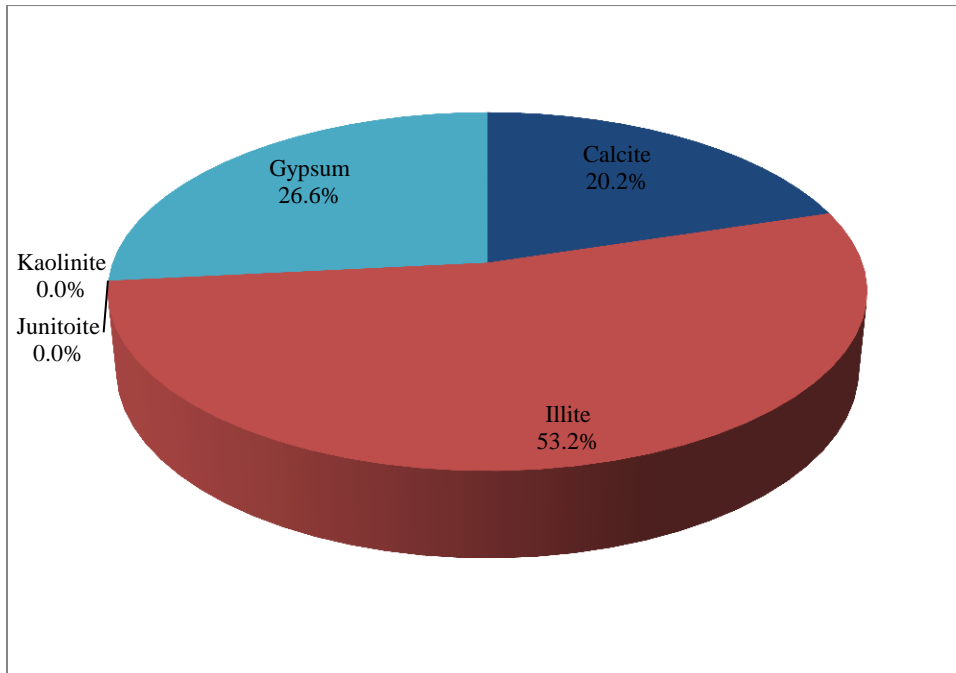
**Figure 41: Treatment scans for the Anthem’s Clay+Silt fraction**



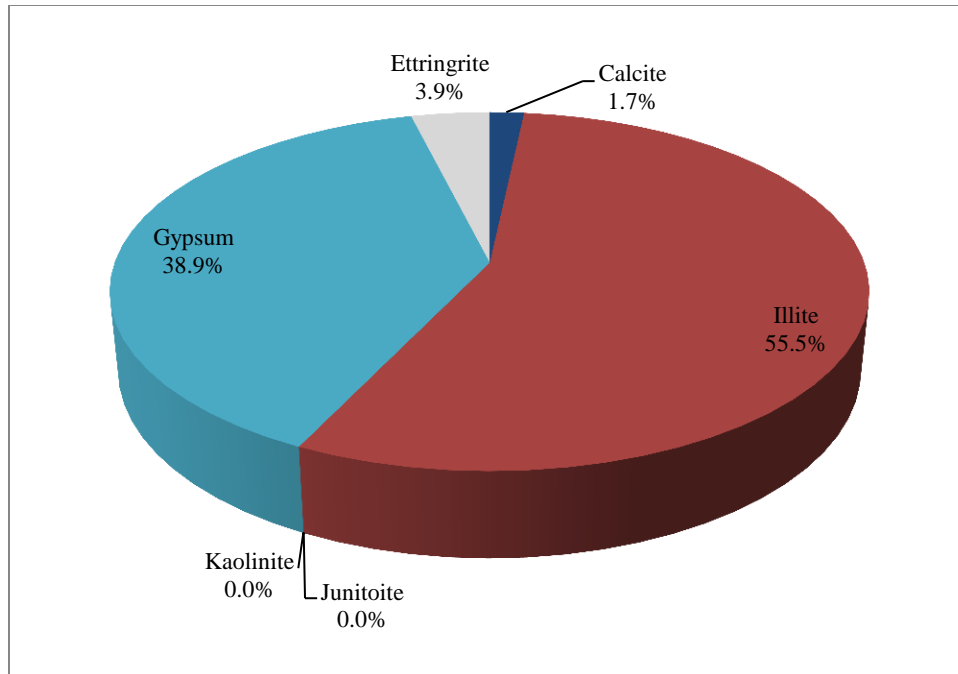
**Figure 42: Mineral quantification of Clay+Silt fraction of Anthem soil for untreated specimen**



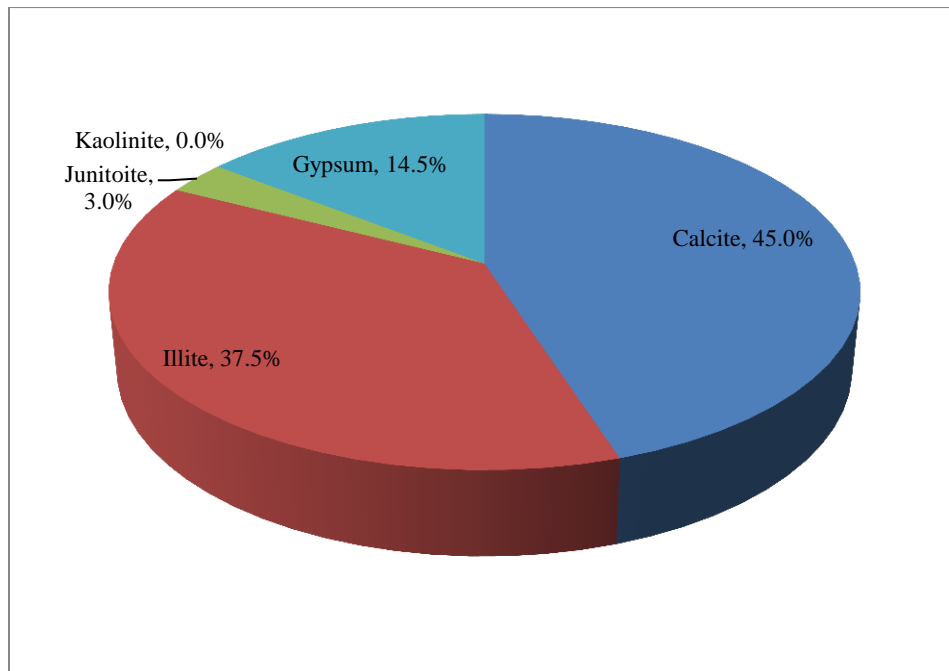
**Figure 43: Mineral quantification of Clay+Silt fraction of Anthem soil for Glycol treated specimen**



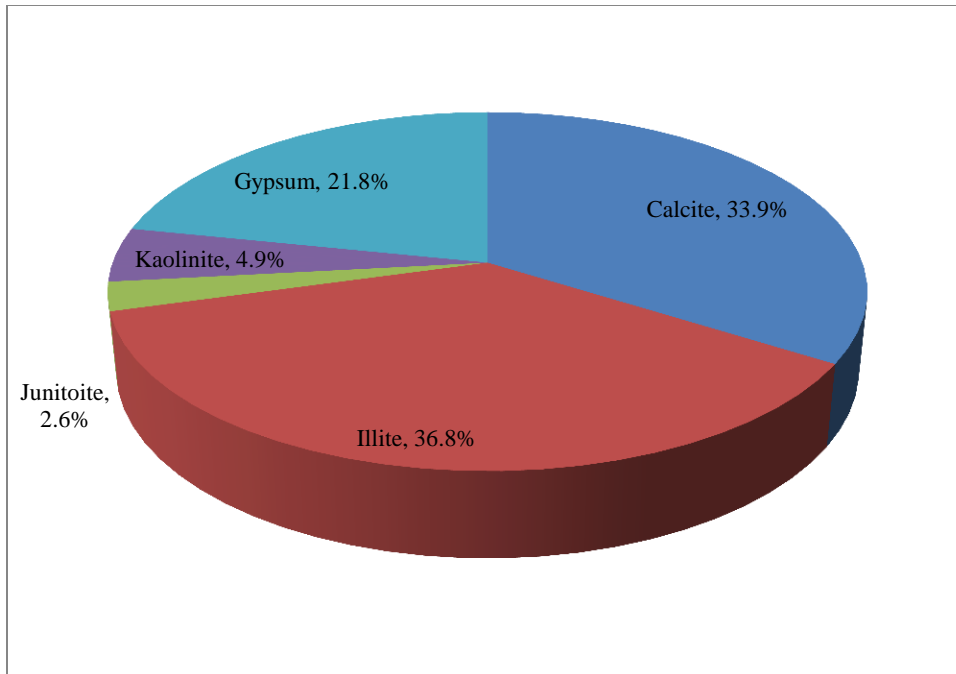
**Figure 44: Mineral quantification of Clay+Silt fraction of Anthem soil for 400°C treated specimen**



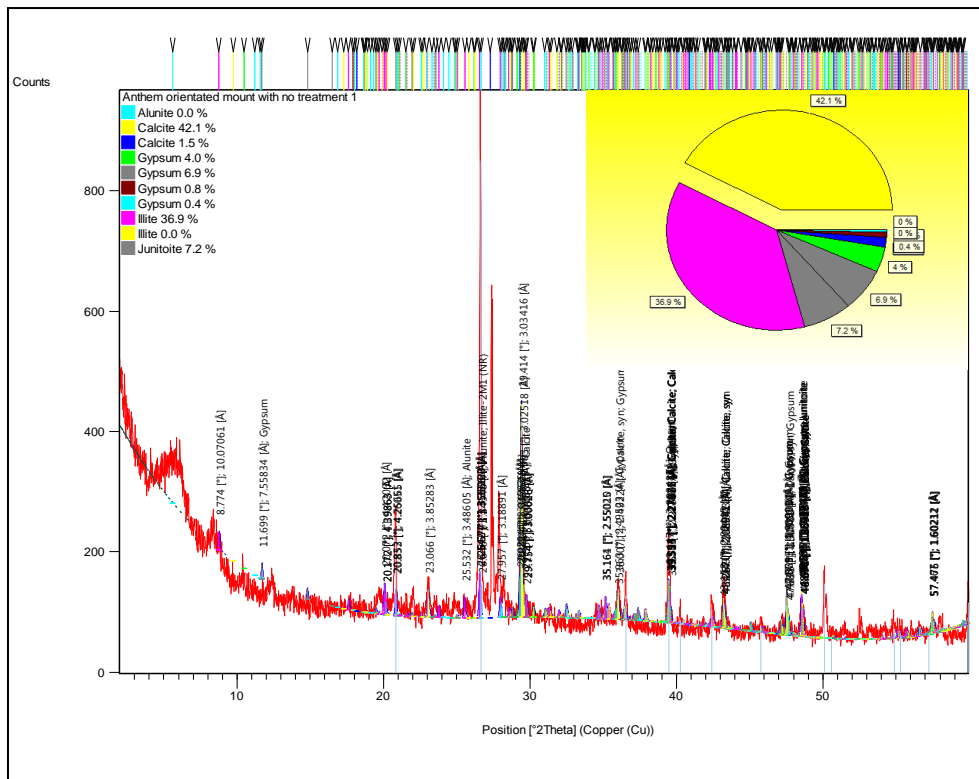
**Figure 45: Mineral quantification of Clay+Silt fraction of Anthem soil for 550°C treated specimen**



**Figure 46: Mineral quantification of Clay+Silt fraction of Anthem soil for wetted short term specimen**



**Figure 47: Mineral quantification of Clay+Silt fraction of Anthem soil for wetted long term specimen**



**Figure 48: Completed signal quantification with labeled peaks**

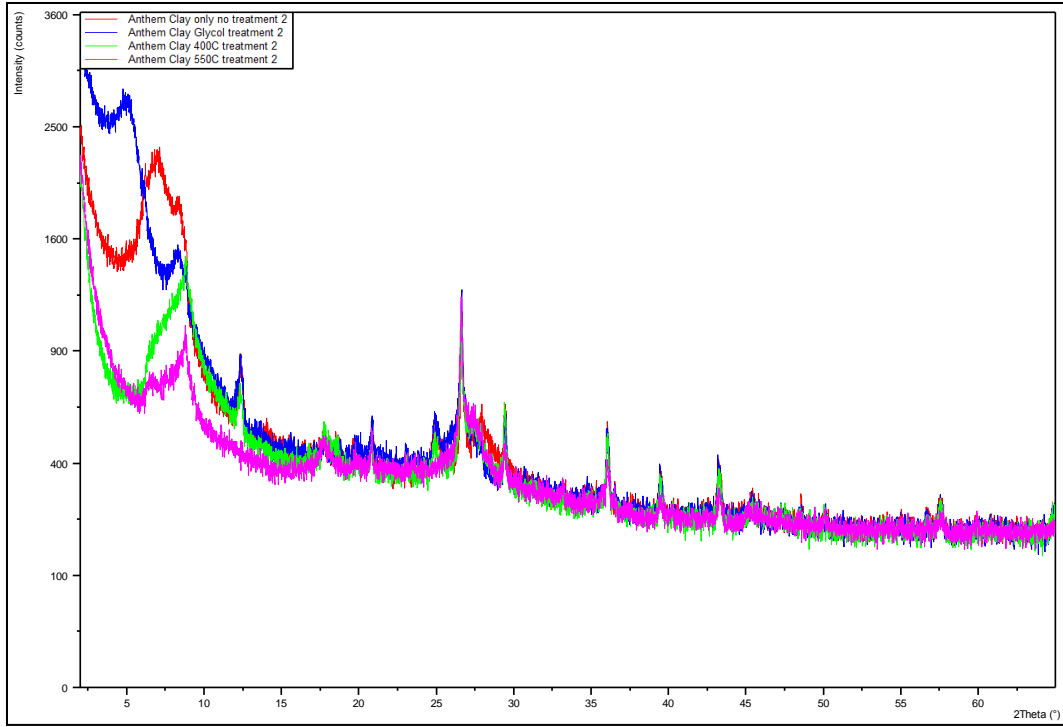
After the mineral quantification was completed, the software allowed labeling the peaks found, as shown in Figure 4.21. With the vast amount of minerals beneath one peak, selecting the top thirty minerals was a difficult task. The quantification for all the treatment for Anthems Clay+Silt fraction can be seen in Table 4.2.

**Table 8: Summary of Anthem Clay+Silt fraction mineral quantification**

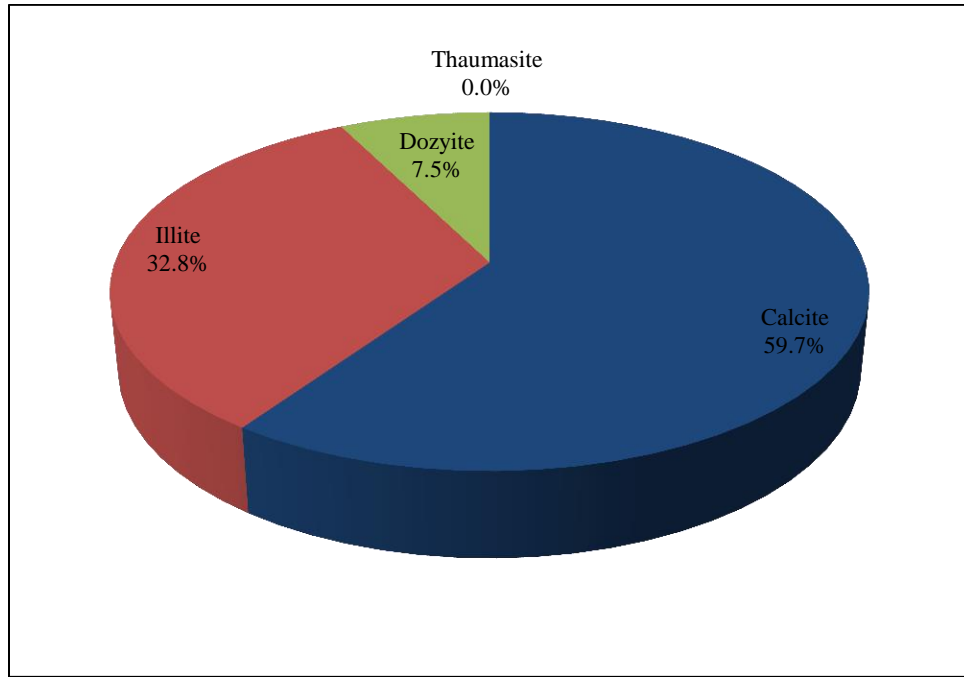
Anthem Clay+Silt Fraction	No (%)	Glycol (%)	400 °C (%)	550 °C (%)	Wet ST (%)	Wet LT (%)
Calcite	57.4	30.0	20.2	1.7	45.0	33.9
Illite	23.1	37.0	53.2	55.5	37.5	36.8
Junitoite	0	7.2	0	0	3.0	2.6
Kaolinite	0	0	0	0	0	4.9
Gypsum	19.5	25.7	26.6	38.9	14.5	21.8
Ettringite	-	-	-	3.9	-	-

Note: % by crystalline weight

The same analysis procedure shown for the Clay+Silt fractions was completed for the clay fraction of Anthem. Figure 4.22 presents the treatment scans for the Anthem's clay fraction soil sample. The red line represents the untreated sample, the blue line is the glycol sample, the green line is the sample subjected to 400°C sample, and the purple line represents the results of the sample subjected to 550°C sample. The mineral quantification for Anthem's clay fraction can be seen in Figures 4.23 to 4.26 for each treatment.

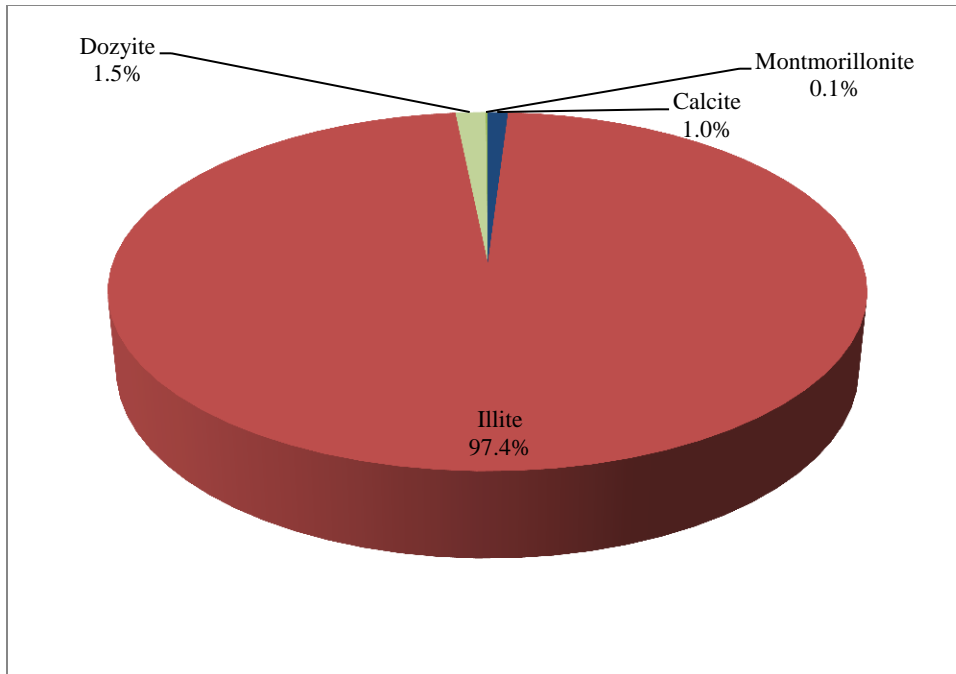


**Figure 49: Treatment scans for the Anthem’s clay fraction**

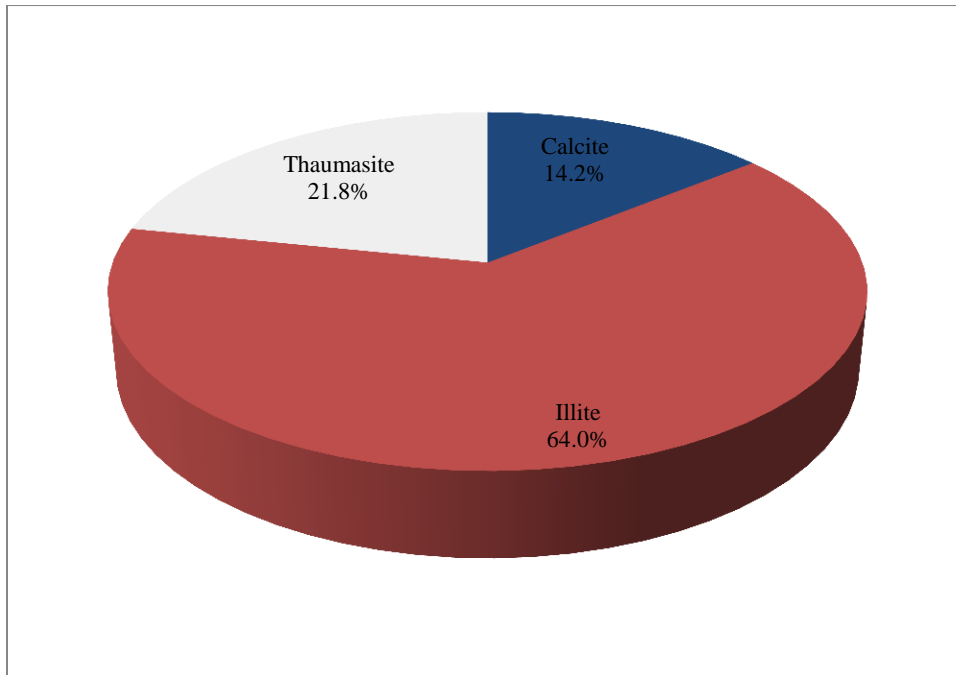


**Figure 50: Mineral quantification of Clay fraction of Anthem soil for untreated specimen**

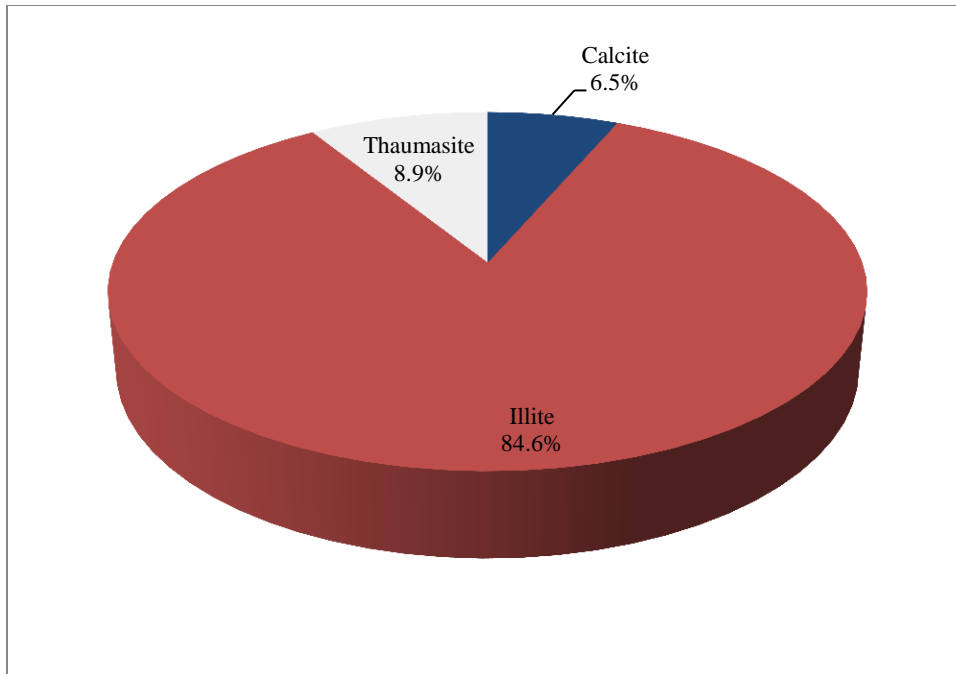




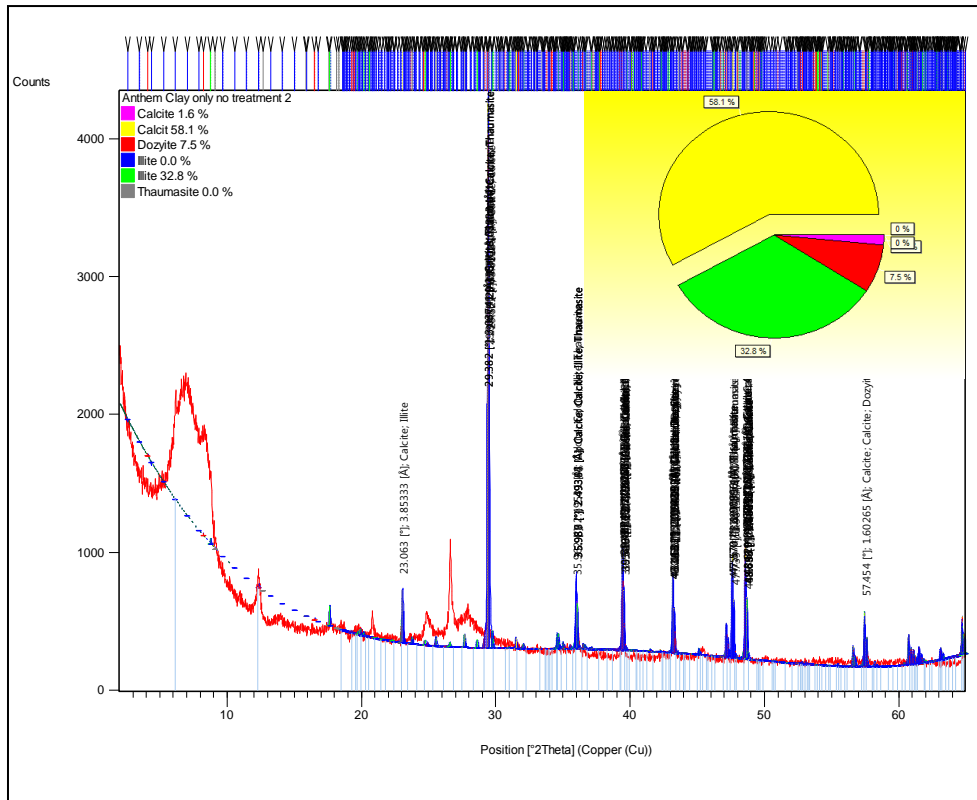
**Figure 51: Mineral quantification of Clay fraction of Anthem soil for Glycol treated specimen**



**Figure 52: Mineral quantification of Clay fraction of Anthem soil for 400°C treated specimen**



**Figure 53: Mineral quantification of Clay fraction of Anthem soil for 550°C treated specimen**



**Figure 54: Completed signal quantification with labeled peaks**

After the mineral quantification was completed, the software allowed labeling the peaks found, as shown in Figure 4.27. The mineral quantification for all the treated specimens for Anthem’s Clay fraction can be seen in Table 4.3.

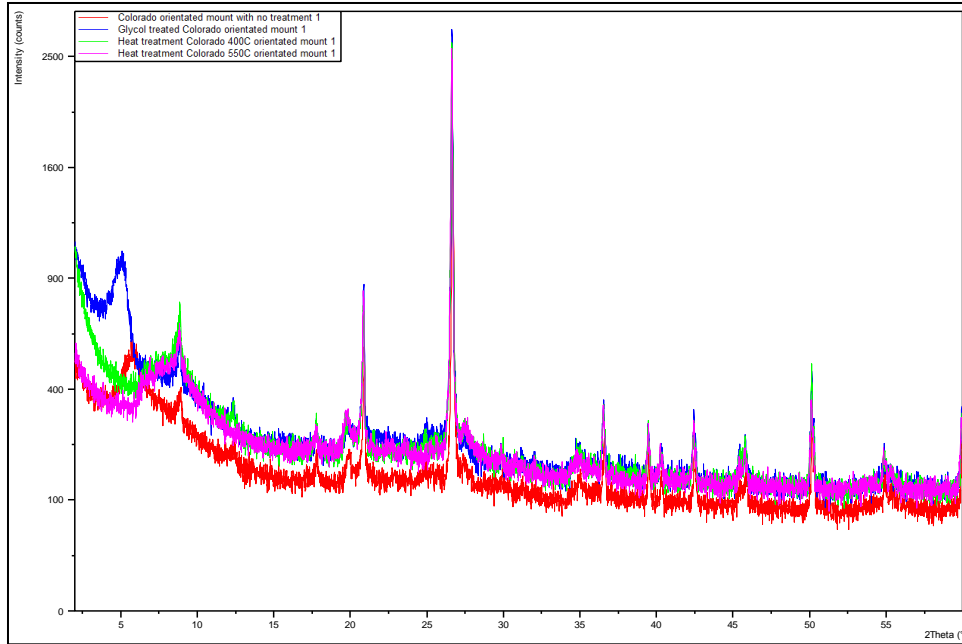
**Table 9: Summary of Anthem Clay fraction quantification**

Anthem Clay Fraction	No Treatment (%)	Glycol Treatment (%)	400 °C Treatment (%)	550 °C Treatment (%)
Calcite	59.7	1.0	14.2	6.5
Dozyite	7.5	1.5	-	-
Illite	32.8	97.4	64.0	84.6
Montmorillonite	-	0.1	-	-
Thaumasite	0	-	21.8	8.9

Note: % by crystalline weight

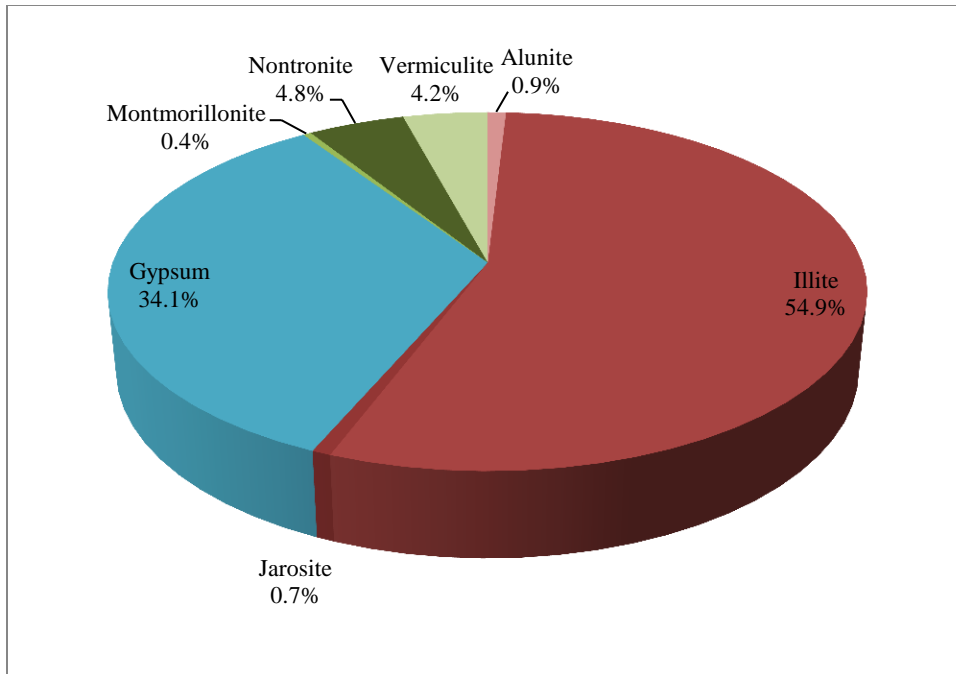
#### 4.4.2 Qualification and Quantification of Colorado Soil

When the scanning of all treated Colorado soil specimen was completed the data was analyzed using the software provided by PANalytical, HighScore Plus. Figure 4.28 present the treatment scans for the Colorado’s clay+silt fraction soil sample. The red line represents the untreated sample, the blue line is the glycol sample, the green line is the sample subjected to 400°C sample, and the purple line represents the results of the sample subjected to 550°C sample.

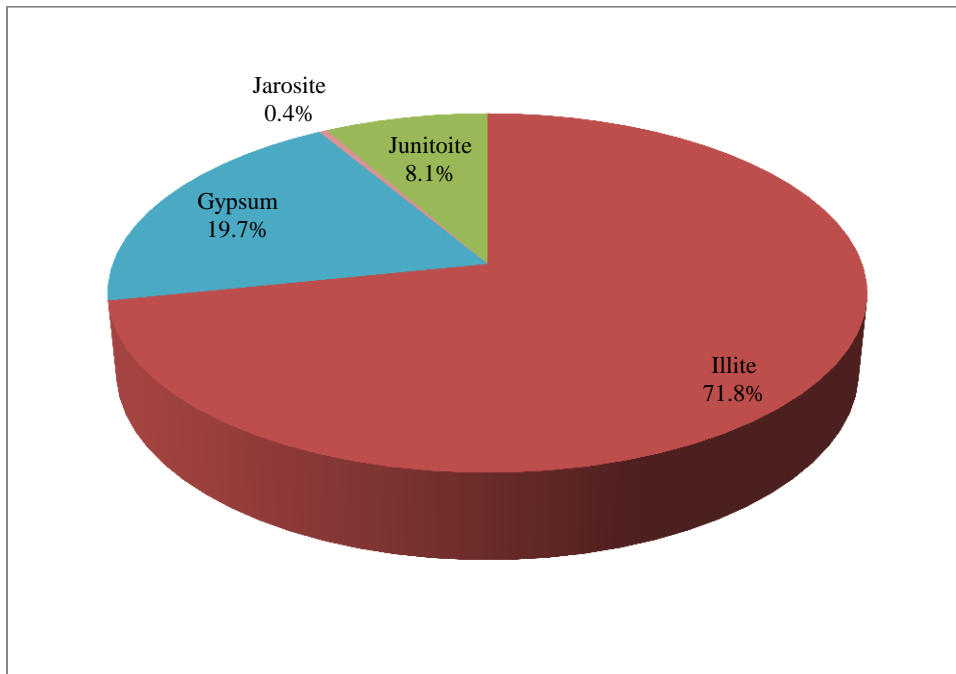


**Figure 55: Treatment scans for the Colorado’s clay+silt fraction**

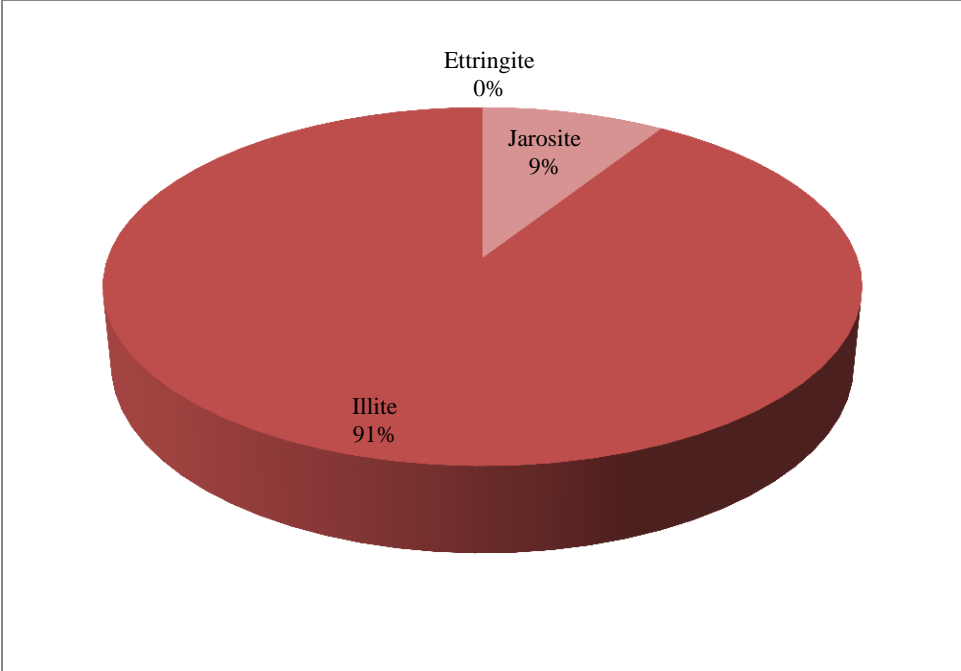
The same analysis procedure described for Anthem was completed on the clay+silt fraction of Colorado soil. Colorado’s clay+silt fraction mineral quantifications for each treatment can be seen in Figures 4.29 to 4.34 below.



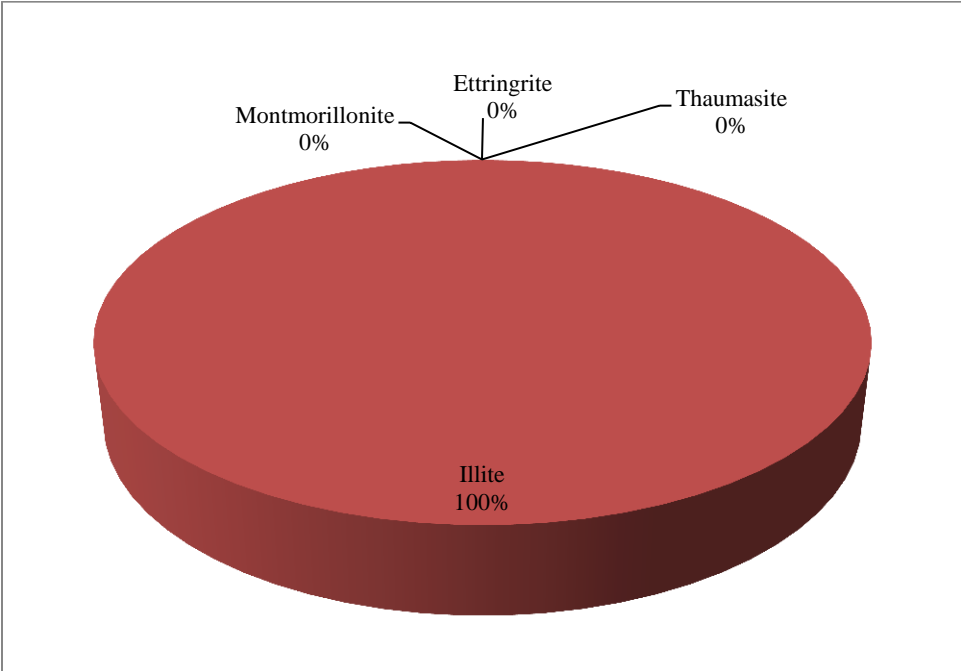
**Figure 56: Mineral quantification of Clay+Silt fraction of Colorado soil for untreated specimen**



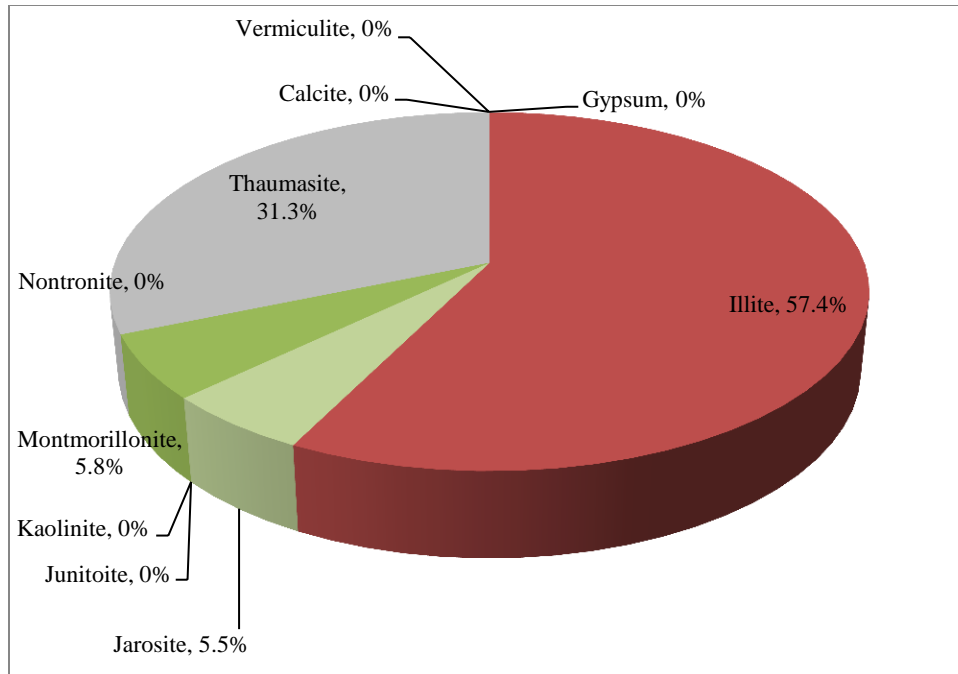
**Figure 57: Mineral quantification of Clay+Silt fraction of Colorado soil for Glycol treated specimen**



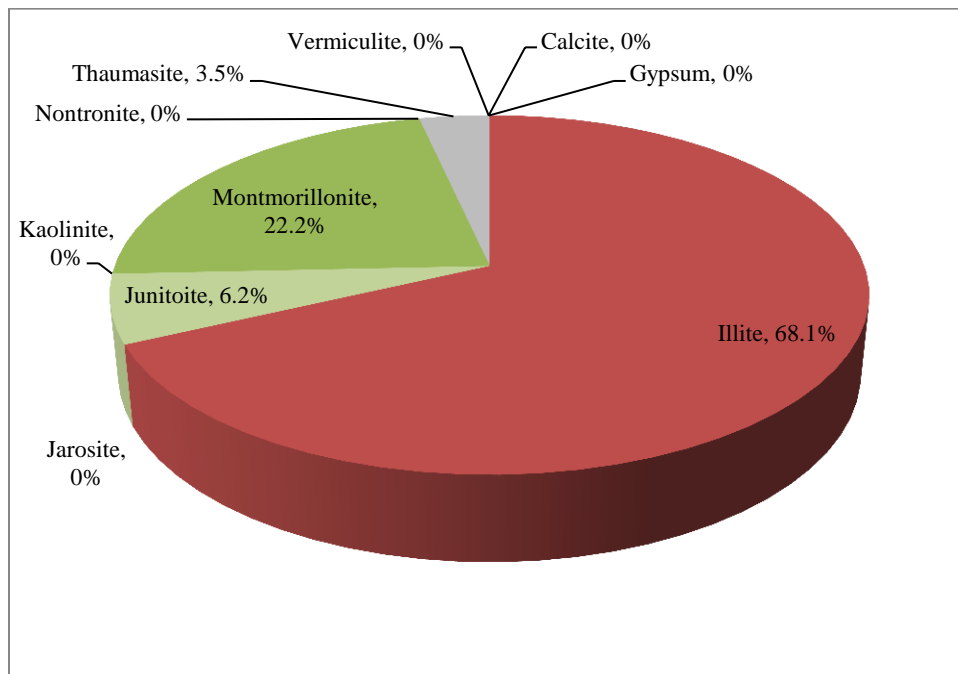
**Figure 58: Mineral quantification of Clay+Silt fraction of Colorado soil for 400°C treated specimen**



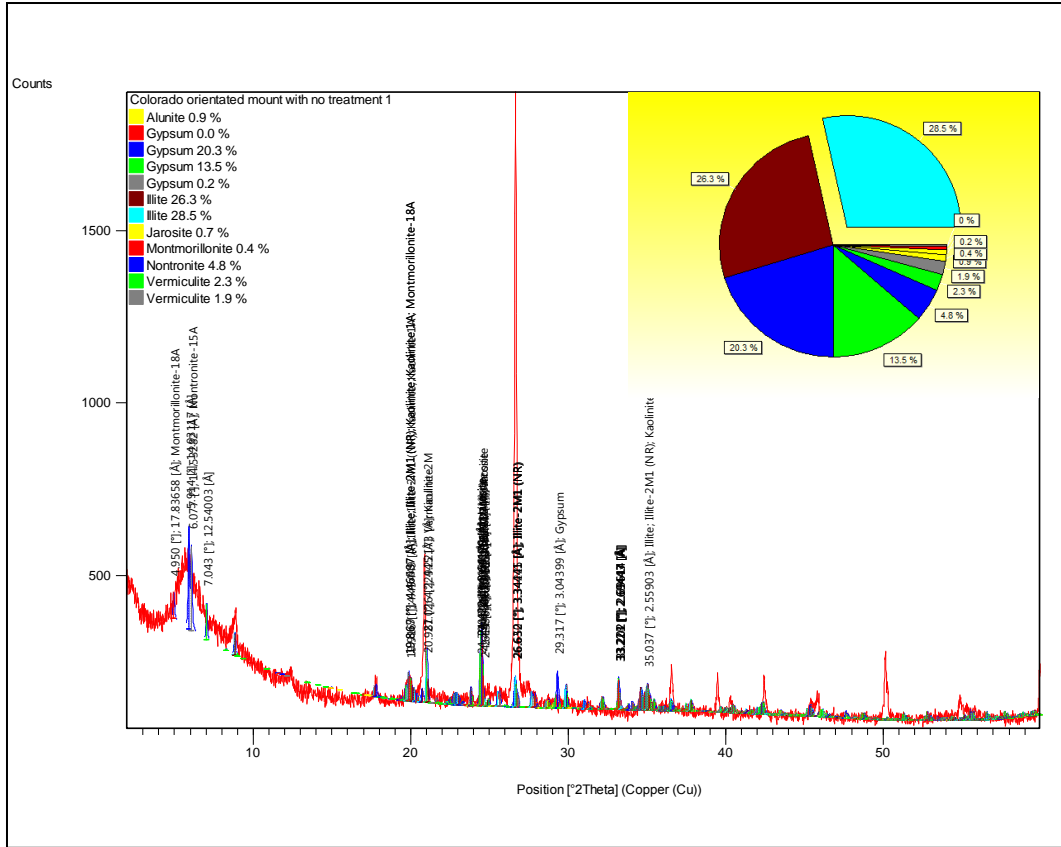
**Figure 59: Mineral quantification of Clay+Silt fraction of Colorado soil for 550°C treated specimen**



**Figure 60: Mineral quantification of Clay+Silt fraction of Colorado soil for wetted short term specimen**



**Figure 61: Mineral quantification of Clay+Silt fraction of Colorado soil for wetted long term specimen**



**Figure 62: Completed signal quantification with labeled peaks**

Once the quantification was complete, the peaks were labeled in Figure 4.35.

With the numerous amounts of minerals beneath one peak, the labels overlapped and the chart becomes difficult to read. The mineral quantification for all the treated specimens for Colorado’s Clay+Silt fraction can be seen in Table 4.4.

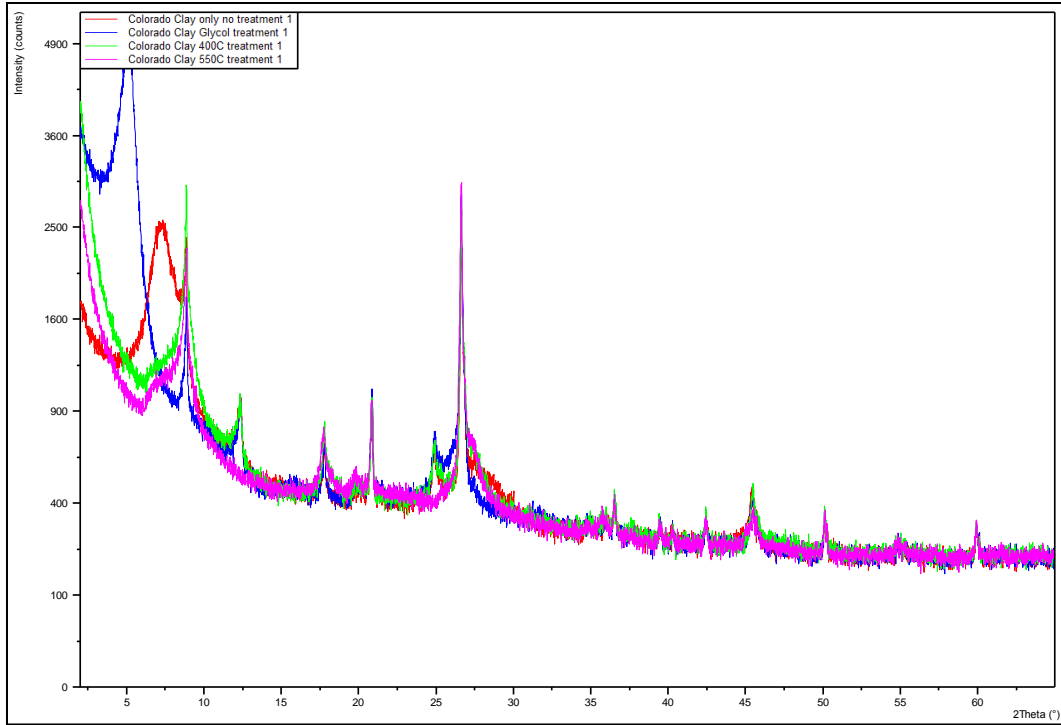


**Table 10: Summary of Colorado Clay+Silt fraction mineral quantification**

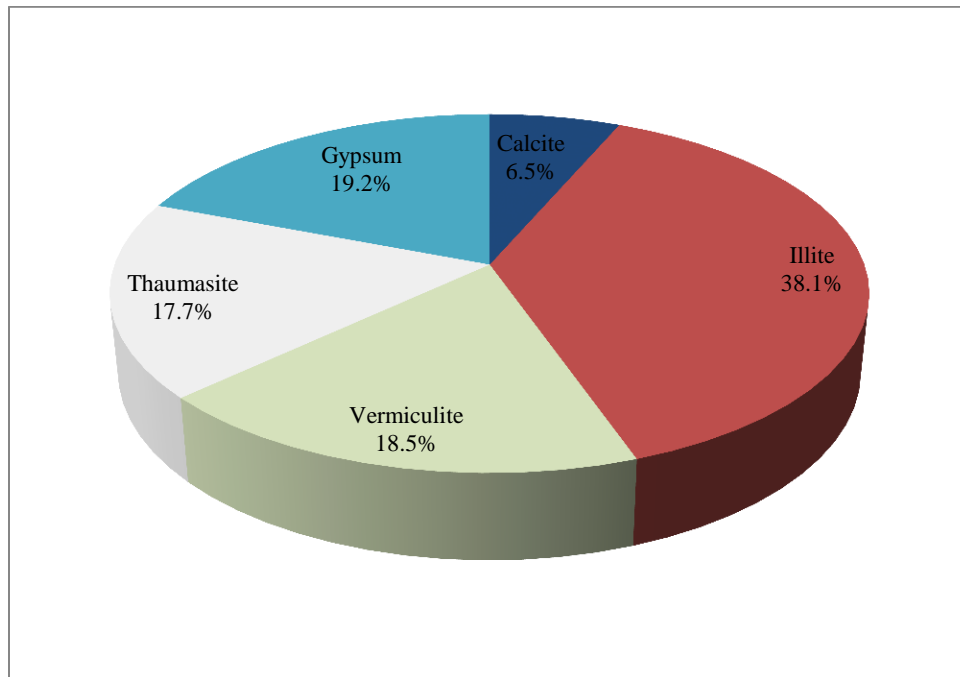
Colorado Clay+Silt Fraction	No (%)	Glycol (%)	400 °C (%)	550 °C (%)	Wet ST (%)	Wet LT (%)
Alunite	0.9	-	-	-	-	-
Calcite	-	-	-	-	0	0
Ettringite	-	-	0	0	-	-
Gypsum	34.1	19.7	-	-	0	0
Illite	54.9	71.8	91.0	100	57.4	68.1
Jarosite	0.7	0.4	9.0	-	5.5	0
Junitoite	-	8.1	-	-	0	6.2
Montmorillonite	0.4	-	-	0	5.8	22.2
Nontronite	4.8	-	-	-	0	-
Thaumasite	-	-	-	0	31.3	3.5
Vermiculite	4.2	-	-	-	0	0

Note: % by crystalline weight

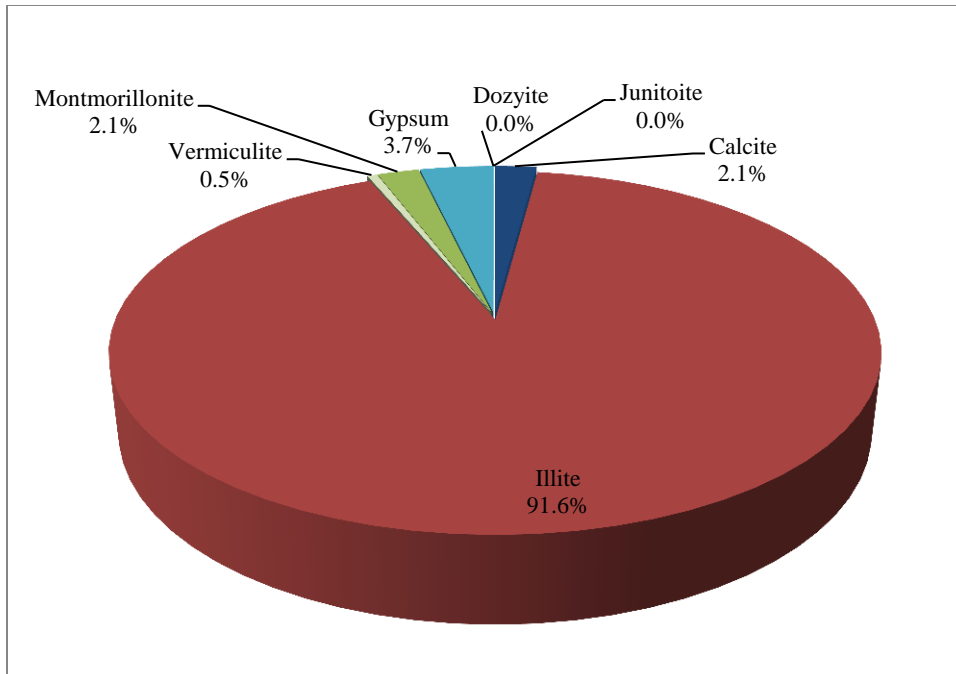
The same analysis procedure was completed on the clay fraction of Colorado. The treatment scans for the Colorado's clay fraction soil sample can be seen in Figure 4.36. The red line represents the untreated sample, the blue line is the glycol sample, the green line is the sample subjected to 400°C sample, and the purple line represents the results of the sample subjected to 550°C sample. Colorado clay mineral quantification for each treated specimen can be seen in Figures 4.37 to 4.40.



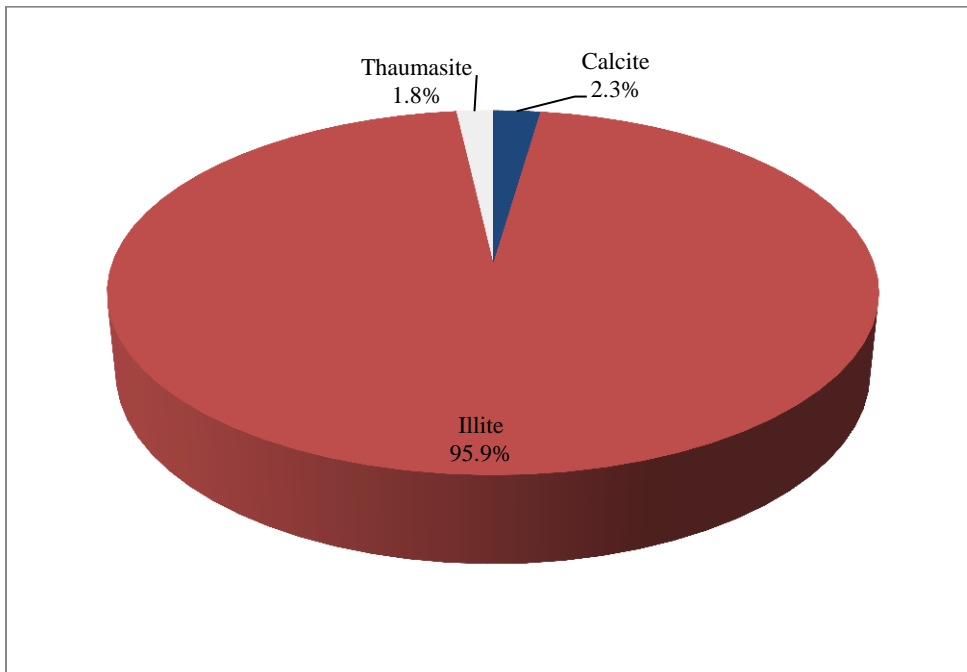
**Figure 63: Treatment scans for the Colorado's clay fraction**



**Figure 64: Mineral quantification of Clay fraction of Colorado soil for untreated specimen**



**Figure 65: Mineral quantification of Clay fraction of Colorado soil for Glycol treated specimen**



**Figure 66: Mineral quantification of Clay fraction of Colorado soil for 400°C treated specimen**



The labeled peaks can be seen in Figure 4.41. With the numerous amounts of minerals beneath one peak, the selected labels for the top thirty minerals overlap and become difficult to read. The mineral quantification for all the treated specimens for Colorado’s Clay fraction can be seen in Table 4.5.

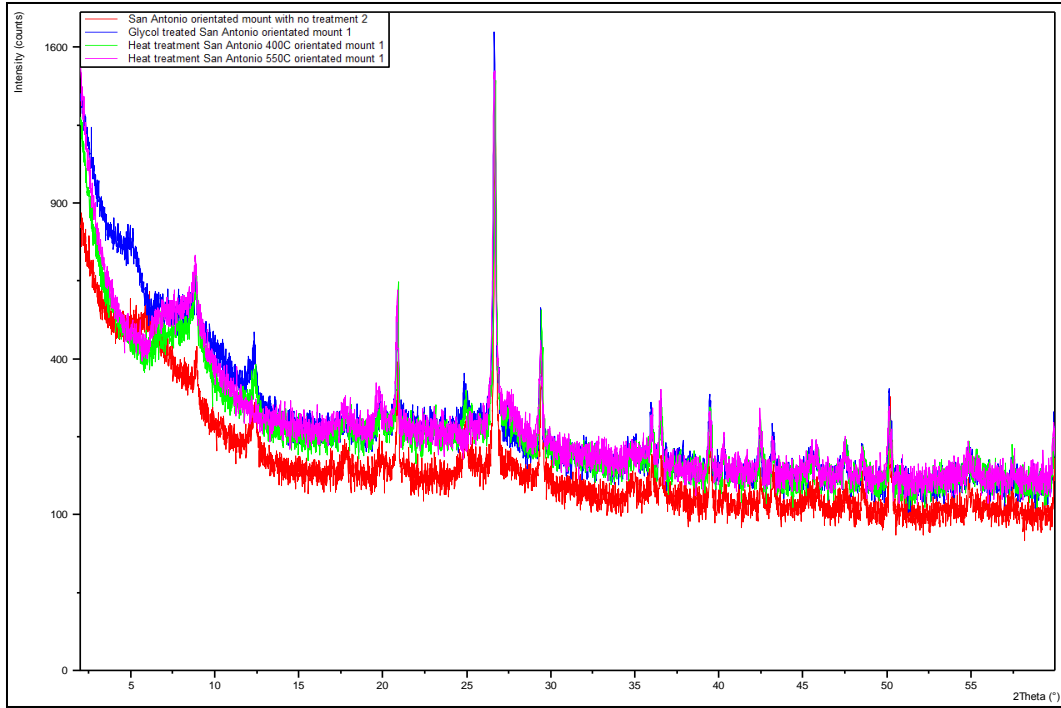
**Table 11: Summary of Colorado Clay fraction mineral quantification**

Colorado Clay Fraction	No Treatment (%)	Glycol Treatment (%)	400 °C Treatment (%)	550 °C Treatment (%)
Calcite	6.5	2.1	2.3	-
Dozyite	-	0	-	-
Gypsum	19.2	3.7	-	-
Illite	38.1	91.6	95.9	96.8
Junitoite	-	0	-	-
Montmorillonite	-	2.1	-	-
Thaumasite	17.7	-	1.8	3.2
Vermiculite	18.5	0.5	-	-

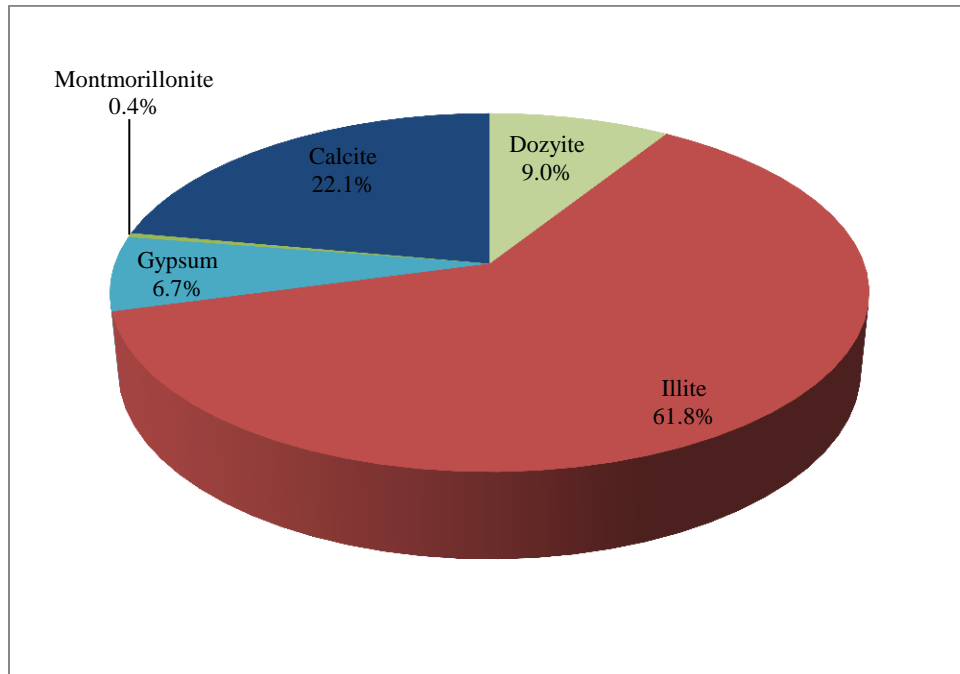
Note: % by crystalline weight

#### 4.4.3 Qualification and Quantification of San Antonio Soil

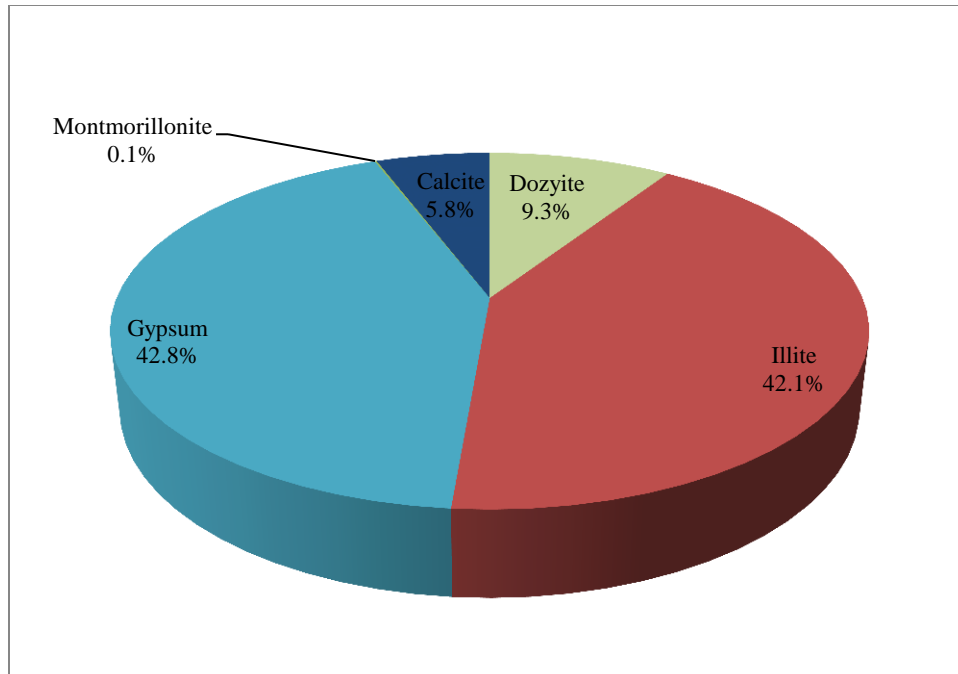
Once the scanning of all treated specimens of San Antonio soil was completed, the data was analyzed using the software provided by PANalytical, HighScore Plus. Figure 4.42 presents the scan obtained for all treatments for the San Antonio’s clay+silt fraction specimens. The red line represents the untreated sample, the blue line is the glycol sample, the green line is the sample subjected to 400°C sample, and the purple line represents the results of the sample subjected to 550°C sample. The same analysis procedure was followed to quantify the minerals found on the clay+silt fraction of San Antonio soil. San Antonio’s clay+silt fraction mineral quantification for each all treated specimens can be seen in Figures 4.43 to 4.48.



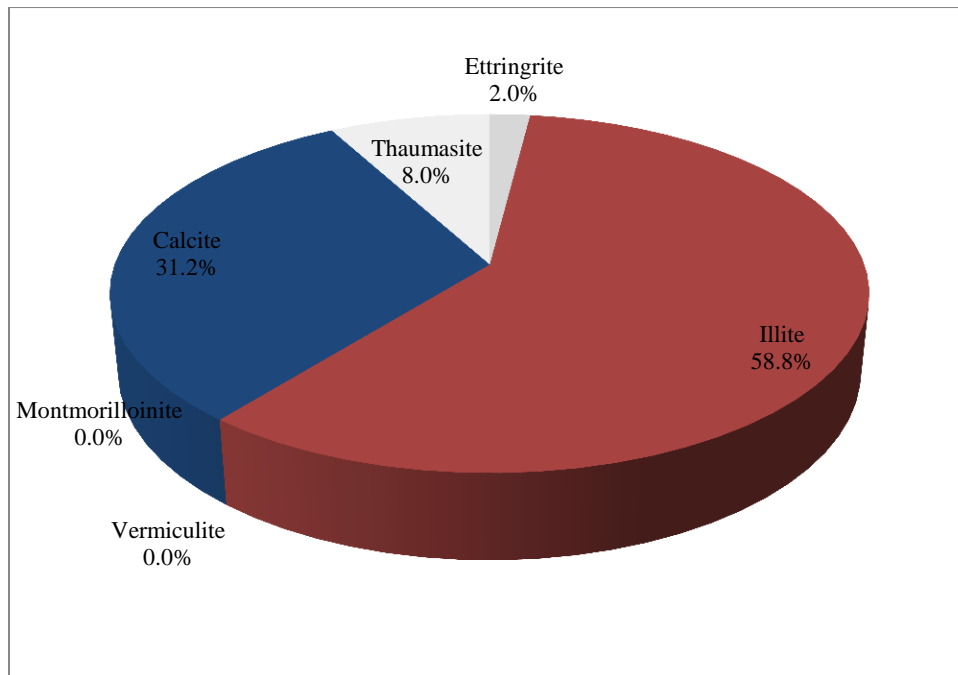
**Figure 69: Treatment scans for the San Antonio's Clay+Silt fraction**



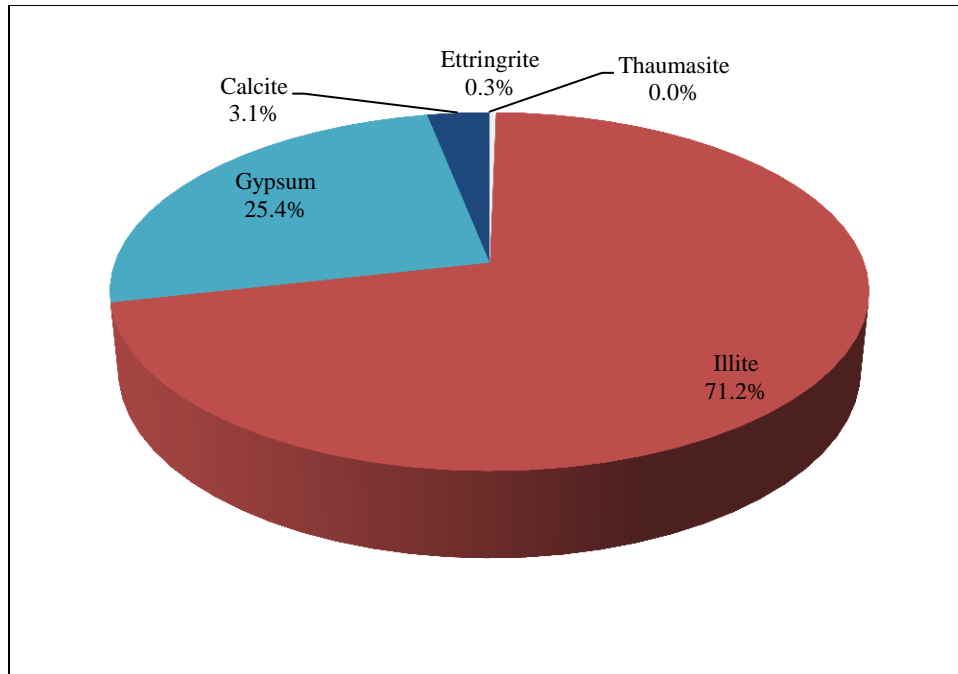
**Figure 70: Mineral quantification of Clay+Silt fraction of San Antonio soil for untreated specimen**



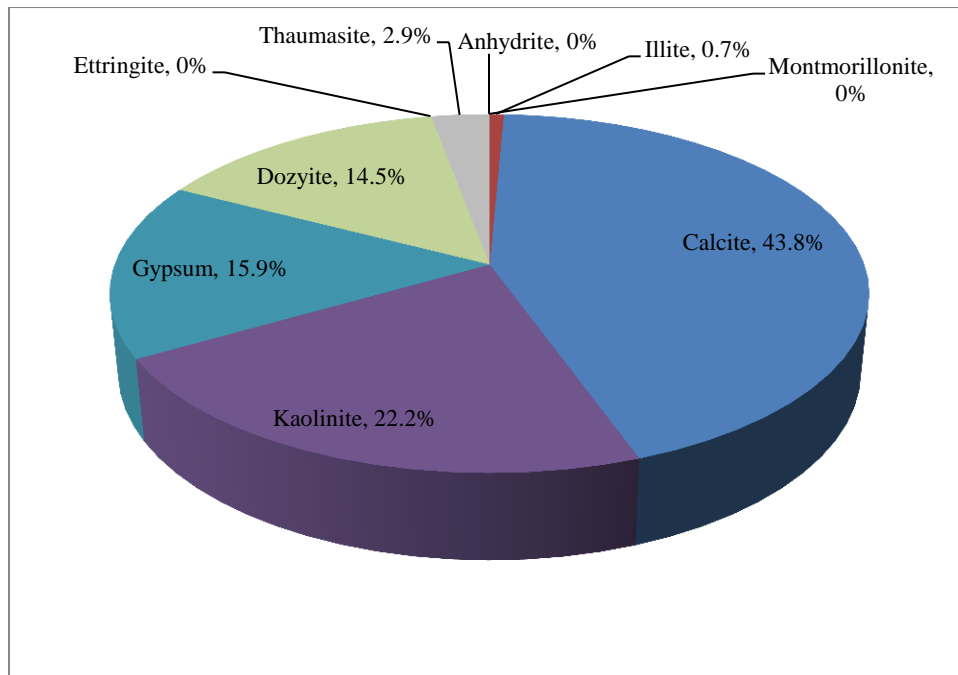
**Figure 71: Mineral quantification of Clay+Silt fraction of San Antonio soil for Glycol treated specimen**



**Figure 72: Mineral quantification of Clay+Silt Fraction of San Antonio soil for 400°C treated specimen**

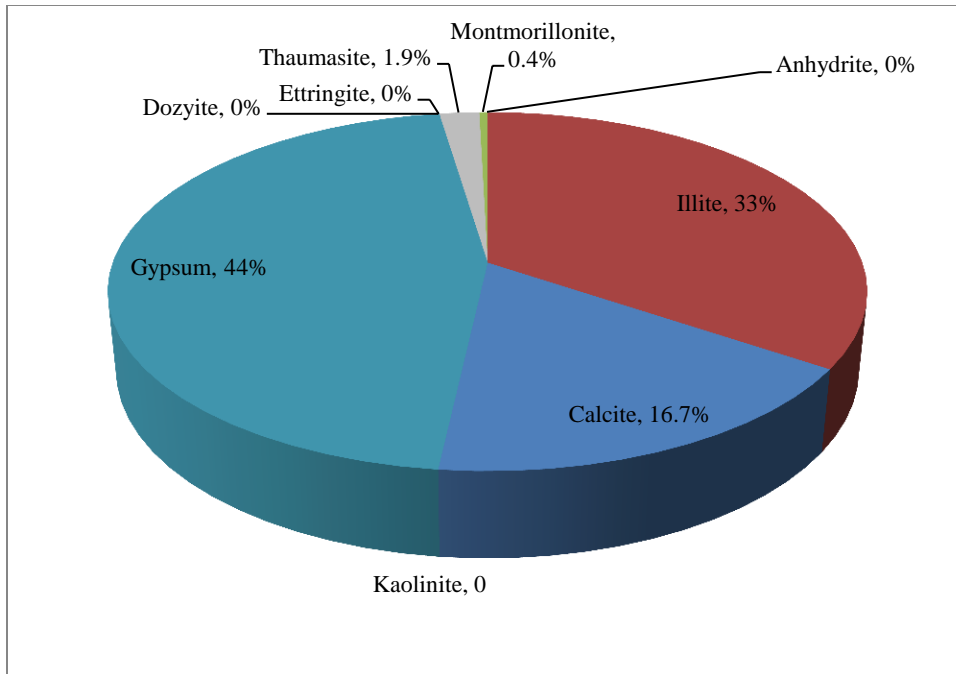


**Figure 73: Mineral quantification of Clay+Silt fraction of San Antonio soil for 550°C treated specimen**

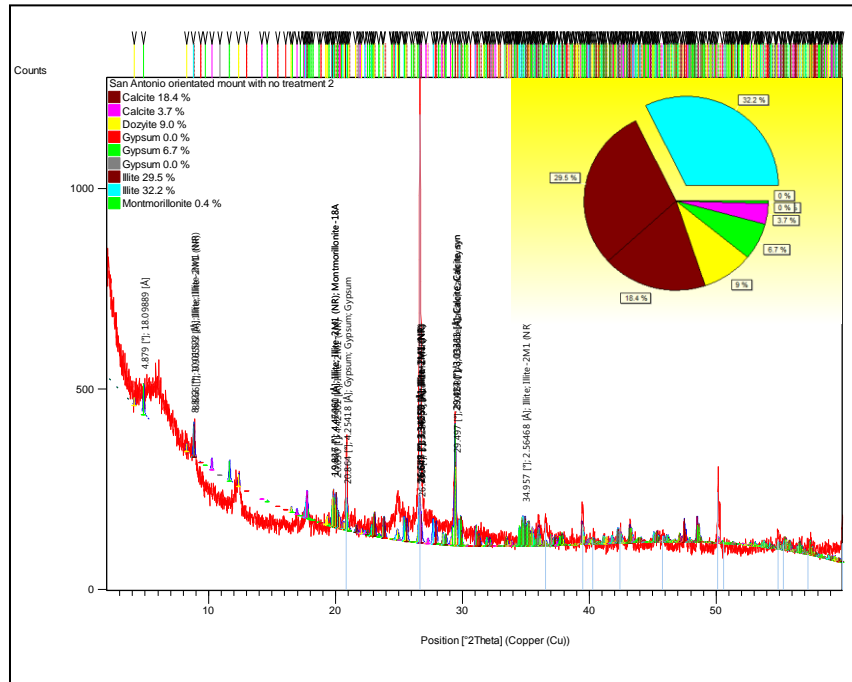


**Figure 74: Mineral quantification of Clay+Silt fraction of San Antonio soil for wetted short term specimen**





**Figure 75: Mineral quantification of Clay+Silt fraction of San Antonio soil for wetted long term specimen**



**Figure 76: Completed signal quantification with labeled peaks**

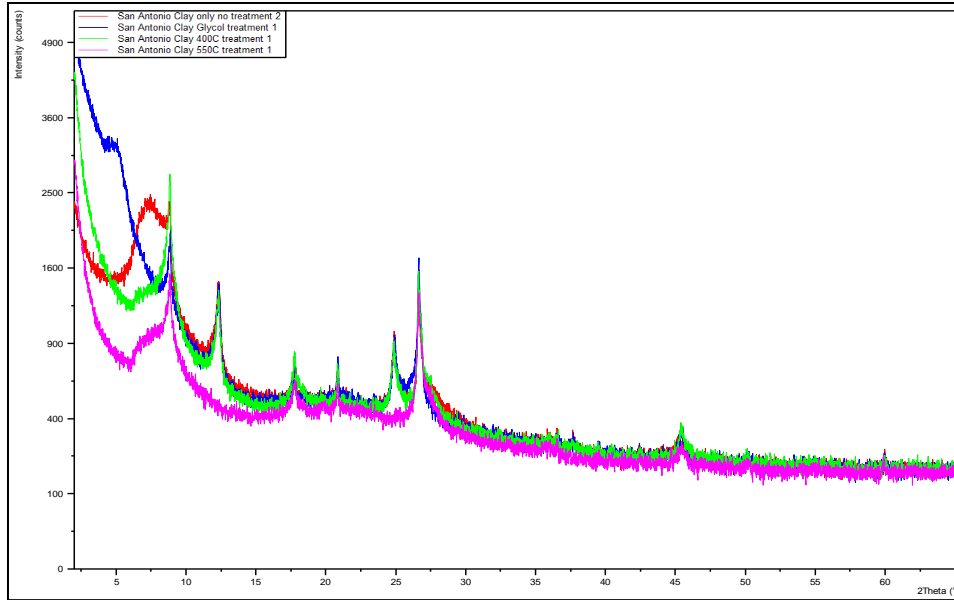
The labeled peaks can be seen in Figure 4.49. With the numerous amounts of minerals beneath one peak, selecting the top thirty minerals becomes difficult as the labels overlap. The mineral quantification for all treatments for San Antonio's Clay+Silt fraction can be seen in Table 4.6.

**Table 12: Summary of San Antonio Clay+Silt fraction mineral quantification**

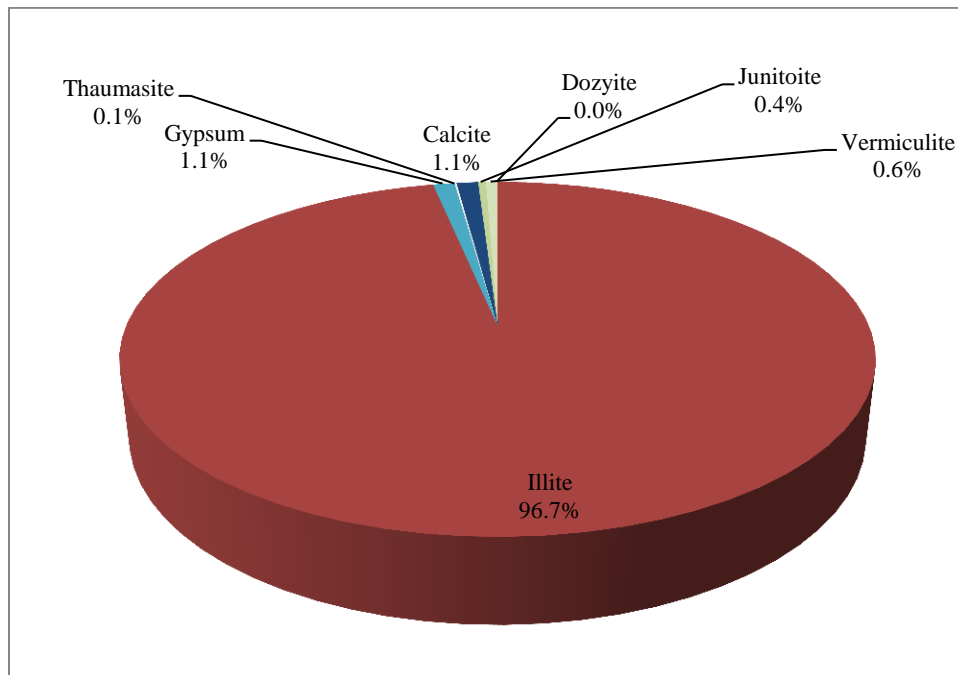
San Antonio Clay+Silt Fraction	No (%)	Glycol (%)	400 °C (%)	550 °C (%)	Wet ST (%)	Wet LT (%)
Calcite	22.1	5.8	31.2	3.1	43.8	16.7
Dozyite	9.0	9.3	-	-	14.5	-
Ettringite	-	-	2.0	0.3	0	-
Gypsum	6.7	42.8	-	25.4	15.9	44.0
Illite	61.8	42.1	58.8	71.2	0.7	33.0
Montmorillonite	0.4	0.1	0	-	-	0.4
Thaumasite	-	-	8.0	0	2.9	1.9
Vermiculite	-	-	0	-	-	-
Kaolinite	-	-	-	-	22.2	-

Note: % by crystalline weight

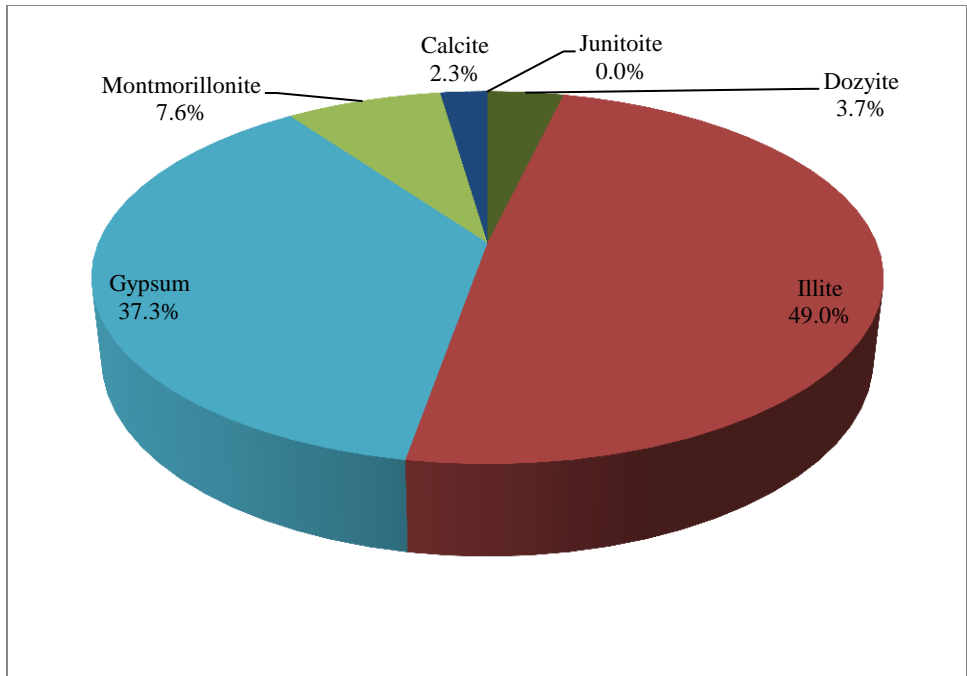
Figure 4.50 presents the scans for the San Antonio's clay fraction soil sample. The red line represents the untreated sample, the blue line is the glycol sample, the green line is the sample subjected to 400°C sample, and the purple line represents the results of the sample subjected to 550°C sample. San Antonio's clay quantifications for each treatment can be seen in Figures 4.51 to 4.54.



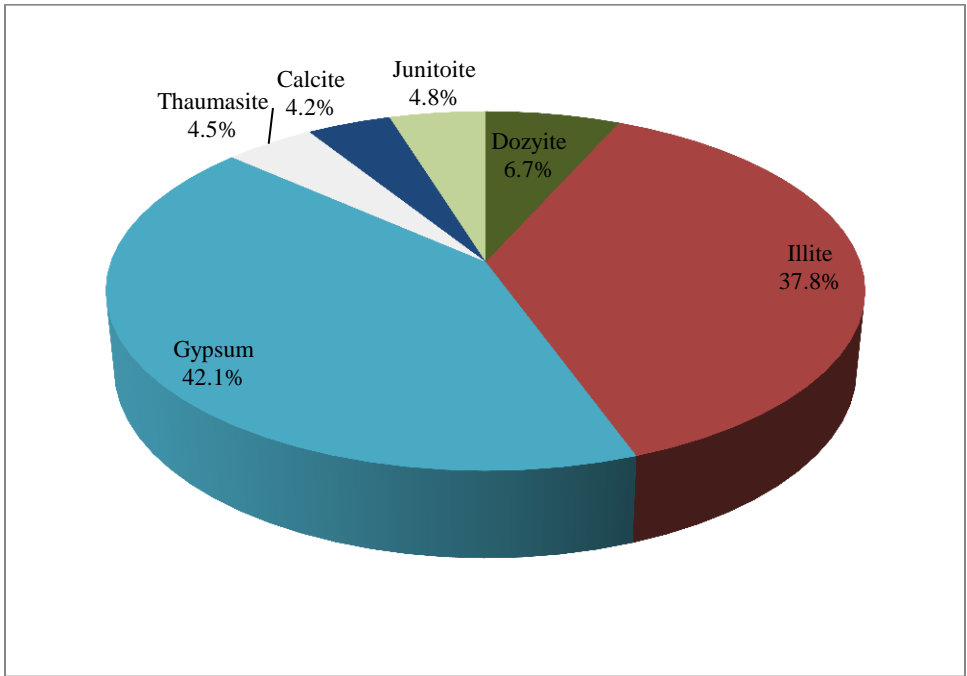
**Figure 77: Treatment scans for the San Antonio’s clay fraction**



**Figure 78: Mineral quantification of Clay fraction of San Antonio soil for untreated specimen**



**Figure 79: Mineral quantification of Clay fraction of San Antonio soil for Glycol treated specimen**



**Figure 80: Mineral quantification of Clay fraction of San Antonio soil for 400°C treated specimen**



The labeled peaks can be seen in Figure 4.55. With the numerous amounts of minerals beneath one peak, selecting the top thirty minerals starts to become overlapped and difficult to read. The quantification for all the treatment for San Antonio's Clay fraction can be seen in Table 4.7 below.

**Table 13: Summary of San Antonio Clay fraction mineral quantification**

San Antonio Clay Fraction	No Treatment (%)	Glycol Treatment (%)	400 °C Treatment (%)	550 °C Treatment (%)
Calcite	1.1	2.3	4.2	-
Dozyite	0	3.7	6.7	-
Gypsum	1.1	37.3	42.1	-
Illite	96.7	49.0	37.8	98.2
Junitoite	0.4	0	4.8	-
Montmorillonite	-	7.6	-	-
Thaumasite	0.1	-	4.5	1.8
Vermiculite	0.6	-	-	-

Note: % by crystalline weight

#### 4.5 Summary and Conclusions

An overview of Bragg's Law was presented, which is the basis of how diffractograms are used to quantify the clay mineralogy of soils. This principle allowed for the PANalytical software to quantify the soil used in this study. Peak interference and the lack of a standard method for interpretation constitute two major obstacles in quantitative analysis. The state of disaggregation, alteration from chemical pretreatment, particle size separation, and preferred orientation of crystallites in the prepared sample and the method of assessing clay mineral proportion for the diffraction pattern may all contribute to errors in quantification (Batchelder, 1998). Published methods of quantitative analysis for clay-bearing samples commonly results in standard deviations of up to 20% (Moore & Reynolds, 1997). Two different interpretation procedures and

several different treatments were applied to the specimens before quantification of the mineral composition of the soil. The quantification analysis done by two interpretation methods and after different treatments revealed scattered results, which made it very different for interpretation. An analysis of the results obtained is presented in the next chapter.

## CHAPTER 5

### COMPARATIVE ANALYSIS OF DATA

#### **5.1 Introduction**

The analysis of the data collected is presented in this Chapter. The analysis was focused on a comparison of the soils mineralogy obtained when the soil was subjected to different treatment techniques prior to XRD testing. This includes results of Gypsification, Mixed-Layer clay identification, Ettringite and Thaumascite formation, and the effect of time on the Gypsification process. Finally, the mineralogy data obtained was compared to the mineral quantification based on the model proposed by the University of Texas, Arlington.

#### **5.2 Comparison of Results from Tests subjected to Different Treatments**

In this section, a comparison of the XRD results obtained after the samples were subjected to different treatment methods is presented. That includes comparisons of the results when different size fractions were used (Clay+Silt fraction and Clay fraction), and also the comparison of the results obtained after three specimens were subjected to different treatments: no treatment, glycol, heat treatment at two different temperatures, and wetting treatments over two different periods of time.

##### **5.2.1 Results Showing Gypsification**

There are several mechanisms that could lead to swelling of soils. One such mechanism is the case of mineral transformation. Table 5.1 presents a list of minerals that can undergo mineral transformation leading to new minerals that can cause volume change of the crystalline solid.



**Table 14: Volume increase of selected mineral transformations (Mitchell & Soga, 2005)**

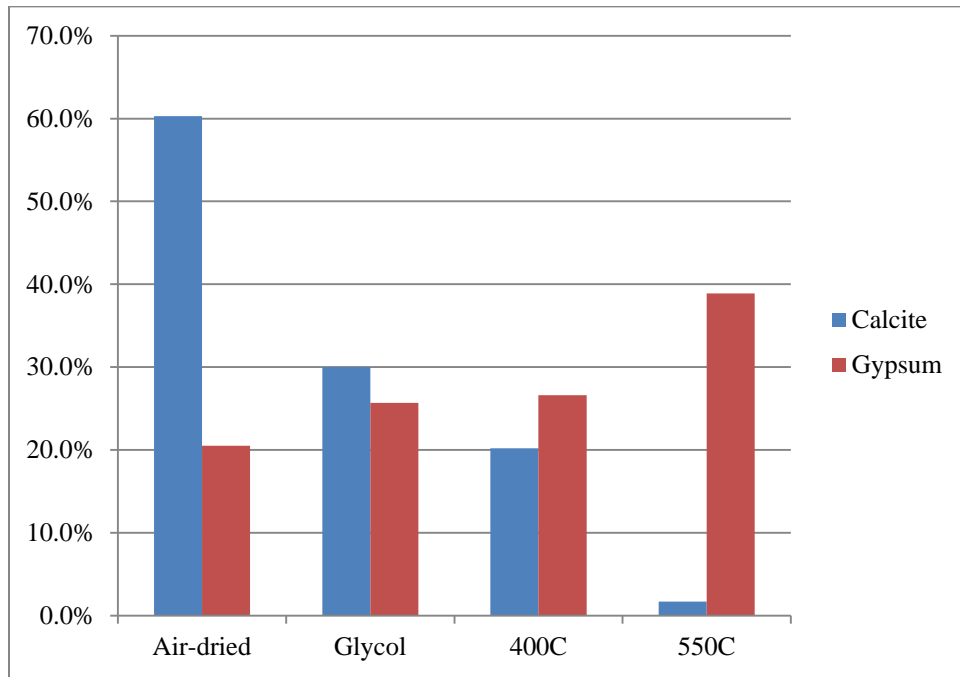
Mineral Transformation		Volume Increase of Crystalline Solids (%)
Original Mineral	New Mineral	
Illite	Alunite	8
Illite	Jarosite	10
Calcite	Gypsum	60
Pyrite	Jarosite	115
Pyrite	Anhydrous ferrous sulfate	350
Pyrite	Melanterite	536

Of this list, the formation of Gypsum is of particular interest as this mineral is abundant in arid regions. Gypsum is formed through the dissociation of Calcite in a weak acid, such as rain water. Calcite can be found in the soil or can be added as part of soil stabilization techniques used when expansive soils are encountered. The dissociation of Calcite frees up Calcium and Carbonate ions. Once the Calcium is freed up, it re-associates with soluble Sulfate (if available in the soil) and water molecules. The re-association of these ions creates the possibility of Gypsum formation.

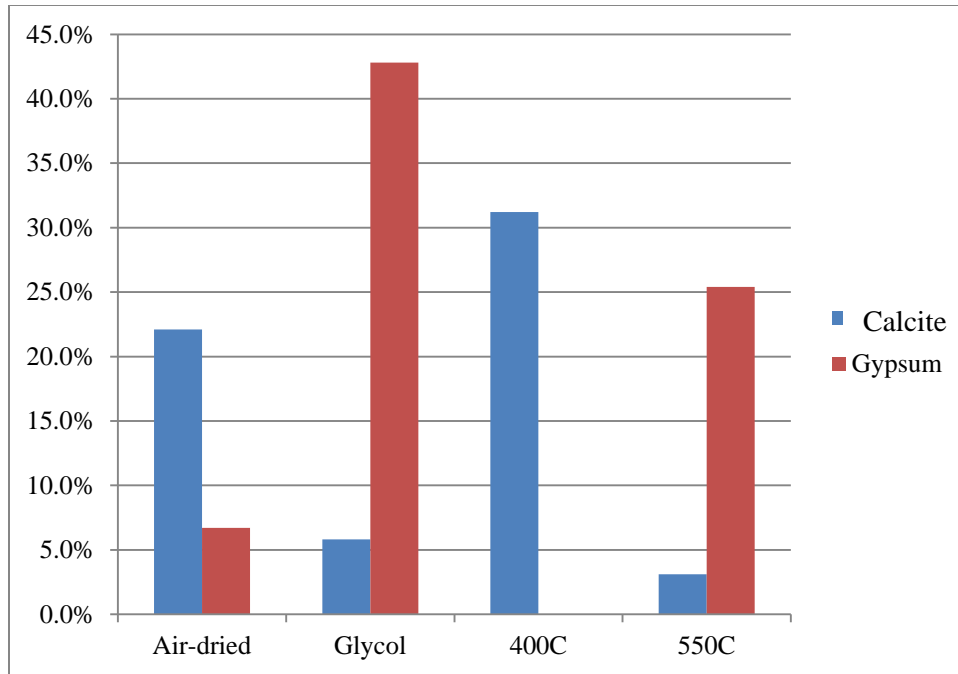
Upon recognition of this phenomenon, an attempt was made to identify the minerals from Table 5.1 in the soils used in this study. The following minerals from this list were found in Anthem soil: Calcite at 57.4% and Gypsum at 19.5% in the untreated specimen. San Antonio presented some amounts of Calcite at 22.1% and Gypsum at 6.7% while Colorado yielded Alunite at 0.9% and Gypsum at 34.1 both in the untreated specimens.

Of particular interest, in the clay+silt fraction of the Anthem soil, it was found that when Calcite was present, Gypsum was absent and vice-versa. Results indicate that

Calcite amounts decrease while Gypsum amounts increase, as the Anthem specimen was subject to the different treatments (Figure 5.1). This was also observed in the San Antonio soil (Figure 5.2).

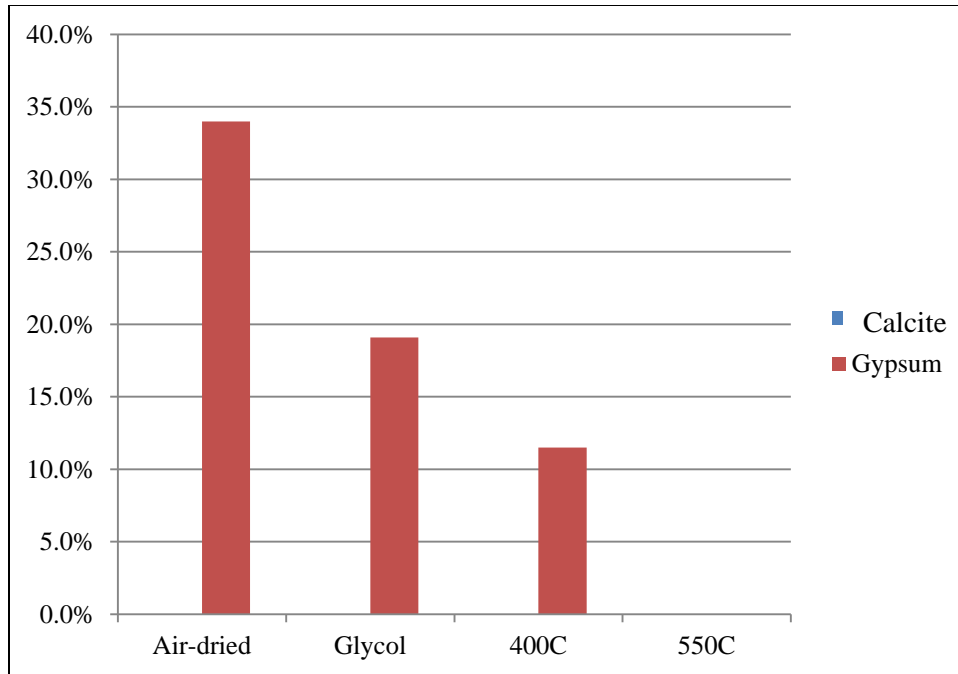


**Figure 83: Anthem's Clay+Silt fraction of possible Calcite transformation into Gypsum**



**Figure 84: San Antonio Clay+Silt fraction of possible Calcite transformation into Gypsum and vice versa**

Although not exactly the same trend was observed in the San Antonio soil as that observed in the Anthem soil, the Calcite was present when the Gypsum was not and vice versa. For the Colorado soil, there were significant amounts of Gypsum (Figure 5.3) but no Calcite was found.



**Figure 85: Amounts of Gypsum observed in the Colorado Clay+Silt fraction.**

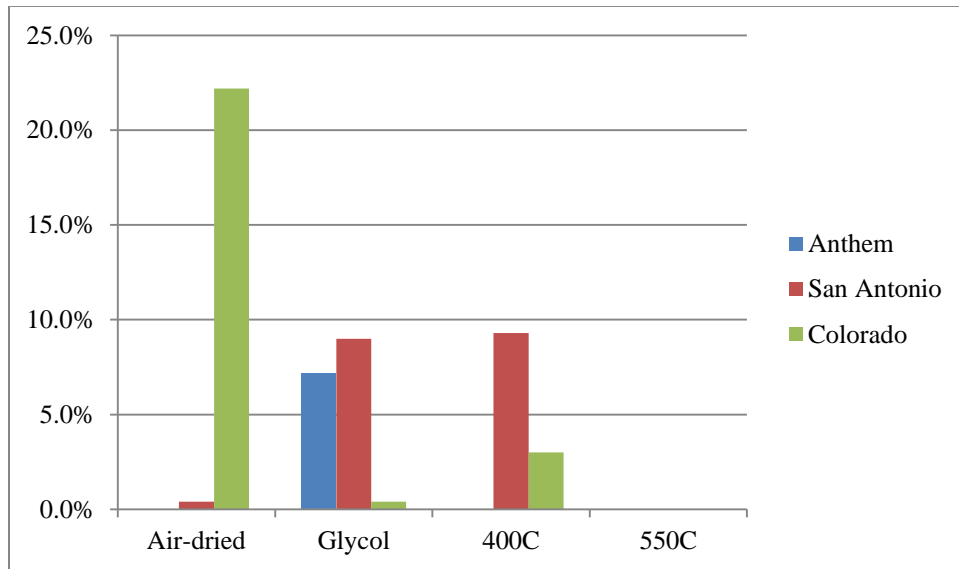
The formation of Gypsum from Calcite in both the Anthem and San Antonio could contribute to the 8.6% and 14.1% free swell on the compacted material measured for these two soils, respectively. The presence of Gypsum and the lack of Calcite observed in the Colorado soil might indicate that the mineral transformation may have already occurred.

Sulfate is the anion in the formation of the mineral Gypsum and therefore, it needs to be present in the soil for the transformation to occur. As indicated in Chapter 3, Anthem and San Antonio have a moderate to high amount of Sulfate, 1800 and 5700 ppm, respectively; while Colorado has only 240 ppm. On the other hand, the amount of Calcium measured in the Anthem and San Antonio were 150 ppm and 1100 ppm respectively; while the amount found in the Colorado soil was 91 ppm. The Sulfate and

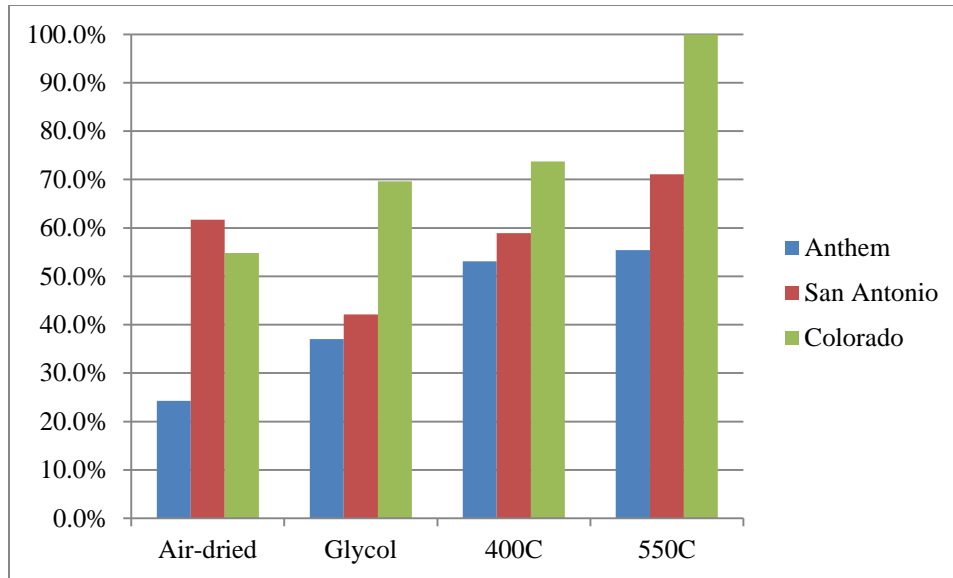
Calcium measured in the former two soils are good indications of possible mineral transformation.

### 5.2.2 Results Showing Mixed-Layer Identification and Smectite Identification

Results of the Anthem clay+silt fraction (Figure 5.4) indicate that there was very little of the common mineral associated with the swelling of soils, Smectite. Colorado exhibited the largest amount (about 20%) when the specimen was air-dried before the XRD analysis. Surprisingly, the Smectite amounts detected after the Glycol and the heat treatments were very small. San Antonio exhibited some amount of the Smectite mineral after the specimens were treated with Glycol and heat. However, there was an extensive amount of Illite present in the three soils, after each treatment, as shown in (Figure 5.5).



**Figure 86: Smectite percentages of the Clay+Silt fraction for the three soils**

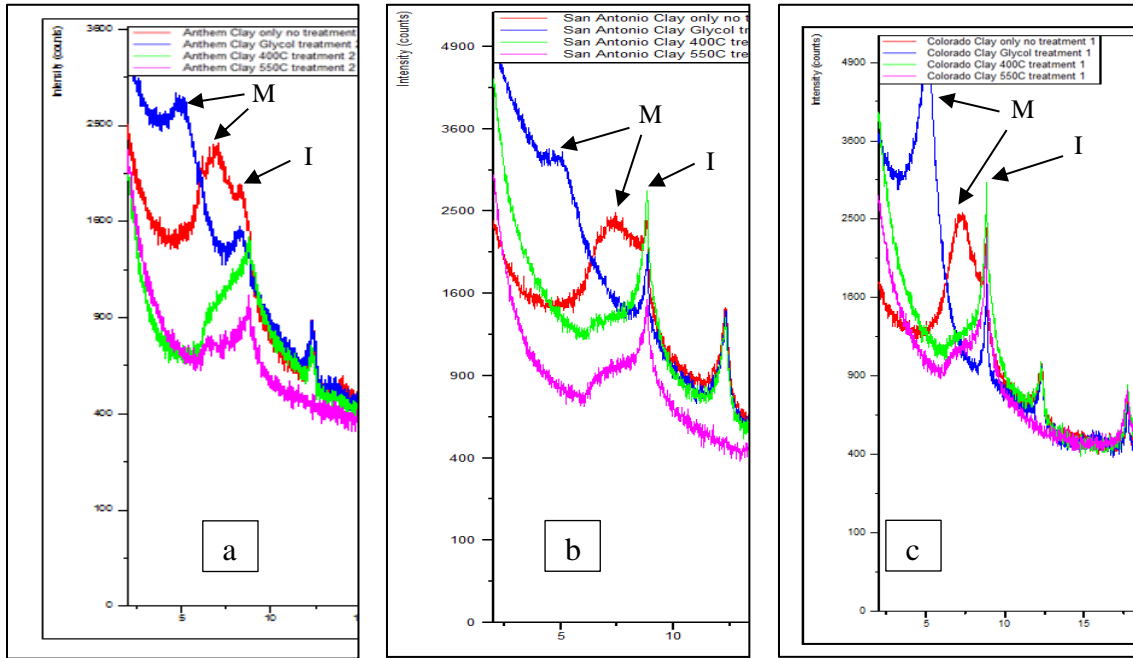


**Figure 87: Illite percentages of the Clay+Silt fraction of the three soils**

Illite is a weathered byproduct of the Smectite mineral and it is considered to be a non-expansive 2:1 mineral (Mitchell & Soga, 2005). When Smectite weathers each individual Smectite mineral does not necessarily weather to Illite at the same time. Actually, only some individual mineral platelets might change creating layered effect (Moore & Reynolds, 1997). This Illite-Smectite layered mineral creates an effect in the XRD diffractogram that may be quantified as Illite mineral only (or Smectite only for this effect). Identifying mixed-layer clay minerals and determining the actual amount of Smectite versus Illite gives a more accurate quantification of the minerals in the soil. Mixed-layer clay can be partially identified using an X-ray diffraction process when different treatments are compared.

In Figure 5.6, it can be seen that the Montmorillonite peak is close to the Illite peak when the no-treatment diffractogram (red line) is observed. As these two peaks are closer, it creates a table top effect between the two. This makes the identification of the Smectite minerals difficult to differentiate from Illite minerals when no treatment is

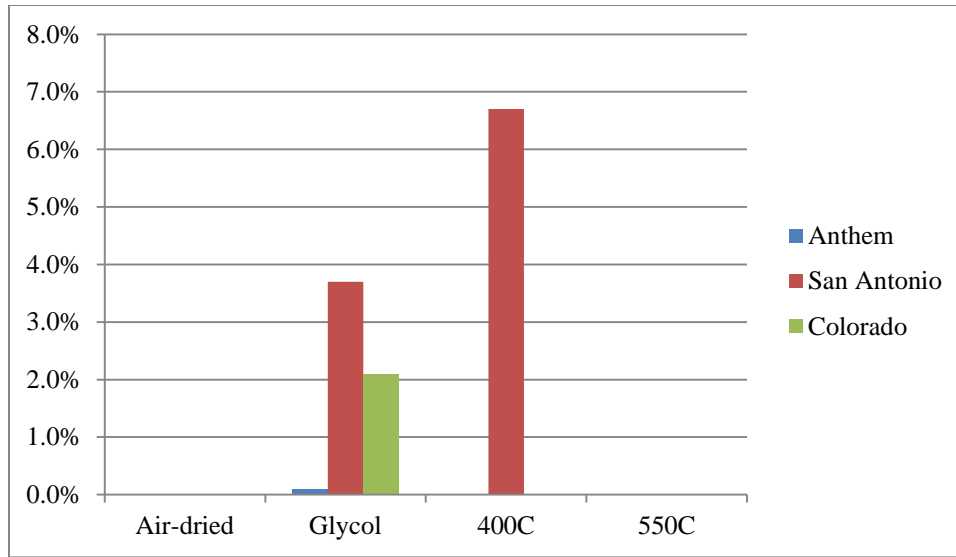
applied to the soil. Also, this affects the accuracy of the quantification of the two minerals due to the peak being so broad. This change in the no treatment signal and the glycol treated signal also yields a change in d-spacing which will be elaborated on later.



**Figure 88: Mixed-layer visual identification in diffractograms (a) Anthem, (b) San Antonio, (c) Colorado**

The same conclusion can be obtained from looking at the diffractograms for the clay fraction of the three soils. In Figure 5.7, it can be observed that here are minimal amounts of Smectite present. Again, this may be due to the close proximity of the primary Montmorillonite peak and the primary Illite peak.

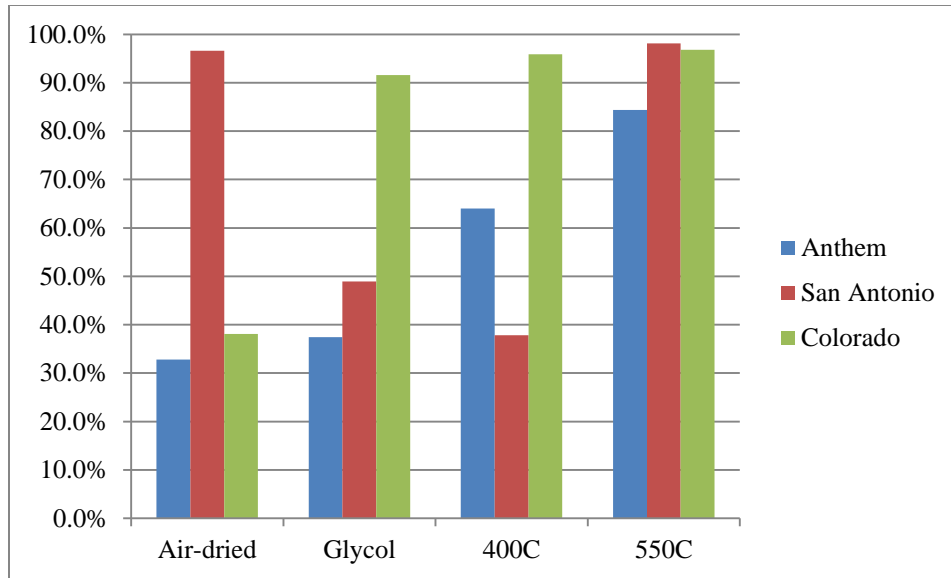
As shown by the blue line in Figure 5.6, there is a definite separation between the two peaks when the three soils were treated with Glycol. This is expected since the inundation of the polar molecules in the Glycol will cause the Smectite minerals to stand out in the X-ray diffraction data collection.



**Figure 89: Spectate identification on the Clay fraction of the studied soils**

It was also noticed that the Illite quantification amount found in the clay fraction of the three soils (Figure 5.8) was extremely high. These numbers reflect the fact that only the clay fraction is being analyzed. Therefore, the user should be careful when quantifying data based on the PANalytical software, as the results are a function of the fraction analyzed and not on the actual amount of minerals present in the specimen. In order to have a more accurate quantification of the entire composition of the soil; the clay+silt fraction should be always used.



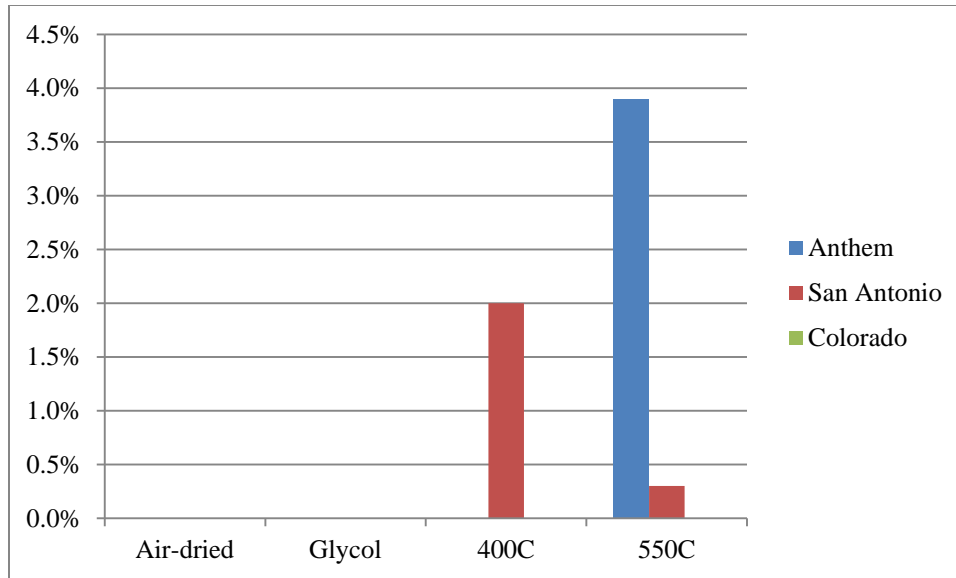


**Figure 90: Illite identification on the Clay fraction of the soils in this study**

Observing the large amount of Illite in all of the soil and that Illite is a byproduct of Smectite weather creating a mixed layer system, shows that Illite quantification masks the quantification of Smectite mineral, particularly Montmorillonite. Also, when comparing the quantification of the clay+silt fraction of Smectite mineral versus the quantification of the clay fraction Smectite minerals, there was a noticeable difference. This was due to the use of only the clay particles of the soil and inundating them with the glycol to create a stronger identification during the X-ray data collection. Finally, the overwhelming amount of Illite present in the three soils in the clay fraction analysis would likely affect the quantification of the other mineral in the system.

### **5.2.3 Results Showing Ettringite and Thaumasite Formation**

Another important trend noticed was the formation of Ettringite after the temperature treatments of the soils in this study (Figure 5.9).

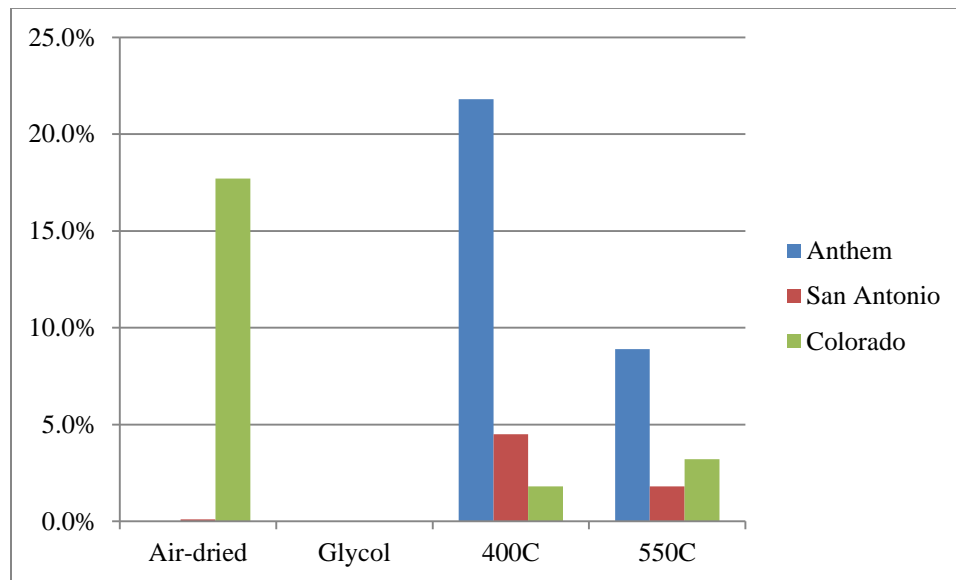


**Figure 91: Formation of Ettringite in Clay+Silt fraction at high temperatures**

Ettringite formation has been shown to form in concrete when subjected to high temperatures. Another term used in petrographic reports is Delayed Ettringite Formation (DEF). This refers to a condition usually associated with heat-treated concrete. Certain concretes of particular chemical makeup which have been exposed to temperatures over about 70°C (158°F) during curing can undergo expansion and cracking caused by Ettringite formation. This can occur because the high temperature decomposes any initial Ettringite formed and holds the Sulfate and alumina tightly in the calcium silicate hydrate (C-S-H) gel of the cement paste (PCA, 2013). The formation of Ettringite not only appears created in the heat treatment of concrete, but also it can form in soils. The amount of damage due to Ettringite formation depends on a number of factors including: (i) the thermodynamic favorability of Ettringite precipitation in specific soils, (ii) the quantity of limiting reactants that stoichiometrically control the mass of Ettringite formed, (iii) the migration of water, Sulfate and other ions that support continued Ettringite nucleation, (iv) the strength of the pozzolanic or cementitious matrix, and (v)

the spatial arrangement of the Ettringite crystals in the soil matrix. It is possible for Ettringite to grow in voids that can accommodate their growth without substantial expansion. It is also possible for Ettringite crystals to grow within a dense matrix that will not accommodate their growth without expansion (Little & Nair, 2007).

Thaumasite, a mineral similar to Ettringite, appeared after the high temperature treatments of the clay fraction of the three soils. Thaumasite and Ettringite compositions are pretty close to each other : Thaumasite composition is  $[Ca_3Si(CO_3)(SO_4)(OH)_6 \cdot 12(H_2O)]$  while Ettringite is  $[Ca_6Al_2(SO_4)_3(OH)_{12} \cdot 26(H_2O)]$ ; and therefore, it also presents swelling behavior. The quantification of the Thaumasite is shown in Figure 5.10.



**Figure 92: Thaumasite formation of the Clay+Silt fraction in this study**

The fact that the expansive mineral Thaumasite occurs again in the high temperature treatments would lead one to believe that temperature has an effect on the formation of this mineral, as reported previously for the Ettringite mineral. As presented in the last two figures, it appears that the presence of sulfates in the soil and high

temperatures favor the formation of Ettringite and Thaumasite. It was also observed that Colorado soil presented Thaumasite in the air-dried specimen, which leads to the conclusion that somehow this soil was subjected to previous periods of higher temperatures when compared to the Anthem and San Antonio soils, which did not show any Thaumasite or Ettringite before the heat treatments.

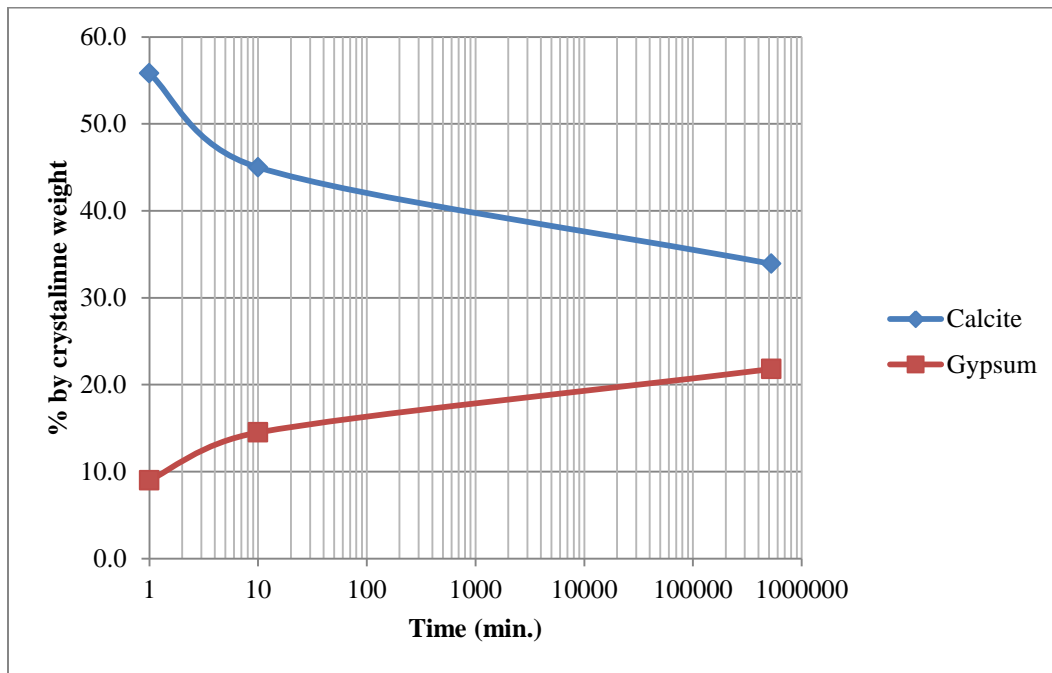
### **5.3 Comparison of Tests Performed on Wet Soil Conditions**

In heavily sulfidic soils the original mineral reacts with the Sulfate minerals present in the soil which creates a different mineral that has the possibility of being expansive. Table 5.1 presents some minerals that once in contact with Sulfates could transform into high volume change minerals.

In order to investigate the possibility of mineral transformation during the wetting treatments (explained in Chapter 4, section 4.4), the XRD results obtained from powder (air-dried) specimens were compared to those obtained after the two wetting treatments: the wet short-term and the wet long-term treatments. After completing the procedure for Anthem, it was observed that the different percentages of Calcite and Gypsum started to develop a pattern. Table 5.2 presents the minerals found during the wet analysis procedure performed on Anthem soil. Since the two wetting treatments were spaced one year period without being disturbed, the percentages of Gypsum and Calcite were plotted vs. time (Figure 5.11).

**Table 15: Anthem soil wet analysis mineral quantification**

Minerals	Anthem		
	Wet Analysis		
	Air-dried	Wet short term	Wet long term
Calcite	55.8%	45.0%	33.9%
Illite	34.1%	37.5%	36.8%
Junitoite	1.1%	3.0%	2.6%
Kaolinite	0.0%	0.0%	4.9%
Gypsum	9.0%	14.5%	21.8%



**Figure 93: Time scale indicating Calcites transformation into Gypsum in Anthem soil**

With the claim made in Table 5.1, that a volume change of 60% can occur when Calcite is transformed into Gypsum (Mitchell & Soga, 2005), and Figure 5.11 showing evidence that Gypsification might happened, indicate that the presence of clay minerals might not explain the swelling behavior of Anthem soil by itself and that other mechanisms of swelling should be taking into consideration. This would have been

unable to be notice without the usage of X-ray diffraction to determine the quantification at different time steps.

The different percentages of Calcite and Gypsum found in the Colorado soil after the wetting treatments did not present any clear trend as that observed in the Anthem soil. Table 5.3 presents the amount of minerals found in Colorado soil, when it was subjected to the wetting processes. As observed in this table, the Calcite and Gypsum minerals did not appear in the wet short term or the wet long term specimens, but they appeared in the air-dried specimen. This result could not be explained and it is suspected that interpretation of the results play an important role in the validity of the same. Notice that while the air-dried specimen presents no measurable amount of Illite, the wet short and long term specimens exhibit Illite quantities comparable with the Gypsum found in the air-dried specimen. Another possibility is that mineral transformation might have already happened in the Colorado specimen based to the high amounts of Gypsum and little amount of Calcite found in the soil (see Table 5.3); but again, that does not explain the lack of minerals after the wetting treatments.

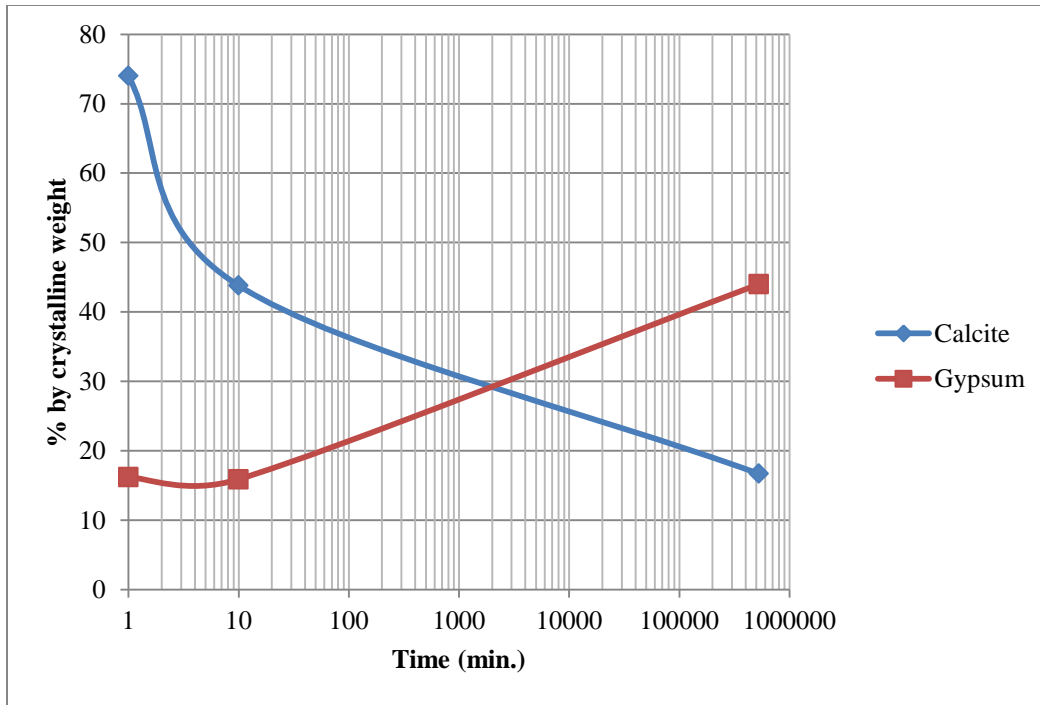
**Table 16: Colorado soil wet analysis mineral quantification**

Minerals	Colorado		
	Wet Analysis		
	Air-dried	Wet short term	Wet long term
Calcite	10.6%	0.0%	-
Gypsum	56.0%	-	-
Illite	0.0%	57.4%	68.1%
Jarosite	-	5.5%	0.0%
Junitoite	-	-	6.2%
Kaolinite	0.0%	-	0.0%
Montmorillonite	4.1%	5.8%	22.2%
Nontronite	0.0%	-	-
Thaumasite	-	31.3%	3.5%
Vermiculite	29.3%	-	-

Table 5.4 presents the amount of minerals found in the San Antonio soil, after the specimens were wetted, for the short term (10-minute time prior) and the long term (1 year) conditions. The percentages of Gypsum and Calcite found were plotted vs. time and the results are shown in Figure 5.12.

**Table 17: San Antonio soil wet analysis mineral quantification**

Minerals	San Antonio		
	Wet Analysis		
	Air-dried	Wet short term	Wet long term
Anhydrite	1.1%	0.0%	-
Illite	0.0%	0.7%	33.0%
Calcite	74.0%	43.8%	16.7%
Kaolinite	0.0%	22.2%	-
Gypsum	16.2%	15.9%	44.0%
Dozyite	-	14.5%	-
Ettringite	0.0%	0.0%	-
Thaumasite	7.4%	2.9%	1.9%
Montmorillonite	1.3%	-	0.4%



**Figure 94: Time scale indicating Calcite transformation into Gypsum in San Antonio soil**

The wet analysis yielded important results regarding other phenomenon's related to swelling of soil through mineral transformation. The changes of Calcite and Gypsum observed throughout the one year period (Calcite decreasing and Gypsum increasing) gives validity to the hypothesis that the volume change of expansive soil is not just due to the presence of expansive clay mineralogy, but also due to the formation of Gypsum via mineral transformation from Calcite when Sulfates are present in the soil. Furthermore, the formation of Gypsum should be expected with time if Sulfate and Calcites are available for the reaction to occur. Therefore, the identification of salts such as Sulfates and Calcium should be imperative in the identification of expansive soil properties.



#### **5.4 Quantification of Minerals by Correlations with Other Properties**

Not only are there direct measurements in the quantification of clay minerals in soil specimens, but there are also ways to quantify minerals through correlations with known properties of clay minerals.

When trying to quantify clay mineralogy it has been customary to lump all the clay minerals into three common categories: Kaolinite, Illite, and Montmorillonite. While this practice has been a good baseline in the quantification of clay minerals, the soil appears to have more components that have been overlooked in reported predictive methods aimed at quantifying expansive clay minerals.

In this study, Arizona State University (ASU) and University of Texas Arlington (UTA) collaborated to embark on the experimentation of soil properties. UTA developed a model that takes soil characteristics such as Total Potassium (K), Specific Surface Area (SSA), and Cation Exchange Capacity (CEC) and relates them to the type of clay minerals present in the soil. The model is solved by a non-linear regression analysis using the Solver® function in Excel® (Chittoori & Puppala, 2011); which uses the aforementioned three known soil properties and determine three unknown quantities: Kaolinite, Illite, and Montmorillonite. Obviously, this method limits the types of clay minerals one can find to only three; which creates a high probability that the model does not capture other important minerals that can be present in the soil specimen; and therefore, overestimates the predicted clay quantities. The results obtained with the UTA model are presented in Table 5.5.

**Table 18: Mineral percentages obtained with UTA method**

Soil	% Kaolinite	% Illite	% Smectite
Anthem	50.27	24.45	25.28
San Antonio	31.21	30.93	37.87
Colorado	29.25	35.00	35.75

When the mineral quantification from UTA was compared with the mineral quantifications obtained at ASU, as shown in Figure 5.6 through 5.8, there seems to be some discrepancies. The data presented from the ASU quantifications are given in a range from lowest quantification to the highest based on the treatments. The Montmorillonite quantification in the ASU observation is the summation of the Smectite family.

**Table 19: Comparison of mineral quantifications of Anthem soil from UTA and ASU**

Soil	% Kaolinite	% Illite	% Smectite
Anthem (UTA)	50.27	24.45	25.28
Anthem (ASU C+S)	4.9	23.1-55.5	2.6-7.2
Anthem (ASU C)	0	32.8-97.4	1.6-7.5

**Table 20: Comparison of mineral quantification of San Antonio soil from UTA and ASU**

Soil	% Kaolinite	% Illite	% Smectite
San Antonio (UTA)	31.21	30.93	37.87
San Antonio (ASU C+S)	22.2	0.7-71.2	0.4-14.5
San Antonio (ASU C)	0	37.8-98.2	0.4-11.5

**Table 21: Comparison of mineral quantification of Colorado soil from UTA and ASU**

Soil	% Kaolinite	% Illite	% Smectite
Colorado (UTA)	29.25	35.00	35.75
Colorado (ASU C+S)	0	54.9-100	5.2-28.4
Colorado (ASU C)	0	38.1-96.8	2.1

As observed, the UTA method considers the entire specimen be made up of the three chosen clay minerals. The analysis is missing not only other clay minerals that can be important to the characterization of swelling behavior but also, it misses other mechanisms affecting the swell potential such as Gypsification and the formation of other expansive minerals during the life of the structure. It is also shown that of the three soils quantified by UTA model, the only mineral that falls within the range measured at ASU is the Illite. This could be justifiable because the element that bonds the 2:1 sheets together in Illite is Potassium. This is one of the dependent variables in UTAs model that helps in the mineral quantification. The other two mineral groups do not fall within the range of values found at ASU. This may indicate that the quantifications indicated by UTA might lump the error in the Kaolinite and Montmorillonite (Smectitie family) quantifications due to the dependent properties used in the model. Though UTA's proposed method gives an approximated estimation of the clay minerals that can affect soil expansivity, the results are considered incomplete.

### **5.5 Summary and Conclusions**

The findings in this chapter have shed some light on the means and methods to quantify expansive minerals. The following conclusions were reached:

- 1) The trend of Calcite leaving the system and Gypsum entering the system indicates that the process of Gypsification was happening. Gypsification occurs after the dissociation of Calcite which reacts with the Sulfates present in the soil. In doing so, Gypsum forms, which is a mineral associated with high volume increase in soils. The formation of Gypsum was observed after one year period, as long as Sulfates and Calcites were available for the reaction to occur.
- 2) Due to the proximity of the two primary peaks of Illite and Montmorillonite in a diffractogram, it is difficult to identify them properly. The treatment of the soil with Glycol allows the two peaks to separate. Therefore, to recognize Smectite minerals in the soil, the specimens should be always treated with Glycol and only the clay fraction of the soil should be used if quantification of expansive minerals is desired. The inundation of samples with the glycol also aids in the identification of mixed-layer clays.
- 3) When considering the amount of Illite present in both sets, clay+silt and clay, it was difficult to quantify the samples when using the PANalytical quantification tool due to the masking effect that Illite creates on Montmorillonite.
- 4) It was shown that the formation of Ettringite and Thaumasite appeared after the high temperature treatments, whether the specimens were composed of the clay+silt fraction or only the clay fraction. This observation agrees and validates a reported process observed in concrete known as Delayed Ettringite Formation (DEF). Though this process has been only referred to Ettringite

formation; it was also shown that Thaumasite can follow suit. This is due to the close chemical composition of the two minerals.

- 5) The results obtained at ASU were compared to a mineral quantification method proposed by the University of Texas at Austin. It was shown the amount of Illite predicted by UTA was close or within the range measured at ASU, for the three soils. The amounts of Kaolinite and Montmorillonite (Smectite) predicted by the UTA method were not in agreement with the results obtained at ASU.
- 6) It has been presented in this Chapter that not only the presence of expansive clay minerals contributes to the swell potential of soil but also processes such as Gypsification and Delayed Ettringite Formation must be considered when Calcite and Sulfates are available in the soil, or when the soil can be subjected to high temperatures.

## CHAPTER 6

### ANALYSIS OF THE EFFECT OF CLAY MINERALS AND SALT CONTENT IN THE ESTIMATION OF SWELLING POTENTIAL

#### **6.1 Introduction**

As mentioned in Chapter 2, there are correlations available in the literature to estimate the swelling potential of soils. These different correlations use engineering index properties as dependent variables but fail to include the impact of parameters related to the soil mineralogy. This Chapter presents an analysis of the significance of the soil index and mineralogy properties in the estimation of free swell on the compacted material for the soils of this study. In order to accomplish this objective, a correlation matrix was obtained, which included the clay minerals and salt quantities found in the three soils after different treatments. The publications of many predictive equations for the swell potential of soil will be compared with the actual data that was collected in this study. The most significant parameters are presented.

#### **6.2 Swelling Correlations Comparison**

As mentioned in previous chapters, the soil free swell can be estimated by using correlations with soil properties available in the literature. Several models that allow for an estimated swelling potential for the soil are presented in Table 6.1.

**Table 22: Predictive equations for the swell potential of soils from different authors**

Author	Year	Predictive Equation
Seed et al.	1962	$S = 3.6 \times 10^{-5} * 60 * PI^{2.44}$
Seed et al.	1962	$S = 3.6 \times 10^{-5} * A^{2.44} * C^{3.44}$
Chen, F.H.	1988	$S = 0.2558e^{0.08381(PI)}$
Basma, A.A.	1993	$S_{100} = 0.00064 * PI^{1.37} * C^{1.37}$
Al-Shayea, N.A.	2001	$S = 0.143C$ <b>when C &lt; 20%</b> $S = 0.55C - 8.25$ <b>when 20% &lt; C &lt; 60%</b>
Yilmaz, I.	2006	$S = 0.155LL - 0.00763CEC - 2.04$
Zapata et al.	2006	$S_{@100\ psf} = 0.2014 * wPI + 1.682$

Where:

$S$  is the Swell Potential @ 6.9 kPa overburden (compacted in the optimum moisture content and the maximum dry density),

$PI$  is the Plasticity Index,

$I_s$  is the Shrinkage Index (LL-SL),

$LL$  is the Liquid Limit,

$SL$  is the Shrinkage Limit,

$C$  is the clay content,

$S_{100}$  is the swell percent at 100% of MDD,

$S_{@ 100\ psf}$  is the Expansion Index @ 100 psf with optimum water content, minus 2%, and compacted to maximum dry density.

Once this list of predictive equations was compiled, the free swell data on the compacted material from this study was compared with their results. The free swell for the three soils in this study is summarized in Table 6.2. Entering in the specific properties that are called for in the predictive equations in Table 6.1 yields the results also shown in Table 6.2.

**Table 23: Measured free swell data for Anthem, Colorado, and San Antonio soils and Results obtained with predictive equations**

	Anthem	Colorado	San Antonio
Measured Free Swell (%)	8.6	18.7	14.1

Author	Year	Anthem	Colorado	San Antonio
Seed et al.	1962	6.71	19.73	20.9
Seed et al.	1962	3.62	15.79	18.78
Chen	1988	2.46	8.64	9.4
Basma.	1993	6.81	21.91	26.01
Al-Shayea.	2001	9.46	18.48	21.34
Yilmaz	2006	4.85	7.34	7.6
Zapata et al.	2006	6.52	9.94	9.34

Analyzing these results show that Seed’s, Basma’s, and Al-Shayea’s predictive equations somewhat match the free swell measured for Anthem and Colorado soils. For the San Antonio soils, none of the predicting equations yielded a reasonable estimation of the free swell obtained in the laboratory. For Anthem soil, results from Seed et al. and Basma models are within 23% to 25% of the measured free swell, while results from Al-Shayea are within 10%. For the Colorado soil, two of the four predicting equations yielded results within 15% to 17% of the measured value for Seed and Basma, respectively; but again, Al-Shayea method predicted a result within 2% of the measured value. Even though four of the equations analyzed yield reasonable prediction of the amount of free swell for two of the expansive soils in this study, there is no one equation that explains the behavior of the three soils on this study.

### 6.3 Correlations Matrix

In order to estimate the significance of different soil index properties and mineralogy properties that affect the swell behavior of the soil, a large set of soils



properties were determined and used to create a correlations matrix. Forty different soil properties were compiled and analyzed in Excel. Table 6.3 presents the results of correlations between index/mineralogy properties and the two parameters that are commonly used to define the swell potential of the soil: free swell percentage and swelling pressure.

**Table 24: Data from the correlation matrix the free swell and pressure data**

	<i>Free Swell %</i>	<i>Swell Pressure (kPa)</i>
Free Swell %	1.00	
Swell Pressure (kPa)	0.99	1.00
F.S.I (%)	0.14	0.03
PI	0.87	0.81
LL	0.85	0.78
PL	0.70	0.62
SL	-0.89	-0.84
% Pass 200	0.83	0.88
% clay	0.77	0.69
Activity	0.35	0.45
wPI	0.96	0.93
GI	-0.93	-0.88
CEC (meq/100g)	0.78	0.70
Ca (ppm)	0.01	-0.10
Na (ppm)	-0.86	-0.91
S (ppm)	-0.23	-0.33
SO4 (ppm)	-0.22	-0.32
% Kaolinite	0.83	0.89
% Illite	-0.94	-0.97
% Montmorillonite	-0.12	-0.23
SSA (m <sup>2</sup> /g)	0.99	1.00
Δ d(001) (Å)	0.95	0.91
C-AD	-0.65	-0.73
C-W ST	-0.85	-0.90
C-W LT	-1.00	-1.00
G -AD	0.90	0.95
G-W ST	-0.79	-0.85
G-W LT	-0.44	-0.54

C-AD <sub>(C+S)</sub>	-1.00	-0.98
C-G <sub>(C+S)</sub>	-0.96	-0.93
C-400C <sub>(C+S)</sub>	-0.59	-0.68
C-550C <sub>(C+S)</sub>	-0.50	-0.59
G-AD <sub>(C+S)</sub>	0.44	0.54
G-G <sub>(C+S)</sub>	-0.21	-0.32
G-400C <sub>(C+S)</sub>	-0.61	-0.52
G-550C <sub>(C+S)</sub>	-0.97	-0.99
E-400C <sub>(C+S)</sub>	0.06	-0.05
E-550C <sub>(C+S)</sub>	-0.92	-0.88
T-400C <sub>(C+S)</sub>	0.86	0.79
T-550C <sub>(C+S)</sub>	0.00	0.00

Where:

$\Delta d(001)$  is the change in d-spacing (see 6.3.1 for definition),

$C-AD$  is the amount of Calcite on air-dried specimens using PANalytical software.

$C-W ST$  is the amount of Calcite on wet (short term) specimens using PANalytical software,

$C-W LT$  is the amount of Calcite on wet (long term) specimens using the PANalytical method,

$G-AD$  is the amount of Gypsum on air-dried specimens using the PANalytical method,

$G-W ST$  is the quantification of the Gypsum wet short term using the PANalytical method,

$G-W LT$  is the quantification of the Gypsum wet long term using the PANalytical method,

$C-AD_{(C+S)}$  is the quantification of the Calcite air-dried of a Clay+Silt fraction sample using the PANalytical method,

$C-G_{(C+S)}$  is the quantification of the Calcite after glycol inundation of a Clay+Silt fraction sample using the PANalytical method,

$C-400C_{(C+S)}$  is the quantification of the Calcite after heating to  $400^{\circ}C$  of a Clay+Silt fraction sample using the PANalytical method,

$C-550C_{(C+S)}$  is the quantification of the Calcite after heating to  $550^{\circ}C$  of a Clay+Silt fraction sample using the PANalytical method,

$G-AD_{(C+S)}$  is the quantification of the Gypsum air-dried of a Clay+Silt fraction sample using the PANalytical method,

$G-G_{(C+S)}$  is the quantification of Gypsum after glycol inundation of a Clay+Silt fraction sample using the PANalytical method,

$G-400C_{(C+S)}$  is the quantification of Gypsum after heating to  $400^{\circ}C$  of a Clay+Silt fraction sample using the PANalytical method,

$G-550C_{(C+S)}$  is the quantification of Gypsum after heating to  $550^{\circ}C$  of a Clay+Silt fraction sample using the PANalytical method,

$E-400C_{(C+S)}$  is the quantification of Ettringite after heating to  $400^{\circ}C$  of a Clay+Silt fraction sample using the PANalytical method,

$E-550C_{(C+S)}$  is the quantification of Ettringite after heating to  $550^{\circ}C$  of a Clay+Silt fraction sample using the PANalytical method,

$T-400C_{(C+S)}$  is the quantification of Thaumasite after heating to  $400^{\circ}C$  of a Clay+Silt fraction sample using the PANalytical method,

$T-550C_{(C+S)}$  is the quantification of Thaumasite after heating to  $550^{\circ}C$  of a Clay+Silt fraction sample using the PANalytical method.

The matrix yields Pearson product-moment correlation coefficient, also known as R. This is a measure of the strength and direction of the linear relationship between two variables that is defined as the covariance of the variables divided by the product of their standard deviations. The values produced are between -1 and 1. The closer to -1 or 1, the more significant the soil property is in explaining the free swell and swell potential result.

**Table 25: Summary of parameters that have high correlation values**

Free Swell		
> 0.90	Index Properties: Mineralogy:	wPI, GI, SSA, %I, C-WLT, G-AD, C-AD, C-G, G-550, Δd, E-550C
> 0.80	Index Properties: Mineralogy:	PI, LL, SL, P200, Na, %K, C-WST, T-400C
Swell Potential		
> 0.90	Index Properties: Mineralogy:	wPI, SSA, Na, C-WST, C-WLT, G-AD, C-AD, C-G, G-550, %I, Δd
> 0.80	Index Properties: Mineralogy:	PI, SL, P200, GI G-WST, %K, E-550C

Looking at the correlation matrix results in Table 6.3, there are several properties (index and mineralogy) that seem to have a significant relationships to the swelling of the soils in this study and the chosen parameters. Those parameters that yield a value of +/- 0.9 or higher have been focused on in Table 6.4. In the following sections, the correlations with free swell and swell potential of the soils will bring about a discussion to how these significant parameters could cause such a significant correlation value.

### 6.3.1 Parameters that Correlate with Free Swell

The soil properties that have traditionally been used in the prediction and identification of swell in soils, in research and practice, are basic index properties such as the plastic limit, plasticity index, liquid limit, shrinkage limit and percent passing #200.

These properties, when used independently, give a moderate indication of swell with a correlation value between 0.7 and 0.89. The index properties that combine one or more single index properties such as wPI and GI yielded stronger correlations, with values higher than +/- 0.93. The wPI was the best performer within the index properties used in the analysis. The wPI combines the percent passing #200 and the plasticity index, as explained in Chapter 2. The GI was the next best performer within the index properties used in the analysis. The GI combines the percent passing #200, the liquid limit and the plasticity index, and was also explained in Chapter 2. When observing these parameters in their coefficient of determination regressions, they both perform well as shown in Table 6.5.

**Table 26: Summary of regressions for parameters with free swell**

Parameter	R	Linear Equation	R <sup>2</sup>	Best fit Regression Equation	R <sup>2</sup>
<b>Index Properties</b>					
wPI	0.96	y = 0.0052x - 0.0418	0.92	y = 0.0313e <sup>0.0415x</sup>	0.97
GI	-0.93	y = 0.0042x - 0.025	0.95	y = 0.036 e <sup>0.0336x</sup>	0.99
<b>Mineralogy Properties</b>					
% Illite	-0.94	y = -0.0155x + 0.1929	0.89	y = -0.0155x + 0.1929	0.89
SSA (m <sup>2</sup> /g)	0.99	y = 0.001x - 0.0733	0.98	y = 0.2115ln(x) - 0.9969	0.995
Δ d <sub>(001)</sub> (Å)	0.95	y = 0.0141x + 0.0305	0.90	y = 0.0555e <sup>0.1129x</sup>	0.96

Not only is Pearson product-moment correlation coefficient shown in Table XX, but the linear regression equation is shown as its independent variable relates to free swell; along with its coefficient of determination, R<sup>2</sup>. Beside the linear regression equation shown in Table 6.5, the regression equation that best fits the data according to the coefficient of determination in regards to its independent variable is also given. In the linear regression the wPIs R<sup>2</sup> value is 0.92 while the GIs R<sup>2</sup> is 0.95. Since not all data

conforms to a straight line the regression analysis also observed what function would result in the best coefficient of determination. As shown in Table 6.5, the wPIs coefficient of determination is 0.97 and GIs is 0.99 both with an exponential function. With such a strong correlation one would need to consider that these two index properties should play a powerful role in the soils free swell capabilities.

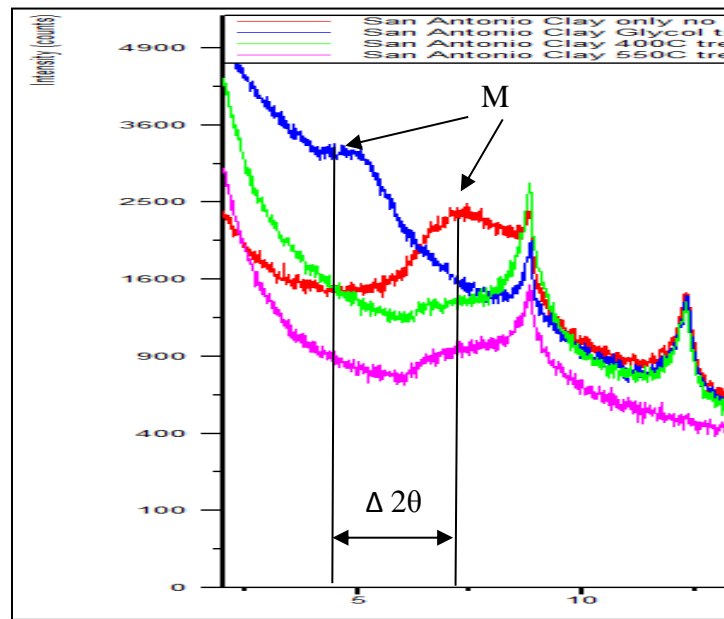
Among the mineralogy parameters, the specific surface area yielded a correlation value of 0.99, (Table 6.5) indicating that its effect on the free swell of soils is very significant and it is an excellent indicator of the free swell measured for the soils in this study. This is interesting because SSA is much like the grain-size distribution of a soil, in that it is unaffected by external variables (Cerato, 2002); however, grain size distribution parameters alone do not explain the swelling behavior of the soil. It is also presented that the SSA has a high significant with both its linear regression and its best fit regression, a logarithmic function, with their coefficients of determination being 0.98 and 0.995, respectively.

In regards to the correlation values that yielded promising indication to the mineralogical study in this paper, there are five other quantities that yielded values greater than +/-0.9 of interest. One of these is the Calcite amount measured after the specimen was wetted and let it soaked for a longer period of time (one year) and then interpreted using the PANalytical software. Its correlation value was found to be -1, which gives a strong indication that as Calcite content decreases, the free swell of the soil increases. The second parameter found to be significant was the amount of Gypsum in the air-dried (untreated) specimen when analyzed with the PANalytical method. The value being greater than 0.90 indicate that there is a strong correlation between the

amount of Gypsum and the free swell of the soil. It should be noted that the Gypsum amount measured on specimens wetted (short term condition) also yielded values greater than -0.79. This gives strong evidence to the theory proposed in this paper regarding mineral transformation. Another interesting correlation shown was the value between the clay+silt specimen heated to 550°C Gypsum quantification and free swell collected in the laboratory. A correlation of -0.97 was found. With Gypsum being a Sulfate based material, the same as Ettringite, gives significance towards the previous statement of Ettringite forming at high temperatures. The same trend can be seen with a correlation value for Ettringite quantification when the clay+silt specimen was heated to 550°C having a correlation value with free swell of -0.92.

Other correlation values of interest are the percentage of Illite and the change in d-spacing. With such a strong correlation, -0.94 and 0.95, respectively, there is a strong indication that the clays having a mixed-layer structure, which was explained in Chapters 2 and 5. Mixed-layers of Illite are usually over looked as just being an Illite mineral or are quantified but not given any attention in practice due to the non-swelling behavior of Illite. Its correlation analysis, which is presented in Table XX, indicated that the linear regression equation has a coefficient of determination of 0.89 which is the same as the best fit regression, a linear equation. Though the coefficient of determination is 0.89, this give a strong indication of the statement presented previously about mixed-layer clays. In regards to the change is d-spacing, this refers to a change in the primary Montmorillonite peak from its natural state, air-died, and the same sample being inundated with glycol. A visual representation is presented in Figure 6.1. The change in d-spacing of the Montmorillonite's dry peak, in the red, to its maximum swell, in the blue, gives the

greatest change in  $2\theta$ . The difference in the  $2\theta$  can be converted using Bragg's Law to yield the maximum change in d-spacing of that soil. The regression analysis of this change in d-spacing has a strong linear regression with an  $R^2$  value of 0.90, but observing the best fit regression an exponential regression has the best coefficient of determination, 0.96. The change in d-spacing is a quantifiable number in Angstroms, and therefore become a good candidate to identify swelling materials out of a diffractogram.



**Figure 95: Change in  $2\theta$  between an air-dried and glycol sample, focusing on the primary Montmorillonite peak.**

### 6.3.2 Parameters that Correlate with Swell Pressure

Observing the swell pressure column in Table 6.3 there are some soil properties that strongly correlate to the swell pressure. Again, the index properties, the plastic index and liquid limit, give a moderate indication to the correlation of swell potential. These properties, plasticity index, liquid limit, plastic limit, shrinkage limit, and the percent passing a #200 sieve, when used independently, give a moderate indication of swell with a correlation value between 0.62 to 0.88. Continuing through the swell potential column,



many of the same high correlation values for swell pressure also have the same correlation, in regards to the same properties, as the free swell column. A summary of the important correlations can be seen in Table 6.6, which includes the Pearson product-moment correlation coefficient, the linear regression equation is shown as its independent variable relates to swell potential; along with its coefficient of determination,  $R^2$ . Beside the linear regression equation shown in Table 6.6, the regression equation that best fits the data according to the coefficient of determination in regards to its independent variable is also given.

**Table 27: Summary of regressions for parameters with swell pressure**

Parameter	R	Linear Equation	$R^2$	Best fit Regression Equation	$R^2$
<b>Index Properties</b>					
wPI	0.93	$y = 6.7632x - 71.347$	0.86	$y = 31.383e^{0.0457x}$	0.94
GI	-0.88	$y = 5.5402x - 50.733$	0.89	$y = 36.434e^{0.0372x}$	0.96
<b>Mineralogy Properties</b>					
% Illite	-0.97	$y = -21.631x + 238.7$	0.95	$y = -21.631x + 238.7$	0.95
SSA ( $m^2/g$ )	1.00	$y = 0.001x - 0.0733$	0.999	$y = 0.001x - 0.0733$	0.999
$\Delta d_{(001)}$ (Å)	0.91	$y = 18.201x + 23.401$	0.83	$y = 59.23e^{0.1239x}$	0.91

In the linear regression the wPIs  $R^2$  value is 0.86 while the GIs  $R^2$  is 0.89. Since not all data conforms to a straight line the regression analysis also observed what function would result in the best coefficient of determination. As shown in Table 6.6, the wPIs coefficient of determination for the best fit regression as 0.94 and GIs is 0.96 both with an exponential function. With such a strong correlation one would need to consider that these two index properties should play a powerful role in the soils swell pressure capabilities.

Among the mineralogy parameters, the specific surface area yielded a correlation value of 1.00, (Table 6.6) indicating that its effect on the swell pressure of soils is very significant and it is an excellent indicator of the swell pressure measured for the soils in this study. It is also presented that the SSA has a high significant with both its linear regression and its best fit regression, also linear, with their coefficients of determination being 0.999.

In regards to the correlation values that yielded promising indication to the mineralogical study in this paper, there are four other quantities that yielded values greater than +/-0.9 of interest. One of these is the Calcite amount measured after the specimen was wetted and let it soaked for a longer period of time (one year) and then interpreted using the PANalytical software. Its correlation value was found to be -1, which gives a strong indication that as Calcite content decreases, the swell pressure of the soil increases. The second parameter found to be significant was the amount of Gypsum in the air-dried (untreated) specimen when analyzed with the PANalytical method. The value being greater than 0.95 indicate that there is a strong correlation between the amount of Gypsum and the swell pressure of the soil. It should be noted that the Gypsum amount measured on specimens wetted (short term condition) also yielded values greater than -0.85. This gives strong evidence to the theory proposed in this paper regarding mineral transformation. Another interesting correlation shown was the value between the clay+silt specimen heated to 550°C Gypsum quantification and swell pressure collected in the laboratory. A correlation of -0.99 was found. With Gypsum being a Sulfate based material, the same as Ettringite, gives significance towards the previous statement of Ettringite forming at high temperatures. The same trend can be seen with a correlation

value for Ettringite quantification when the clay+silt specimen was heated to 550°C having a correlation value with swell pressure of -0.88.

Lastly, the other correlation values of interest are the percentage of Illite and the change in d-spacing. With such a strong correlation, -0.97 and 0.91, respectively, there is a strong indication that the clays having a mixed-layer structure, which was explained in Chapters 2 and 5. Mixed-layers of Illite are usually over looked as just being an Illite mineral or are quantified but not given any attention in practice due to the non-swelling behavior of Illite. Its correlation analysis, which is presented in Table 6.6, indicated that the linear regression equation has a coefficient of determination of 0.89 which is the same as the best fit regression, a linear equation. Though the coefficient of determination is 0.89, this give a string indication of the statement presented previously about mixed-layer clays. In regards to the change is d-spacing, the regression analysis of this change in d-spacing has a strong linear regression with an  $R^2$  value of 0.83, but observing the best fit regression an exponential regression has the best coefficient of determination, 0.91.

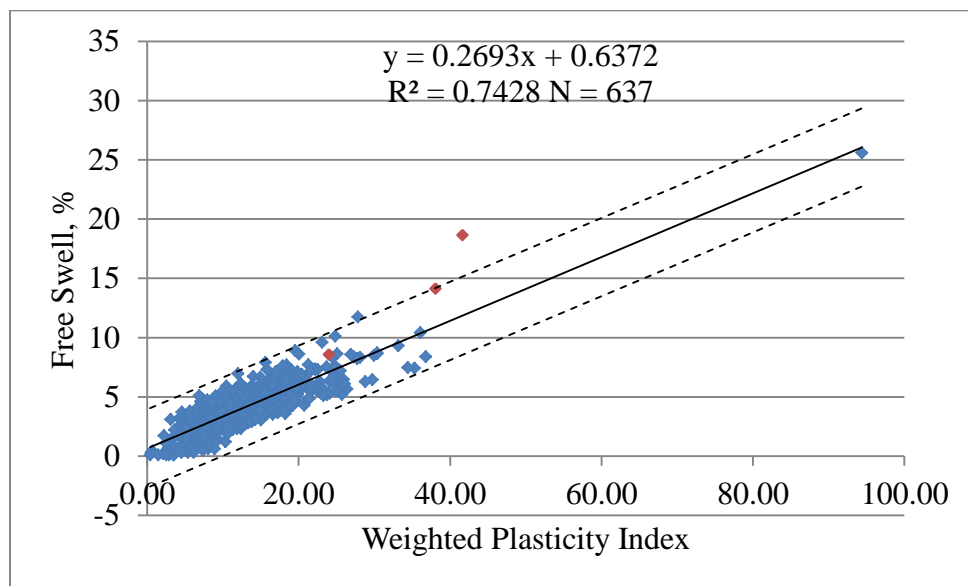
#### **6.4 A closer look at properties that have a strong correlation with free swell**

In order to consider the relationship presented previously regarding wPI, Group Index, and the change in d-spacing, the next section is dedicated to these parameters and their effect on the swell properties of soils. The wPI and Group Index were evaluated with a collection of data point from Arizona, while the data for determining the d-spacing is shown. The data was obtained from geotechnical engineering firms around the Phoenix (Arizona) valley and from field sampling and laboratory testing performed by ASU under a project funded by the Homebuilders Association of Central Arizona, HBACA, aimed at studying the performance of slab on grade residential foundations on expansive soils

(Houston et al., 2006). The data collected included, among others, the maximum (free) swell or expansion and soil index properties such as Atterberg limits and grain-size distribution.

#### 6.4.1 Correlation of wPI and Free Swell

The data collected was used to determine the weighted plasticity index of the soils gathered from the Phoenix geotechnical engineering firms. There was 637 data points, shown in Appendix B, that were applicable for observation of the weighted plasticity index with the free swell collected. This data can be seen in Figure 6.2, along with a linear regression and its coefficient of determination,  $R^2$ .



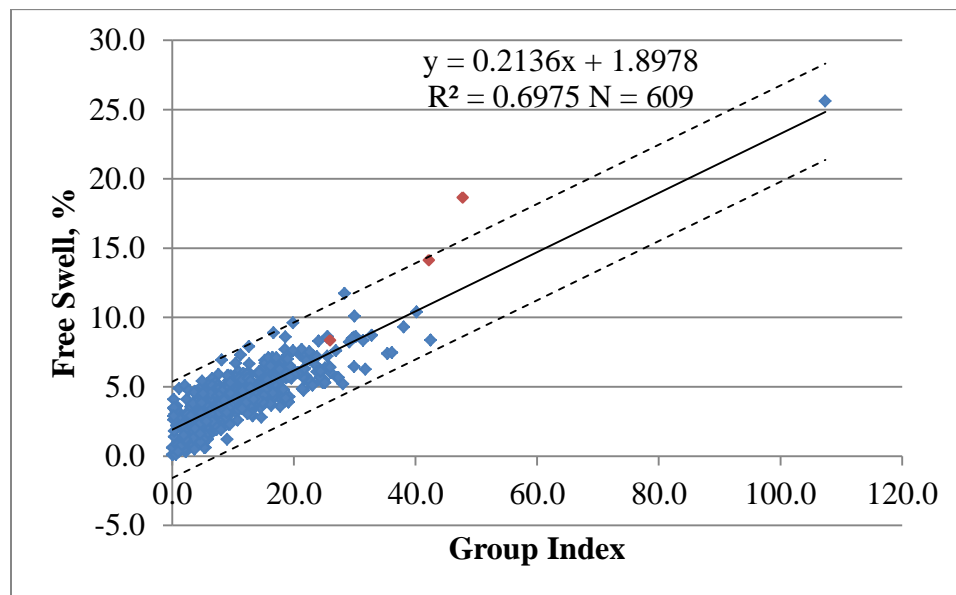
**Figure 96: Linear regression of Free Swell vs. Weighted Plasticity Index with this study's data in red.**

Among the 637 data points, the three soils from this study were also included, as shown in red. Also shown on Figure 6.2 is a  $3\sigma$  standard deviation of the collected data. This shows that more than 99% of the data is within this standard deviation indicating the goodness of fit of the data. This is reinforced by the coefficient of determination of the

linear regression being 0.74, which shows a strong relationship between the free swell of the soil and its weighted plasticity index.

#### 6.4.2 Correlation of GI and Free Swell

The same pool of data from the Phoenix area was used to find the Group Index of the soils. There was 609 data points, shown in Appendix B, that were applicable for observation of the Group Index with the free swell collected. This data can be seen in Figure 6.3, along with a linear regression and its coefficient of determination,  $R^2$ .



**Figure 97: Linear regression of Swell Pressure vs. Group Index with this study's data in red.**

Among the 609 data points, the three soils from this study were also included, as shown in red. Also shown on Figure 6.3 is a  $3\sigma$  standard deviation of the collected data. This shows that more than 99% of the data is within this standard deviation indicating the goodness of fit of the data. This is reinforced by the coefficient of determination of the linear regression being 0.70, which shows a strong relationship between the free swell of the soil and its group index.

### 6.4.3 The correlation of D-spacing

The data acquired for the change in d-spacing is presented in Tables 6.7, 6.8, and 6.9, which include the  $2\theta$  values for each soil at their untreated state, after glycol treatment, after wet short term, and wet long term treatments, for the three soils, respectively., The d-spacing can be found with Braggs Law once the  $2\theta$  data is known. Once the d-spacing was determined for each treatment the difference between the untreated and Glycol, wet short term, and wet long term were determined. This yields a quantifiable value that is measurable in Angstroms. No data presented indicates that the Montmorillonite peak could not be found.

**Table 28: Anthem soil  $2\theta$ , d-spacing, and  $\Delta$ d-spacing data obtained from the different treatments shown**

Anthem	$2\theta$ , degrees	d-spacing, Å	$\Delta$ d-spacing
Untreated	6.1996	14.25	-
Glycol	4.9776	17.7391	3.489
Wet short term	-	-	-
Wet long term	-	-	-

**Table 29: San Antonio soil  $2\theta$ , d-spacing, and  $\Delta$ d-spacing data obtained from the different treatments shown**

San Antonio	$2\theta$ , degrees	d-spacing, Å	$\Delta$ d-spacing
Untreated	7.4086	11.9229	-
Glycol	4.3926	20.100	8.1773
Wet short term	-	-	-
Wet long term	4.3903	20.1107	8.1878

**Table 30: Colorado soil 2θ, d-spacing, and Δd-spacing data obtained from the different treatments shown**

Colorado	2θ, degrees	d-spacing, Å	Δd-spacing
Untreated	7.3306	12.04995	-
Glycol	5.0036	17.64698	5.59703
Wet short term	-	-	-
Wet long term	4.3903	20.11071	8.06076

As shown in Table 6.7, 6.8, and 6.9, 2θ data is easily obtained from the untreated specimens. While, though an easier method of preparation, the wet data is missing due to the primary Smectite peak not being easily identifiable. This was not the case for the Glycol treated samples, where the primary Smectite peak was easily defined. Though the Glycol treatment process is more involved, it yielded the most consistent results.

### **6.5 Summary and Conclusion**

After reflecting on this chapter there are many soil properties that have an effect on the swelling of the soils in this study. The properties that you would expect such as the plastic limit, liquid limit, shrinkage limit, etc. have a respectable correlation value. These index properties have been used through soil mechanics to identify behaviors of soil, swelling of soil being one of them. Computed values such as wPI and GI use the index properties, such as PI, percent passing a #200 sieve, and SL, to determine their value. It is no wonder that the acquired values of wPI and GI have such a strong correlation to the swelling of the soils in this study. This gives strong indication that use of correlation to represent swelling with a single parameter can give an okay representation, but to achieve more detail the use of combined parameters yields much better correlations which in turn gives a better representation of the swell potential. What correlation values that made head way in this study were the correlation which linked the Gypsification theory of

Calcite and Sulfate creating Gypsum over time. With Gypsum being a swelling material, just the knowledge of the soils index properties to determine swell gives a limited understand of how the soil behaviors. The same can be said for the formation of Ettringite, since this mineral is a Sulfate bearing material and as shown with its correlation value related to the swelling of soils. Knowing the complete composition, such as the Sulfate, Calcite, and Gypsum content, reveals a much larger picture as to what is the cause of swelling soils, in specific cases, and should be considered in the swell potential of expansive soils. Another link to swelling found in this study was the use of diffractograms determined in the X-Ray Diffraction (XRD) analysis to identify Montmorillonite peaks at its natural state, air-dried, and the same sample inundated with glycol to give the Montmorillonite its maximum swell. The change in the two tests would give a change in d-spacing. This change in d-spacing is related to how much the soil swells. This is shown with its strong correlation value in Table 6.3. This gives an indication that d-spacing could be used as a computed value to help examine how the swell behavior of a soil could be determined using XRD diffractograms.



## CHAPTER 7

### CONCLUSIONS AND RECOMMENDATIONS FOR FUTURE RESEARCH

#### **7.1 Introduction**

When this study was in its infancy the investigation was set out to identify the clay minerals that were highly expansive in three different soils, San Antonio, Texas, Denver, Colorado, and Anthem Arizona. In turn, this investigation grew in to five main objectives for this study, as indicated in Chapter 1. This final chapter covers the main conclusions of the research described in this thesis, together with recommendations for future work expanding on phenomenon presented.

#### **7.2 Conclusions of study**

Upon completion of the research described in this thesis it has provided considerable insight into expansive soils and the identification of the minerals that govern the expansive nature of said soils. In the following sections, conclusions of the objectives of this study and the various aspects regarding this research are summarized.

##### **7.2.1 Objective 1**

A detailed analysis of the methods currently used to quantify clay minerals was investigated along with state-of-the-art methods. X-ray diffraction (XRD) is a common practice used to qualify the soil physical make-up, but however it is able to quantify the composition. Through relentless use of XRD analysis used to investigate and compare methods of this analysis yielded interesting results. The two different methods compared, PANalytical and RockJock, took two different approaches. The two methods gave inconclusive results that were difficult to compare, not to say that the data was not helpful in understanding soil behavior. The quantities might have had different values due to the

different size fractions used in each of the two tests. Also, the PANalytical method observed the signal from  $0^\circ - 65^\circ 2\theta$  while the RockJock method quantified the signal from  $20^\circ - 65^\circ 2\theta$ . The different quantities could also be attributed to the use of an internal standard of aluminum oxide in the RockJock method while the PANalytical method is a non-standardized method. Even the way the two methods justify the quantification is different. The PANalytical method used a Rietveld analysis based on the crystalline structure while the RockJock method uses an internal database of pure mineral standards. If mineral quantification was to be used again in another study, the PANalytical method would be the preferred method. This is due to the minerals passing the #200 sieve, which were used in this study, yield typical behaviors of different soils specimens. These fines are quantifiable in this method, which include expansive clay and other minerals of interest, such as Salts and Sulfates. Further analysis will be needed on the reliability of the data obtained with different interpretation method and after different treatments.

### **7.2.2 Objective 2**

Identifying expansive clay minerals that cause volume change was revealed during the XRD analysis, though not without complications. In the PANalytical analysis, all three soils in this study showed a wide fluctuation in the Smectite swelling minerals.

In the Anthem soil it was revealed that not a lot of swelling minerals were present in the soil. Even after glycolnation of the soil and scanning, the specimen yielded only 7.2% Junitoite, a Smectite mineral that was in our list of minerals of consideration in Chapter 4, section 4.5. What was predominantly present was the mineral Illite. This mineral is known to have a mixed-layer structure, as indicated in Chapter 5. An Illite

mineral interlayered with a Smectite mineral can be difficult to determine if the swelling of the Smectite mineral is going to have any effect on the volume change potential of the soil. Though as indicated in Chapter 6, the identification of the change in d-spacing from an air-dried sample to a glycol treated sample creates a separation of the Smectite peak and the Illite peak which yields a more accurate identification of expansive clay minerals. Other swelling minerals were observed in the temperature treatment of the study. There was a 3.9% increase in the identification in Ettringite and a 21.8% increase in the identification of Thaumasite in the clay fraction of the Anthem specimen once heated to 550°C and 400°C, respectively. This formation of Ettringite after heating could indicate a possibility of a Delayed Ettringite Formation (DEF). Even though Thaumasite is not Ettringite, the chemical make-up of Thaumasite is similar to Ettringite and could develop in the same manner.

The PANalytical analysis of the San Antonio indicates the same type of behavior of mixed-layered clay was also identified, though also having individual swelling minerals in the XRD analysis. This indicates that the San Antonio soil has not only Smectite minerals causing swelling but also mixed layer swelling from the Illite mineral composition. There was also a DEF in the San Antonio soil. It showed that Ettringite had a 2.0% increase and Thaumasite had a 4.5% increase in the 400°C treatment. Thus, San Antonio has many different mechanisms that could relate to the expansivity of the soil.

The PANalytical analysis of the Colorado soil yielded many different minerals that have been known to swell when hydrated. These Smectite minerals include Juncoite, Montmorillonite, Nontronite, and Vermiculite. This indicates that the Colorado's soil swelling behavior has strong influence related to the Smectite mineral

present. Along with the swelling behavior due to the Smectite minerals there is strong evidence that there is a mixed-layer swelling effect on the Colorado soil based on the diffractograms shown in Chapter 4. There was also a slight increase of Thaumasite during the 400°C temperature treatment which strengthens the soil's ability to create this swelling mineral in hot environments, such as the placement of Portland Concrete Cement and Asphaltic Concrete.

These observations and knowledge of minerals that cause volume change when hydrated allow these techniques to gather the quantification of the minerals within the specimens permitted the identification of said minerals and gave insight to the behavior of soil specimens.

### **7.2.3 Objective 3**

Soil in the ground is a completely open system. Substances, water, etc. can move in and out of the system and alter the behavior of the soil. These geochemical reactions can contribute to the swelling behavior of the soil through many different processes. One of which, mineral transformation, was examined in this study.

Observing the quantification of Anhydrite in the PANalytical method explained in Chapter 4, the amount of Calcite had a decreasing trend in its quantification as the time period from an initial wetting period to a long term wetting period progressed. This happened in conjunction with the quantification of Gypsum, where its trend indicated as the time period increases so does the amount of Gypsum. This was presented in Chapter 5.3. With Gypsum having an anion of Sulfate and a cation of Calcium the Calcite mineral can dissociate and re-associate with the free Sulfate in the system. As indicated by Mitchell (2005) the mineral transformation from Calcite to Gypsum creates a 60%

increase in volume. It has been shown that this is happening in the Anthem and would contribute to the soils volume change given the lack of traditional swelling minerals. This was observed in the San Antonio soil as well, with its greatest change in the final time period. The Colorado soil yielded a different result. The Gypsum was present in the beginning stages of the study and was not created in the later stages. This leads one to believe that the mineral transformation has already taken place within the system due to the lack of Calcite in the quantification or that the Calcium or Sulfate has depleted in the system, given the little amounts present in the soils shown in Chapter 3.

The trend of Calcite leaving the system and Gypsum entering the system indicates that the process of Gypsification was happening. Gypsification occurs after the dissociation of Calcite which reacts with the Sulfates present in the soil. In doing so, Gypsum forms, which is a mineral associated with high volume increase in soils. The formation of Gypsum was observed after one year period, as long as Sulfates and Calcites were available for the reaction to occur.

#### **7.2.4 Objective 4**

As mentioned in Chapter 2 there have been publication which give predicative equations that relate index properties to the swelling characteristic of soil. These equations were shown in Chapter 6, Table 6.1. Upon entering the index properties found in this study, the predicted swell was compared with the actual free swell of the soil. Of these predictive equations there were a few that were relative close to the actual free swell of the soils in this laboratory. Of the seven equations three of them had promising results that were relatively close to the data found in the laboratory.

The Seed, Basma, and Al-Shayea predictive equations are the three that match the free swell measured for Anthem and Colorado soils with some relative degree. For the San Antonio soils, none of the predicting equations yielded a reasonable estimation of the free swell obtained in the laboratory. For Anthem soil, results from Seed et al. and Basma models are within twenty-three to twenty-five percent of the measured free swell, while Al-Shayea is within ten percent. For the Colorado soil, two of the four predicting equations yielded results within fifteen to seventeen percent of the measured value for Seed and Basma, respectively; but again, Al-Shayea method predicted a result within two percent of the measured value. Even though four of the equations analyzed yield reasonable prediction of the amount of free swell for two of the expansive soils in this study, there is no one equation that explains the behavior of the soils on this study.

#### **7.2.5 Objective 5**

This objective indicates that the study would identify the most significant parameters associates with swell potential. This was done in Chapter 6 through a correlation matrix and regression analysis. Through this analysis it was shown that there are many soil properties that have an effect on the swelling of the soils in this study. The properties that you would expect such as the plastic limit, liquid limit, shrinkage limit, etc. have a respectable correlation value between 0.62 to 0.88. These index properties have been used through soil mechanics to identify behaviors of soil, swelling of soil being one of them. Computed values such as wPI and GI use the index properties, such as PI, percent passing a #200 sieve, and SL, to determine their value. It is no wonder that the acquired values of wPI and GI have such a strong correlation to the swelling of the soils in this study. This gives strong indication that use of correlation to represent swelling

with a single parameter can give an okay representation, but to achieve more detail the use of combined parameters yields much better correlations which in turn gives a better representation of the swell potential. What correlation values that made head way in this study were the correlation which linked the Gypsification theory of Calcite and Sulfate creating Gypsum over time. With Gypsum being a swelling material, just the knowledge of the soils index properties to determine swell gives a limited understand of how the soil behaviors. The same can be said for the formation of Ettringite, since this mineral is a Sulfate baring material and as shown with it correlation value related to the swelling of soils. Knowing the complete composition, such as the Sulfate, Calcite, and Gypsum content, reveals a much larger picture as to what is the cause of swelling soils, in specific cases, and should considered in the swell potential of expansive soils. Another link to swelling found in this study was the use of diffractograms determined in the X-Ray Diffraction (XRD) analysis to identify Montmorillonite peaks at its natural state, air-dried, and the same sample inundated with glycol to give the Montmorillonite its maximum swell. The change in the two tests would give a change in d-spacing. This change in d-spacing is related to how much the soil swells. This is shown with its strong correlation value in Table 6.3. This gives an indication that d-spacing could be used as a computed value to help examine how the swell behavior of a soil could be determined using XRD diffractograms. After observing the correlation presented it shows that a response to wetting test on compacted soils is a good predictor to identify the effects of expansive soils, but practicing engineers should also consider the Sulfates present in the soil. This is done all the time with the issue of Sulfate attack on concrete, but has not been considered in the context of swell potential. In conjunction with the response to

wetting test on compacted soils, the inclusion of Sulfate testing will link the consideration of Gypsification and Delayed Ettringite Formation.

### **7.3 Future research recommendations**

After completing a task one usually thinks what they would have done differently or would have changed to receive a different outcome. In this section completing a factored tests and X-ray diffraction simplification will be explored.

Knowing what was presented in this study, a more stringent analysis can be implicated. This would include creating a factored test to determine the significance of the presented thesis. First one would need plenty of different soils from around the country. This would include bulk samples and undisturbed samples to create a large factored experiment. Once the samples are acquired the basic properties would need to be determined. This would also include the amount of soluble Sulfates, Calcite, Sodium, etc. A baseline mineral test using the PANalytical method explained in this study would also give the composition of the soils before any changes are done when altering the soils for different factored levels. From here many different theories can be explored. Some of the bulk samples can be spiked with different amounts of Sulfate, Calcite, both Calcite and Sulfate, etc. Knowing the baseline composition and controlling the amounts of which you spike the soil you are able to apply this to swelling test. This can be compared to the baseline swell of the soil without any mineral additions to the soil. One can also evaluate the amount of mineral transformation. Though, as indicated in this study the testing would take a sufficient amount of time for the transformation to take place. To evaluate mineral transformation effects on the swelling of soils, a baseline of the soil samples can be started with, both bulk and undisturbed samples. These samples would be placed in



consolidometers and distilled water or water that is free of ions. Letting these samples sit under a free load weight and observing their swell for a substantial amount of time to allow the mineral change to occur, a year or more, should suffice. When the mineral transformation has taken place the sample should be removed and a XRD analysis completed on them using the same PANalytical procedure that was done for the baseline results. If more specimens can be made to evaluate the mineral composition at different time periods, three months, six months, etc. this would give a better of the time phase needed for the transformation to be completed. This procedure can also be done with spiked sample to do a statistical comparison of significance.

Given these recommendations there would need to be careful consideration to how the test would need to be observed and performed given the complexity of spiking samples, mineral identification, the amount of samples to have a reasonable distribution, and time needed to complete the test. The completion of these recommendations would further improve on the thesis presented in this study.

## REFERENCES

- Arnepalli, D. N. (2008). Comparison of Methods for Determining Specific-surface Area of Fine-grained Soils. *Geotechnical and Geological Engineering*, 121-132.
- Association, P. C. (2013, August 11). *PCA*. Retrieved from Portland Cement Association: [http://www.cement.org/tech/faq\\_DEF.asp](http://www.cement.org/tech/faq_DEF.asp)
- Attom, M. F., & Barakat, S. (2000, August). Investigation of three methods for evaluating swelling pressure of soils. *Environmental & Engineering Geoscience*, pp. 293-299.
- Azam, S., & Abduljawwad, S. N. (2000). Influence of Gypsification on Engineering Behavior of Expansive Clay. *Journal of Geotechnical and Geoenvironmental Engineering*, 638-642.
- Batchelder, M. (1998). Radid, Accurate Phase Quantification of Clay-bearing Samples Using a Position-sensitive X-ray Detector. *Clays and Clay Minerals*, 183-194.
- Blatt, H., Middleton, G., & Murray, R. (1980). *Origin of sedimentary rocks*. New York: Prentice-Hall .
- Bolt, G. H. (1956). Physical-Chemical Analysis of the Compressibility of Pure Clays. *Geotechnique*.
- Brady, N., & Weil, R. (2007). *The Nature and Properties of Soils*. New Jersey: Prentice Hall.
- Carlton, R. W. (1978). *Method of Analysis and Precision of X-ray Diffraction Data form Ohio Shale*. Columbus: Division of Geological Survey.
- Celik, H. (2010). Technological characterization and industrial application of two Turkish clays for the ceramic industry. *Applied Clay Science*, 245-254.

- Cerato, A. B. (2002). Determination of Surface Area of Fine-Grained Soils by the Ethylene Glycol Monoethyl Ether (EGME) Method. *Geotechnical Testing Journal*, 1-7.
- Chen, F. H. (1975). *Development in Geotechnical Engineering 12: Foundations on Expansive Soils*. The Netherlands: Elsevier Scientific.
- Chittoori, B., & Puppala, A. J. (2011). Quantitative Estimation of Clay Mineralogy in Fine-Grained Soils. *Journal of Geotechnical and Geoenvironmental Engineering*, 997-1008.
- Coduto, D. P. (1999). *Geotechnical Engineering: Principles and Practices*. Upper Saddle River, NJ: Prentice-Hall Inc.
- Das, B. M. (2009). *Principles of Geotechnical Engineering*. Stamford, CT: Cengage Learning.
- Davidtz, J. C., & Low, P. F. (1970). Relation Between Crystal-Lattice Configuration and Swelling of Montmorillonites. *Clays and Clay Minerals*, 325-332.
- Derkowski, A., & Bristow, T. F. (2012). On the Problems of Total Specific Surface Area and Cation Exchange Capacity Measurements in Organic-Rich Sedimentary Rocks. *Clays and Clay Minerals*, 348-362.
- Deu, A., Romero, E. E., & Berdugo, I. R. (2013). *Laboratory experiments in swelling due to crystal growth in sulphate argillaceous rocks*. London: Taylor & Francis Group.
- Downs, R. T., & Hall-Wallace, M. (2013, June 25). *The American Mineralogist Crystal Structure Database*. Retrieved from American Mineralogist: <http://rruff.geo.arizona.edu/AMS/amcsd.php>

- Eberl, D. D. (1984). Clay mineral formation and transformation in rocks and soils. *Philosophical Transactions of the Royal Society of London*, 241-257.
- Holtz, R. D., & Kovacs, W. D. (1981). *An Introduction to Geotechnical Engineering*. Upper Saddle River, NJ: Prentice-Hall Inc.
- Houston, S. Z. (2006). *A Study of the Performance of Slab on Grade Residential Foundations on Expansive Soils in Arizona. Final Report to HBACA*. Tempe: Arizona State University.
- Jürgens, D. (2013, October 18). *Institute of Physics*. Retrieved from Atomic and Nuclear Physics: [http://physik2.uni-goettingen.de/research/2\\_hofs/methods/XRD](http://physik2.uni-goettingen.de/research/2_hofs/methods/XRD)
- Klug, H. P., & Alexander, L. E. (1974). *X-Ray Diffraction Procedures For Polycrystalline and Amorphous Materials*. New York: John Wiley & Sons.
- Lin, B., & Cerato, A. B. (2012). Prediction of expansive soil swelling based on four micro-scale properties. *The Bulletin of Engineering Geology and the Environment*, 71-78.
- Little, D. N., & Nair, S. (2007). *Sensitivity of Selected Colorado Soils to Form Ettringite with Calcium-Based Stabilizers and When Soluble Sulfates are Available*. Denver: Colorado Department of Transportation.
- Merriam-Webster*. (2013, March 18). Retrieved from Merriam-Webster.com: <http://www.merriam-webster.com/dictionary/osmosis>
- Mitchell, J. K., & Soga, K. (2005). *Fundamentals of Soil Behavior*. Hoboken: John Wiley & Sons, Inc.
- Moore, D. M., & Reynolds, J. R. (1997). *X-Ray Diffraction and the Identification and Analysis of Clay Minerals*. New York, NY: Oxford University Press Inc.

- Murray, H. H. (2007). *Applied Clay Mineralogy*. Netherlands: Elsevier.
- Oldecop, L., & Alonso, E. (2012). Modelling the degradation and swelling of clay rocks bearing calcium-sulphate. *International Journal of Rock Mechanics & Mining Sciences*, 90-102.
- Poppe, L. J. (2002). *A Laboratory Manual for X-Ray Power Diffraction*. U.S. Geological Survey.
- Rauh, F., Spaun, G., & Thuro, K. (2006). Assessment of the swelling potential of anhydrite in tunnelling projects. *The Geological Society of London*, 1-8.
- Ravina, I., & Low, P. F. (1972). Relation Between Swelling, Water Properties and b-dimension in Montmorillonite-water Systems. *Clays and Clay Minerals*, 109-123.
- Smith, D. K. (2013, October 18). *ICDD and the The Powder Diffraction File Past, Present and Future*. Retrieved from ICDD: <http://www.icdd.com/products/ICDD.PDF>
- Srodon, J. (1980). Precise Identification of Illite/Smectite Interstratifications by X-ray Power Diffraction. *Clays and Clay Minerals*, 401-411.
- van Olphen, H. (1963). *A Introduction to Clay Colloid Chemistry: For Clay Technologists, Geologists, and Soil Science*. New York, NY: John Wiley & Sons, Inc.
- Yitagesu, F. A. (2009). Quantifying engineering parameters of expansive soils from their reflectance spectra. *Engineering Geology*, 151-160.

## APPENDIX A

RockJock is another guide/program that is indorsed by the USGS. The program is aimed at determining quantitative mineralogy from powder X-ray diffraction data. The sample preparation procedure needed for this analysis can be summarized as follows:

- 1) Weigh out 1.000g of soil that has been passed through a 425  $\mu\text{m}$  sieve.
- 2) Pour in to McCrone micronizing milling container. The milling container has corundum grinding elements stacked to allow optimal grinding between particles and the soil.
- 3) Weigh out 0.2500g of 99.9% aluminum oxide power and add to the milling container.
- 4) Measure out 5 *mL* of Ethanol and add to the milling container. The container is closed up and placed the McCrone micronizing unit and mixed for 5 minutes.
- 5) When micronization is complete pour the sample into a container and place in an oven at 60°C to dry overnight.

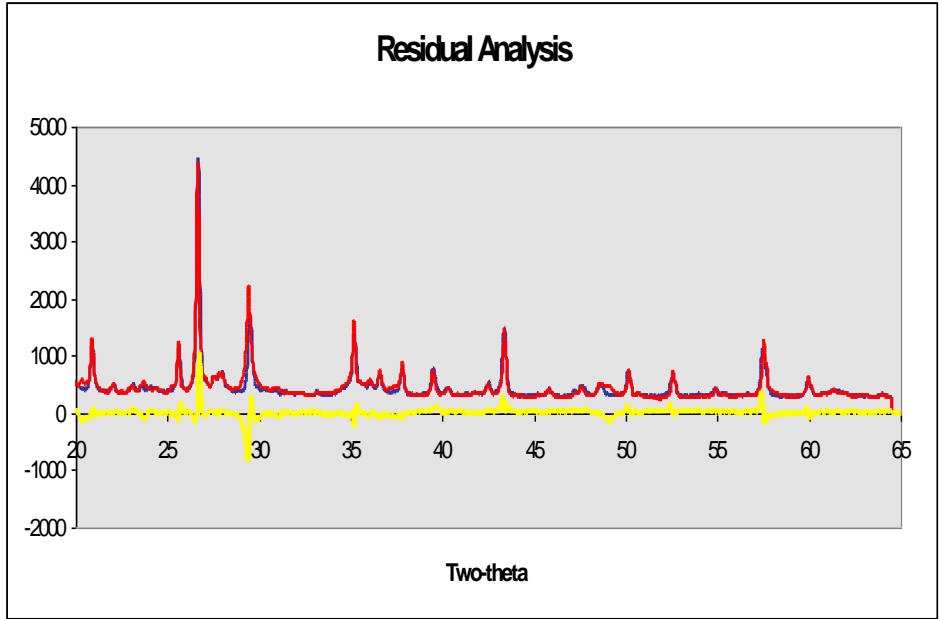
When the sample was dry, three plastic balls and 1 *mL* of Vertrel® XF Cleaning Agent was added to the container. With the container capped, shaking the container vigorously was done to break-up the particles for their drying stage. After shaking for 3-5 minutes, the sample was passed through a #80 sieve. The sample was then side packed into an XRD holder against a quartz slide by tapping the holder on a hard surface. This procedure creates a random particle orientation. Sample should be X-rayed for 5 to 65 degrees two-theta using Cu K-alpha radiation, with a step size of 0.02 degrees two-theta, and a counter time of two seconds per step. Though the analysis used the X-rayed signal

from  $20^{\circ} - 65^{\circ} 2\theta$ . The X-ray set up consist of 1degree slit, soller slits, 1 degree slit, sample, 1 degree slit, no filter, and 0.6 degree slit, scintillation detector.

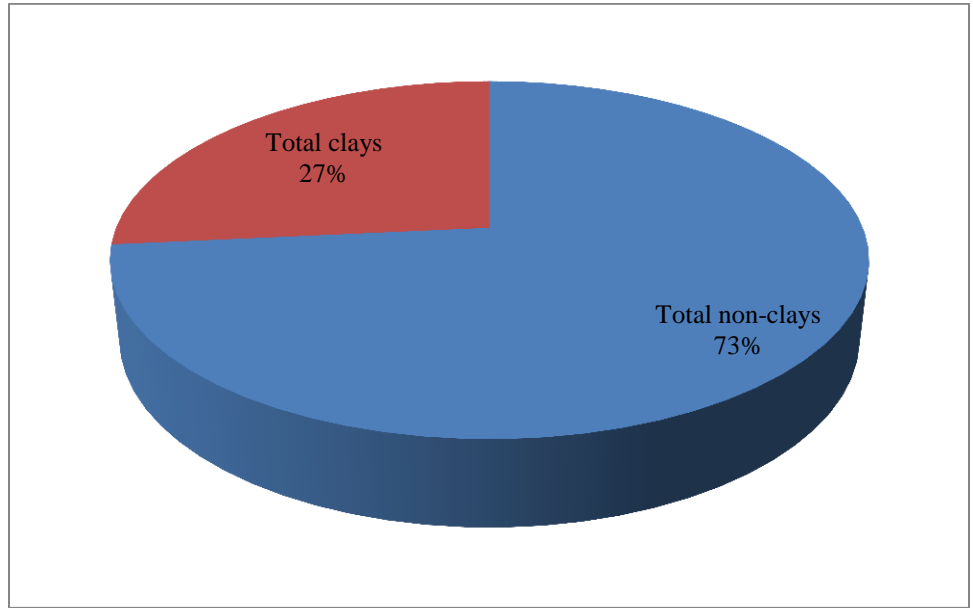
For the RockJock method, minerals were selected based on the lowest degree of fit, as recommended in the RockJock manual. The lowest degree-of-fit corresponds to the program fitting the measured data with the software's internal pure mineral database. The lower the degree-of-fit, the more accurate the quantification is.

### **1: RockJock Analysis for Anthem Soil**

With the sample X-rayed, a software package called Jade was used to convert the intensity and two-theta data into a text format, which can be imported into an Excel® spreadsheet. The measured data was then compared with the programs database, which is comprised of pure mineral signals, until the comparison yielded a degree-of-fit between the measured and calculated signals. The smaller the value of the degree-of-fit, the more precise the quantification is. The RockJock manual recommends the degree-of-fit to be less than 0.1. In Figure A-1, the red pattern represents the calculated pattern, while the blue pattern represents the measured pattern, and the yellow signal is where the red while the blue pattern represents the measured pattern, and the yellow signal is where the red and blue patterns don't match up.



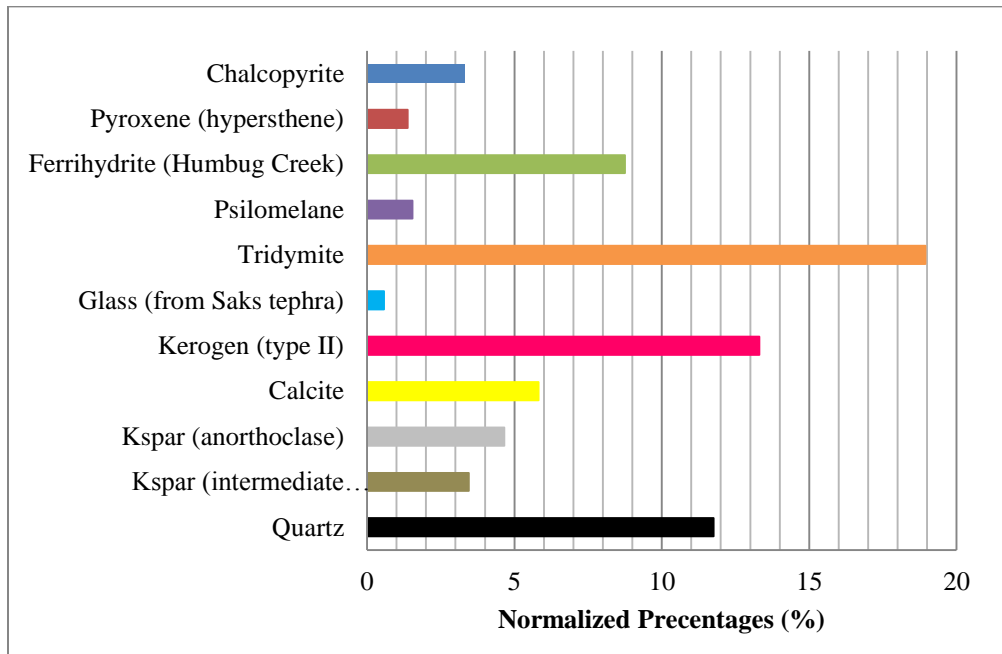
**Figure 98: Residual analysis of Anthem**



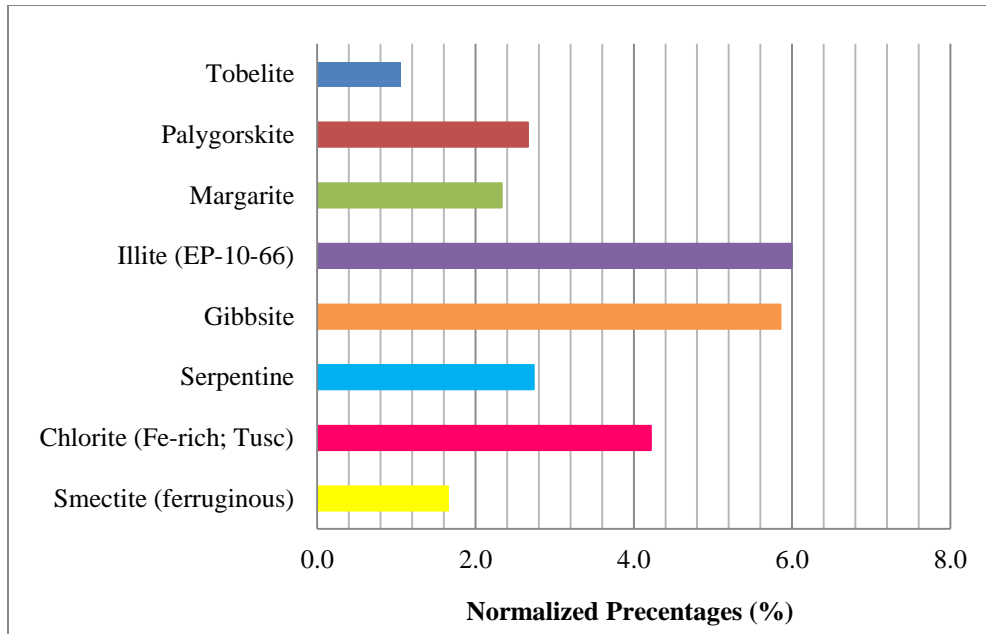
**Figure 99: RockJock quantification of Clay and Non-clay for Anthem soil**



For the Anthem soil, the total amount of clay minerals was found to be 27%, while the total amount of non-clay minerals was found to be 73%, as presented in Figure A-2. These two quantities comprise individual minerals within each category. The individual quantifications for each category are shown in Figure A-3 and A-4.



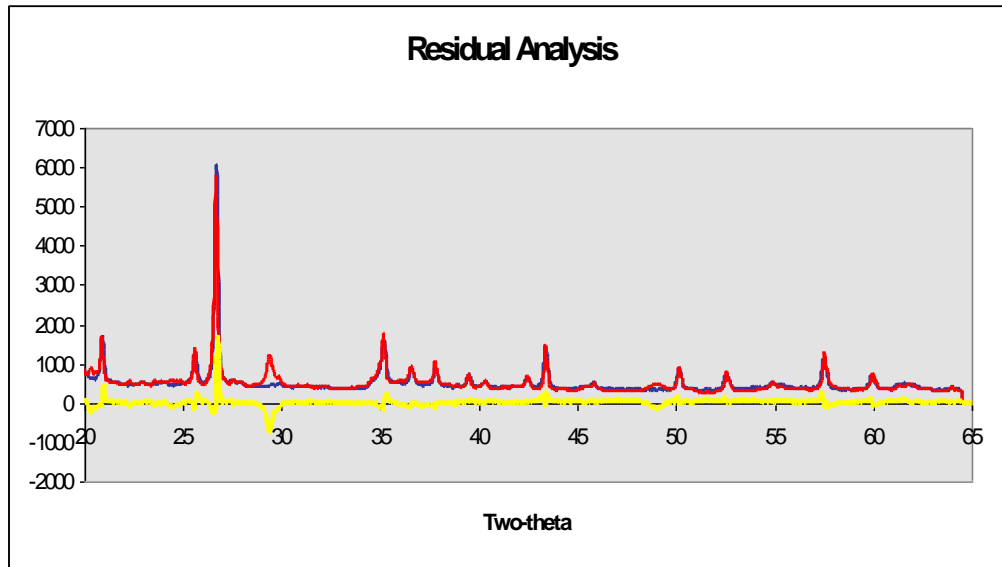
**Figure 100: RockJock quantification of non-clay minerals found in Anthem soil**



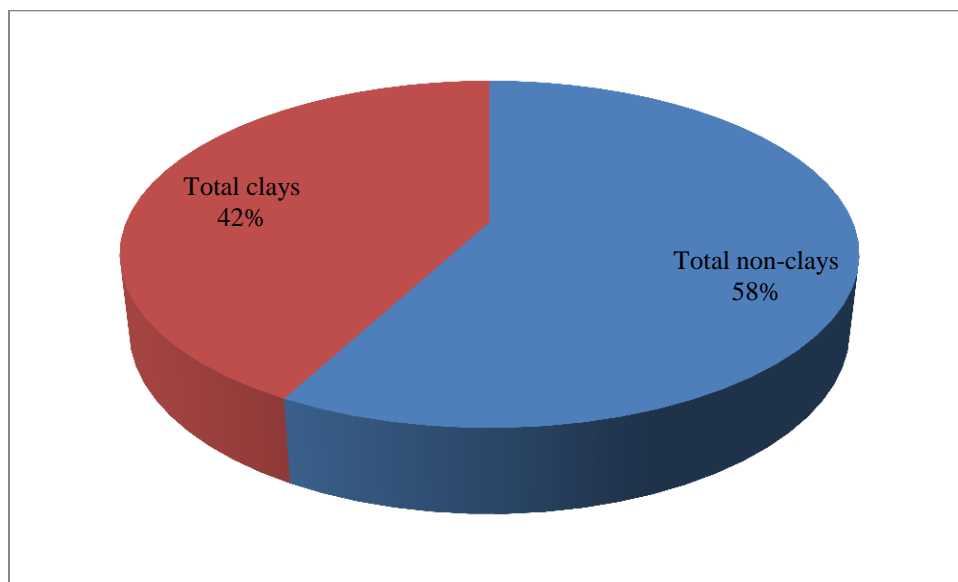
**Figure 101: RockJock quantification of clay minerals found in Anthem soil**

## **2: RockJock Analysis for Colorado Soil**

A software named Jade was used to convert the intensity and two-theta data obtained for the XRD analysis into a text format, which subsequently imported into an Excel® spreadsheet. The measured signals were then compared with the programs database, which is comprised of pure mineral signals. The analysis is complete when the comparison yields the smaller degree-of-fit between the measured and calculated signal. Figure A-5 below, the red pattern represents calculated pattern, while the blue pattern represents the measured pattern, and the yellow signal is where the red and blue patterns don't match up.



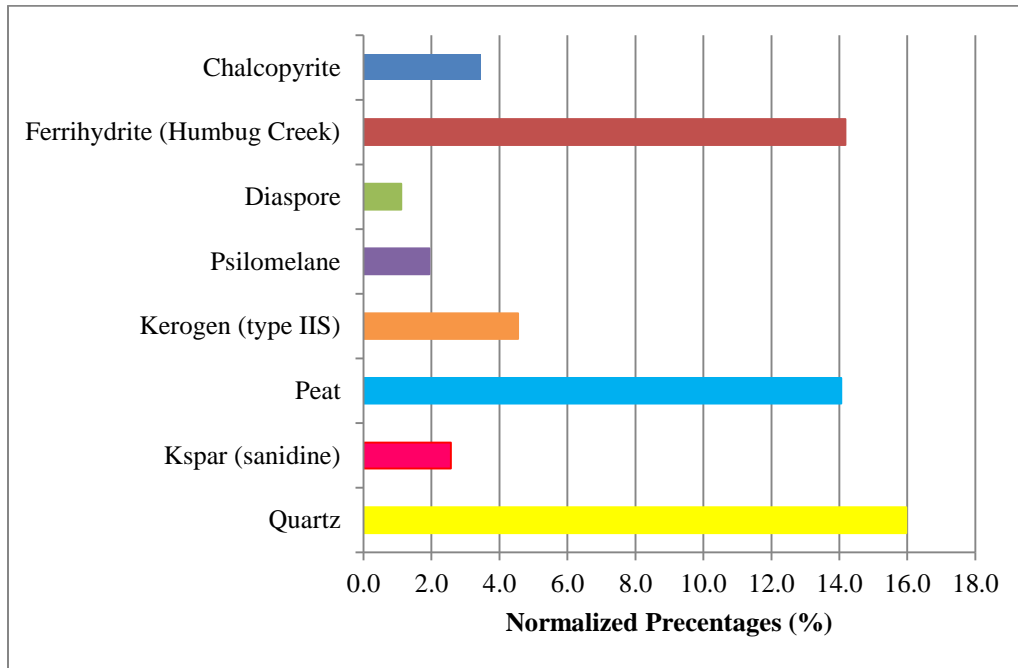
**Figure 102: Residual analysis of Colorado**



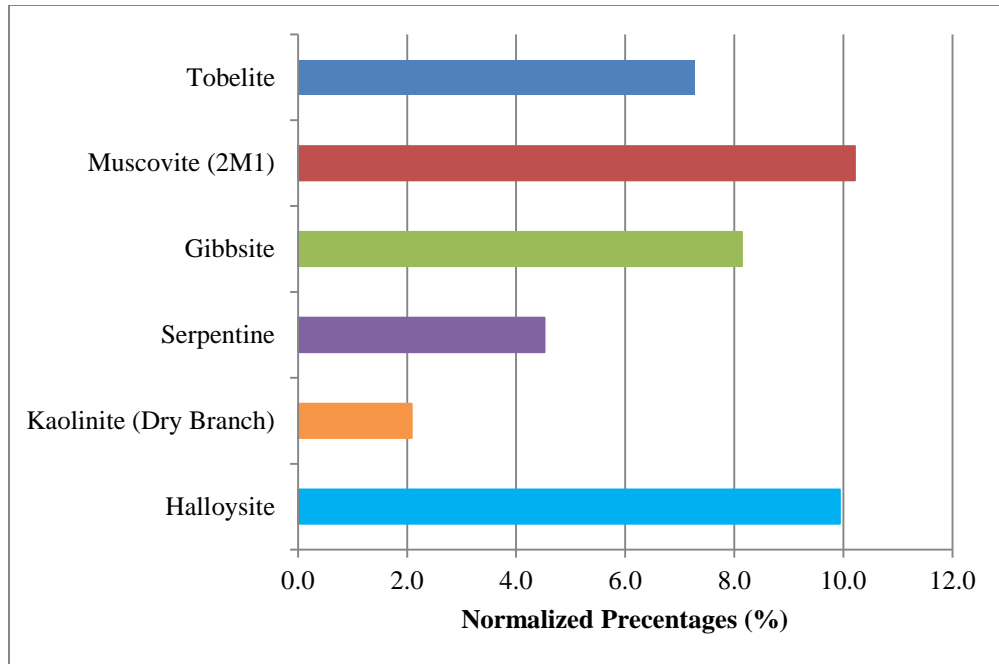
**Figure 103: RockJock quantification of Clay and Non-clay minerals for Colorado soil**

For Colorado soil, the total clays percentage was found to be 42% while the total non-clays percentage was 58%, as shown in Figure A-6. Each of those individual

percentages can be quantified into the individual mineral within those categories. The individual quantifications for each category can be observed in Figure A-7 and A-8.



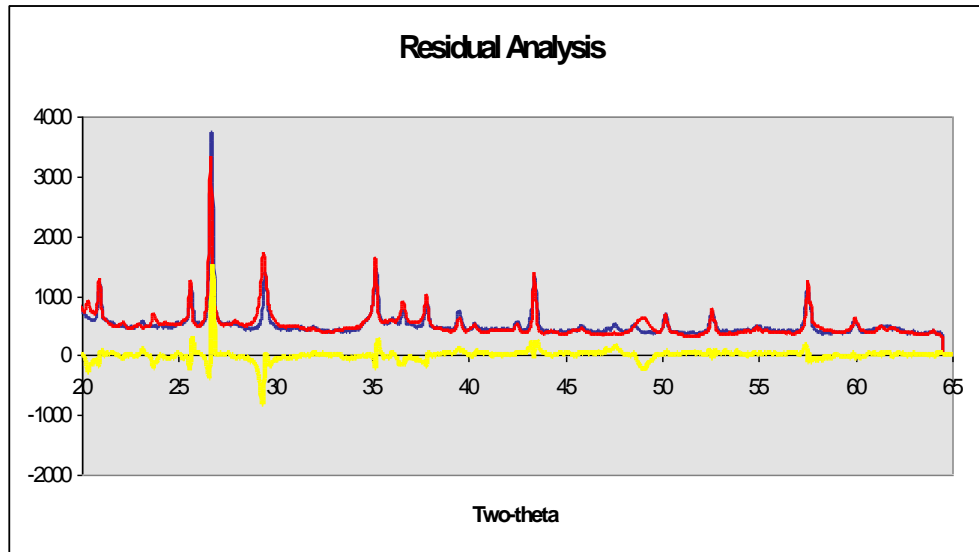
**Figure 104: RockJock quantification of non-clay minerals found in Colorado soil**



**Figure 105: RockJock quantification of clay minerals found in Colorado soil**

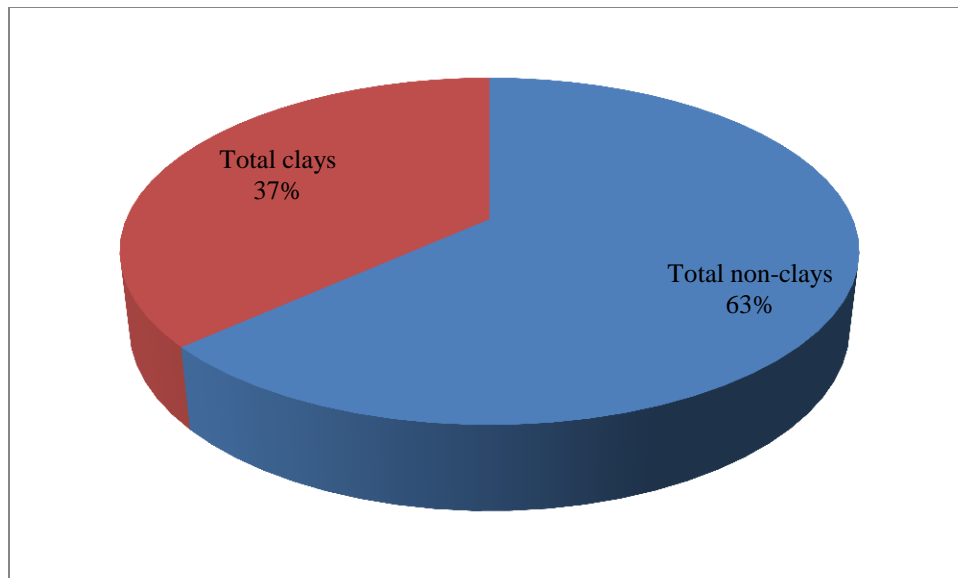
### **3: RockJock Analysis for San Antonio**

With the sample X-rayed, a software named Jade was used to convert the intensity and two-theta data into a text format, which in turn was imported in to an Excel® spreadsheet. The measured signals were then compared with the programs database, which it is comprised of pure mineral signals. During the analysis, the measured signal is compared with the pure minerals selected until it yields a degree-of-fit (residual) of less than 0.1. In Figure A-9, the red pattern represents the calculated pattern, while the blue pattern represents the measured pattern.

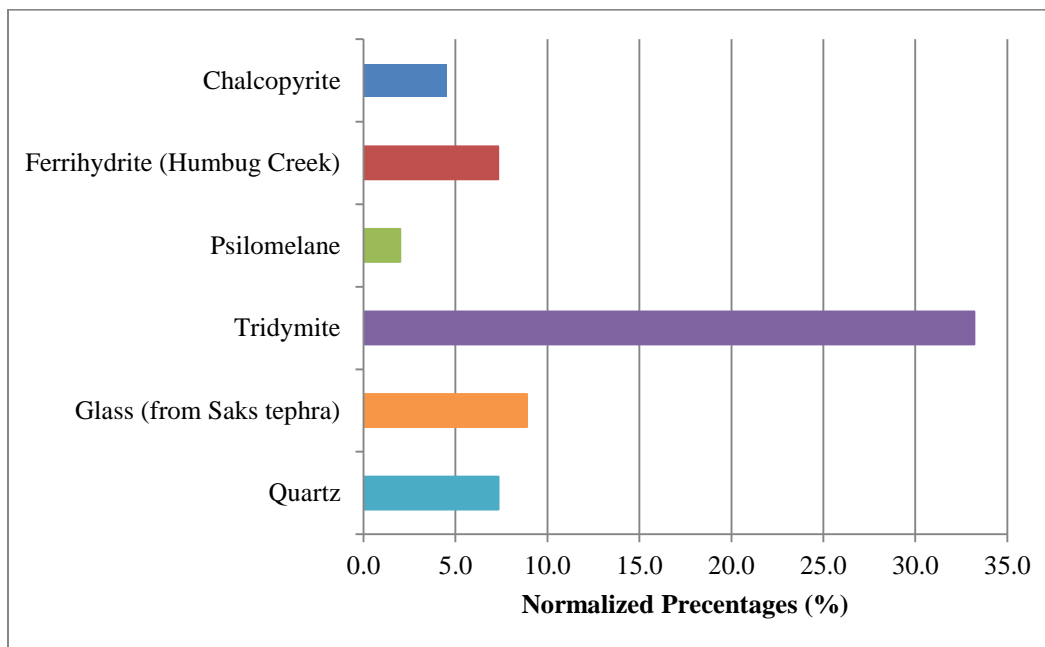


**Figure 106: Residual analysis of San Antonio**

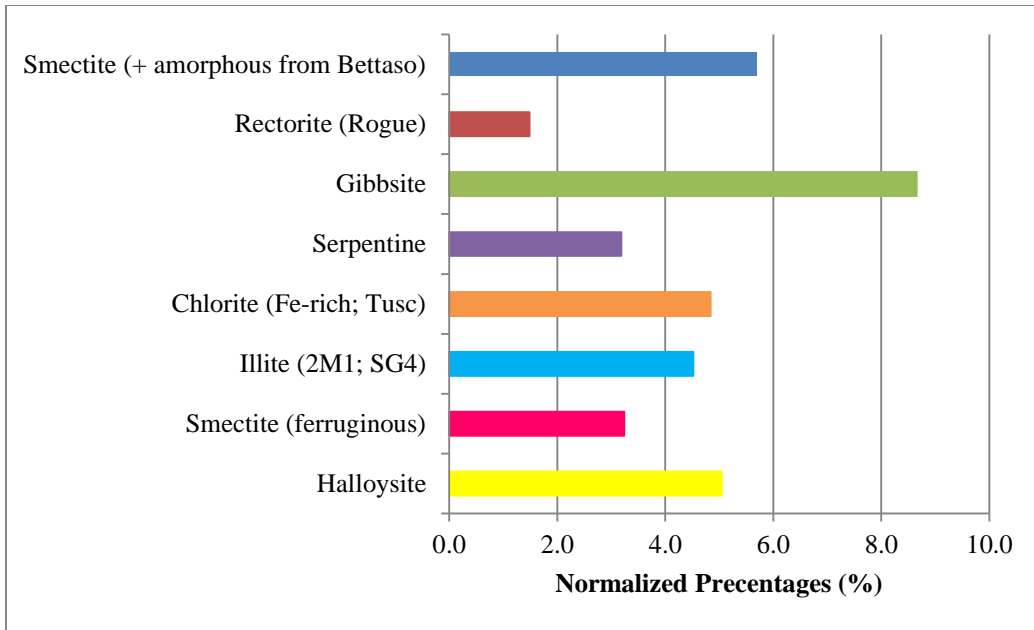
As shown in Figure A-10, for the San Antonio soil, the total clay mineral percentage was found to be 37% while the total non-clay minerals were found to be 63%. Each of those individual percentages can be quantified in to the individual mineral within those categories. The individual quantifications for each category can be observed in Figure A-11 and A-12.



**Figure 107: RockJock quantification for Clay and Non-clay minerals for San Antonio soil**



**Figure 108: RockJock quantification of Non-Clay minerals in San Antonio**



**Figure 109: RockJock quantification of clay minerals in San Antonio**

Applying a full specimen analysis is the only way to retrieve the correct mineral quantification of soils specimens. Using the RockJock program and analysis method seems to be the best option to find all minerals present in the soil specimen. The quantities that were determined using the RockJock program can be seen in Table A-1.



**Table 31: Mineral percentages from ASU using the RockJock method**

Mineral	Anthem	San Antonio	Colorado
Calcite	5.80%	-	-
Illite	6.00%	4.50%	-
Kaolinite	-	0.00%	2.10%
Montmorillonite	1.7%	8.90%	-
Chlorite	4.20%	4.80%	-
Serpentine	2.70%	-	-
Gibbsite	5.90%	8.70%	8.10%
Margarite	2.30%	-	-
Palygorskite	2.70%	-	-
Tobelite	1.10%	-	7.30%
Quartz	11.80%	7.30%	16.00%
Kspar	3.50%	-	2.60%
Kspar	4.70%	-	-
Kerogen	13.30%	-	4.50%
Glass	0.60%	8.90%	-
Tridymite	18.90%	33.20%	-
Psilomelane	1.50%	2.00%	1.90%
Ferrihyrite	8.80%	7.30%	14.20%
Pyroxene	1.40%	-	-
Chalcopyrite	3.30%	4.50%	3.50%
Halloysite	-	5.00%	9.90%
Smectite	-	3.20%	-
Serpentine	-	3.20%	4.50%
Rectorite	-	1.50%	-
Smectite	-	5.70%	-
Muscovite	-	-	10.20%
Peat	-	-	14.10%
Diaspore	-	-	1.10%

As shown, the RockJock program not only gives clay minerals, but it also gives non-clay minerals; allowing for a complete composition analysis and a complete picture of what is actually in the soil specimen. Though, with the program not using the complete signal,  $20^\circ - 65^\circ 2\theta$ , there is missing the primary peaks of Illite and Montmorillonite.

APPENDIX B

		Group Index Data					wPI Data	
IDN	Location	MaxSwell	LL	PI	%P200	GI	MaxSwell	wPI
553.0	Avondale	0.6	24.0	7.0	53.1	1.0	3.7	9.1
469.0	Surprise	2.6	36.2	15.5	65.2	8.2	1.0	3.1
392.0	Peoria	0.9	26.2	9.0	54.5	2.2	0.6	3.7
84.0	Phoenix	3.2	41.0	24.0	39.0	4.2	2.6	10.1
259.0	Phoenix	2.6	28.0	15.0	62.0	6.1	1.2	2.8
437.0	Phoenix	1.3	41.0	22.0	33.0	1.8	0.9	4.9
456.0	Glendale	3.7	25.0	16.0	57.0	5.3	2.2	5.5
37.0	Scottsdale	3.8	27.0	14.0	58.0	4.8	3.2	9.4
57.0	Phoenix	3.3	39.0	23.0	51.0	7.8	2.6	9.3
563.0	Chandler	2.1	30.0	13.0	43.4	2.1	3.7	4.6
591.0	Gilbert	6.7	41.0	25.0	56.0	10.5	1.3	7.3
708.0	Phoenix	1.6	27.0	13.0	52.1	3.4	3.7	9.1
363.0	Goodyear	1.4	30.1	8.2	40.2	0.3	1.8	5.7
446.0	Phoenix	2.6	38.5	13.8	67.6	8.3	3.8	8.1
162.0	Cave Creek	3.0	41.0	22.0	29.0	0.5	3.3	11.7
159.0	Phoenix	2.3	32.0	18.0	61.0	7.8	2.1	5.6
478.0	Surprise	6.1	42.0	26.0	68.0	15.4	6.7	14.0
527.0	Chandler	3.5	32.0	16.0	51.0	4.7	0.5	3.5
69.0	Phoenix	5.0	31.0	20.0	68.0	10.4	0.1	1.4
77.0	Phoenix	2.8	35.0	20.0	43.0	4.2	1.6	6.8
158.0	Glendale	5.0	36.0	18.0	62.0	8.6	1.4	3.1
253.0	Glendale	3.6	33.0	17.0	42.0	3.0	1.4	3.3
356.0	Glendale	3.1	45.0	31.0	43.0	7.7	2.6	9.3
449.0	Phoenix	2.7	42.0	22.0	36.0	2.7	3.0	6.4
637.0	Mesa	0.3	27.0	11.0	49.0	2.2	2.3	11.0
639.0	Mesa	0.1	26.0	7.0	41.5	0.0	6.1	17.7
641.0	Mesa	0.3	26.0	7.0	51.1	1.0	3.5	8.2
642.0	Mesa	0.3	25.0	7.0	51.7	1.0	5.0	13.6
673.0	Phoenix	3.6	36.0	17.0	32.3	0.7	2.8	8.6
682.0	Laveen	0.6	28.0	10.0	39.3	0.6	2.5	4.2
712.0	Phoenix	2.8	33.0	19.0	48.0	5.1	5.0	11.2
163.0	Paradise Valley	2.8	48.0	25.0	35.0	3.0	3.6	7.1
274.0	Glendale	2.5	36.0	12.0	72.1	7.8	3.1	13.3
138.0	Phoenix	3.3	41.0	22.0	43.0	5.0	2.7	7.9
143.0	Highley	3.5	38.0	23.0	72.0	14.4	0.3	5.4
480.0	Surprise	3.4	29.0	14.0	62.0	5.8	0.1	2.9

180.0	Glendale	4.7	38.0	21.0	41.0	4.0	0.3	3.6
427.0	Paradise Valley	4.3	36.0	19.0	62.0	9.1	0.3	3.6
129.0	Cave Creek	3.4	38.0	18.0	31.0	0.5	3.6	5.5
194.0	Scottsdale	2.1	29.0	13.0	62.0	5.3	0.6	3.9
390.0	Mesa	3.3	38.0	15.1	56.0	6.1	0.4	2.7
399.0	Peoria	3.2	30.0	10.0	42.0	1.1	2.8	8.8
51.0	Fountain Hills	3.3	33.0	15.0	33.0	0.6	2.5	8.7
81.0	Phoenix	4.3	35.0	19.0	58.0	7.9	3.3	9.5
136.0	Phoenix	5.0	36.0	20.0	63.0	9.8	3.5	16.6
137.0	Chandler	3.9	34.0	19.0	49.0	5.4	3.4	8.7
315.0	Chandler	2.1	34.0	20.0	41.0	3.6	4.7	8.6
371.0	Mesa	3.8	35.0	20.0	58.0	8.3	4.3	11.8
246.0	Chandler	0.9	31.5	5.8	86.5	5.1	0.4	0.7
564.0	Chandler	1.4	25.0	10.0	50.8	2.0	3.4	5.6
575.0	El Mirage	2.1	30.0	14.0	58.8	5.3	2.1	8.1
588.0	Gilbert	4.9	34.0	18.0	51.2	5.6	3.3	8.5
638.0	Mesa	3.0	28.0	12.0	55.7	3.7	3.2	4.2
666.0	Peoria	3.1	34.0	21.0	35.7	2.4	3.3	5.0
723.0	Scottsdale	1.6	28.0	12.0	52.6	3.2	4.3	11.0
724.0	Sun City	0.6	30.0	13.0	61.9	5.4	5.0	12.6
725.0	Sun City	0.6	30.0	14.0	42.0	2.1	3.9	9.3
726.0	Sun City	1.5	34.0	18.0	36.6	2.0	2.1	8.2
732.0	Surprise	2.2	26.0	8.0	44.8	0.7	3.8	11.6
168.0	Phoenix	4.0	34.0	17.0	81.0	12.4	0.9	5.0
181.0	Peoria	4.8	33.0	18.0	55.0	6.5	0.9	3.1
258.0	Phoenix	3.3	38.0	20.0	48.0	5.8	1.4	5.1
382.0	Mesa	3.6	38.0	22.0	50.0	7.1	2.1	8.2
396.0	Peoria	3.9	31.0	15.0	60.0	6.1	4.9	9.2
25.0	Glendale	3.6	32.0	17.0	54.0	5.8	3.0	6.7
144.0	Phoenix	3.9	31.0	14.0	55.0	4.7	3.1	3.1
234.0	Phoenix	5.5	37.0	22.0	49.0	6.7	3.1	7.5
397.0	Peoria	3.6	41.0	24.0	50.0	8.0	1.6	6.3
413.0	Phoenix	4.4	40.0	20.0	58.0	8.9	0.6	8.0
516.0	Phoenix	2.5	27.0	13.0	51.0	3.2	0.6	5.9
117.0	Phoenix	2.9	33.0	15.0	62.0	6.8	1.5	6.6
388.0	Mesa	3.1	27.0	13.0	65.0	5.6	2.2	3.6
124.0	Phoenix	6.0	39.0	18.0	92.0	17.3	4.0	13.8
134.0	Cave Creek	5.6	48.0	28.0	42.0	6.5	4.8	9.9
174.0	Glendale	3.6	45.0	24.0	76.0	17.8	3.3	9.6
257.0	Litchfield Park	2.7	37.4	12.1	68.6	7.4	3.6	11.0

317.0	Chandler	4.7	37.0	20.0	43.0	4.3	3.9	9.0
403.0	Peoria	3.4	28.0	15.0	57.0	5.2	3.6	9.2
463.0	Scottsdale	3.8	52.0	32.0	38.0	5.8	3.9	7.7
256.0	Surprise	3.2	36.1	18.2	63.1	9.0	5.5	10.8
470.0	Surprise	3.7	39.0	22.0	57.0	9.3	3.6	12.0
50.0	Mesa	3.9	37.0	20.0	51.0	6.6	4.4	11.6
75.0	Chandler	4.6	34.0	18.0	73.0	11.1	2.5	6.6
107.0	Phoenix	3.8	42.0	20.0	51.0	7.0	2.9	9.3
311.0	Chandler	4.9	37.0	21.0	51.0	6.9	3.1	8.5
76.0	Phoenix	2.5	41.0	22.0	49.0	7.0	6.0	16.6
78.0	Phoenix	6.1	39.0	23.0	71.0	14.3	5.6	11.8
142.0	Phoenix	4.1	41.0	25.0	66.0	14.0	3.6	18.2
145.0	Phoenix	3.6	34.0	19.0	56.0	7.3	2.7	8.3
148.0	Chandler	5.3	39.0	24.0	48.0	7.2	4.7	8.6
215.0	Scottsdale	3.0	37.0	22.0	58.0	9.4	3.4	8.6
284.0	Phoenix	4.8	37.0	19.0	67.0	10.6	3.8	12.2
318.0	El Mirage	3.7	33.0	17.0	61.0	7.5	3.2	11.5
349.0	Glendale	5.4	44.0	26.0	51.0	9.3	3.7	12.5
423.0	Phoenix	5.0	53.0	33.0	56.0	15.0	3.9	10.2
474.0	Surprise	4.0	28.0	14.0	59.0	5.1	4.6	13.1
155.0	Scottsdale	4.3	35.0	18.0	76.0	12.1	3.8	10.2
231.0	Scottsdale	3.4	36.0	18.0	30.0	0.3	4.9	10.7
280.0	Gilbert	4.2	38.0	22.0	63.0	11.1	2.7	7.0
379.0	Mesa	3.3	33.0	15.0	51.0	4.4	2.5	10.8
49.0	Fountain Hills	6.9	39.0	23.0	52.0	8.1	6.1	16.3
61.0	Phoenix	3.6	32.0	14.0	72.0	8.2	4.1	16.5
298.0	Carefree	5.1	53.0	31.0	47.0	9.9	3.6	10.6
319.0	El Mirage	4.0	33.0	17.0	61.0	7.5	5.3	11.5
454.0	Phoenix	5.1	33.0	16.0	63.0	7.5	3.0	12.8
22.0	Sun City West	3.3	37.0	20.0	54.0	7.4	4.8	12.7
23.0	Peoria	5.9	37.0	19.0	73.0	12.3	3.7	10.4
106.0	Tempe	4.7	35.0	20.0	64.0	10.0	5.4	13.3
178.0	Cave Creek	2.7	39.0	24.0	30.0	1.1	5.0	18.5
220.0	Phoenix	4.3	34.0	17.0	71.0	10.0	4.0	8.3
297.0	Carefree	3.4	40.0	24.0	41.0	4.8	4.3	13.7
376.0	Mesa	3.4	39.0	20.0	53.0	7.3	3.4	5.4
452.0	Phoenix	6.9	34.0	20.0	84.0	15.2	4.2	13.9
552.0	Avondale	3.4	41.0	24.0	63.5	12.6	3.3	7.7
555.0	Avondale	1.1	27.0	8.0	64.9	3.0	6.9	12.0
571.0	Chandler	1.8	26.0	11.0	36.1	0.4	3.6	10.1

574.0	Chandler	2.2	32.0	13.0	40.8	1.7	5.1	14.6
581.0	Gilbert	2.7	30.0	15.0	50.0	4.0	0.3	0.5
596.0	Gilbert	0.8	31.0	14.0	40.4	1.9	4.0	10.4
599.0	Glendale	3.8	44.0	28.0	55.5	11.8	5.1	10.1
609.0	Glendale	2.5	33.0	18.0	55.7	6.7	3.3	10.8
610.0	Glendale	1.2	30.0	14.0	39.5	1.7	5.9	13.9
622.0	Goodyear	2.4	28.0	9.0	60.1	3.1	4.7	12.8
631.0	Maricopa County	1.2	27.0	8.0	62.3	2.7	2.7	7.2
636.0	Mesa	0.8	35.0	16.0	44.6	3.5	4.3	12.1
640.0	Mesa	1.4	32.0	15.0	51.5	4.5	3.4	9.8
658.0	Peoria	2.4	29.0	11.0	59.1	3.9	3.4	10.6
667.0	Peoria	1.2	33.0	13.0	47.3	3.0	6.9	16.8
678.0	Phoenix	2.3	35.0	16.0	65.4	8.3	3.4	15.2
681.0	Phoenix	2.2	29.0	8.0	80.2	5.2	1.1	5.2
684.0	Phoenix	2.9	35.0	16.0	86.1	13.2	1.8	4.0
719.0	Scottsdale	3.8	32.0	13.0	66.9	6.7	2.2	5.3
731.0	Surprise	1.5	35.0	17.0	54.3	6.1	2.7	7.5
737.0	Surprise	0.7	42.0	19.0	30.0	0.3	0.8	5.7
741.0	Surprise	1.4	35.0	13.0	59.5	5.6	3.8	15.5
742.0	Tempe	1.9	28.0	11.0	55.3	3.2	2.5	10.0
749.0	Tempe	0.1	20.0	1.0	38.0	0.0	1.2	5.5
17.0	Phoenix	4.3	39.0	22.0	57.0	9.3	2.4	5.4
36.0	Surprise	3.5	39.0	21.0	38.0	3.1	0.4	3.2
173.0	Mesa	3.4	33.0	15.0	53.0	4.9	1.2	5.0
358.0	Peoria	4.1	35.0	17.0	39.0	2.4	0.8	7.1
394.0	Peoria	3.6	37.0	20.0	53.0	7.1	1.4	7.7
1.0	Gilbert	4.7	42.0	27.0	64.0	14.4	2.4	6.5
12.0	Tempe	3.1	35.0	20.0	66.0	10.5	1.2	6.1
52.0	Fountain Hills	4.5	48.0	34.0	55.0	14.4	2.3	10.5
88.0	Gilbert	4.1	32.0	15.0	65.0	7.3	2.2	6.4
407.0	Phoenix	4.6	38.0	20.0	46.0	5.2	2.9	13.8
48.0	Chandler	2.5	37.0	20.0	61.0	9.4	0.4	2.7
130.0	Phoenix	4.1	32.0	16.0	65.0	7.8	3.8	8.7
210.0	Peoria	3.8	34.0	17.0	51.0	5.2	1.5	9.2
286.0	Fountain Hills	4.1	48.0	28.0	27.0	0.2	0.7	5.7
153.0	Phoenix	4.9	39.0	22.0	67.0	12.5	1.4	7.7
211.0	Carefree	4.3	48.0	29.0	60.0	14.6	1.9	6.1
265.0	Gilbert	4.5	35.0	18.0	60.0	8.0	0.1	0.4
494.0	Sun City	6.1	44.3	19.5	63.4	10.9	4.3	12.5
9.0	Phoenix	4.1	37.0	21.0	69.0	12.2	3.5	8.0

335.0	Gilbert	4.8	38.0	21.0	50.0	6.7	3.4	8.0
485.0	Tempe	3.2	29.0	14.0	64.0	6.2	4.1	6.6
55.0	Phoenix	4.7	40.0	25.0	37.0	3.7	3.6	10.6
123.0	Phoenix	5.5	32.0	16.0	74.0	9.8	4.7	17.3
165.0	Glendale	3.8	40.0	23.0	55.0	9.2	3.1	13.2
183.0	Peoria	4.1	40.0	23.0	62.0	11.5	4.5	18.7
229.0	Tempe	3.6	36.0	19.0	66.0	10.2	4.1	9.8
465.0	Scottsdale	6.1	46.0	26.0	59.0	12.6	4.6	9.2
20.0	Fountain Hills	3.3	42.0	24.0	48.0	7.4	2.5	12.2
43.0	Phoenix	0.5	47.0	21.0	35.0	2.2	4.1	10.4
97.0	Phoenix	4.8	38.0	21.0	64.0	10.9	3.8	8.7
102.0	Phoenix	2.9	32.0	19.0	54.0	6.6	4.1	7.6
108.0	Phoenix	4.3	44.0	28.0	74.0	19.2	4.9	14.7
126.0	Phoenix	3.3	33.0	17.0	63.0	8.0	4.3	17.4
275.0	Phoenix	4.0	39.0	20.0	70.0	12.3	4.5	10.8
308.0	Chandler	5.1	30.0	25.0	45.0	6.0	6.1	12.4
389.0	Mesa	4.5	32.0	16.0	64.0	7.6	4.1	14.5
402.0	Peoria	3.9	40.0	23.0	59.0	10.5	4.8	10.5
481.0	Surprise	4.4	36.0	20.0	58.0	8.4	3.2	9.0
13.0	Mesa	3.3	32.0	15.0	51.0	4.4	4.7	9.3
157.0	Phoenix	5.1	39.0	21.0	61.0	10.1	5.5	11.8
186.0	Gilbert	5.6	40.0	25.0	55.0	10.0	3.8	12.7
206.0	Peoria	3.3	42.0	26.0	50.0	8.8	4.1	14.3
255.0	El Mirage	5.7	45.0	30.0	60.0	14.6	3.6	12.5
293.0	Avondale	3.7	38.0	21.0	55.0	8.2	6.1	15.3
441.0	Phoenix	3.7	38.0	22.0	69.0	12.9	3.3	11.5
58.0	Mesa	3.5	37.0	19.0	66.0	10.3	0.5	7.4
82.0	Phoenix	6.7	41.0	23.0	65.0	12.7	4.8	13.4
195.0	Chandler	3.9	33.0	19.0	53.0	6.4	2.9	10.3
227.0	Phoenix	3.9	36.0	18.0	68.0	10.2	4.3	20.7
401.0	Peoria	5.8	36.0	19.0	64.0	9.6	3.3	10.7
457.0	Apache Junction	4.1	39.0	19.0	50.0	6.1	4.0	14.0
21.0	Sun City	7.3	45.0	30.0	75.0	21.0	5.1	11.3
160.0	Tempe	3.6	39.0	20.0	55.0	7.9	4.5	10.2
189.0	Peoria	4.0	36.0	18.0	65.0	9.4	3.9	13.6
300.0	Cave Creek	4.9	40.0	24.0	30.0	1.1	4.4	11.6
354.0	Glendale	4.8	38.0	20.0	61.0	9.5	3.3	7.7
410.0	Phoenix	4.3	33.0	16.0	65.0	8.0	5.1	12.8
432.0	Phoenix	4.2	39.0	21.0	71.0	13.2	5.6	13.8
560.0	Casa Grande	5.2	34.0	19.0	65.8	9.8	3.3	13.0

567.0	Chandler	0.8	30.0	12.0	41.4	1.5	5.7	18.0
573.0	Chandler	3.0	27.0	11.0	51.2	2.5	3.7	11.6
613.0	Glendale	5.8	40.0	23.0	61.5	11.3	3.7	15.2
617.0	Goodyear	2.3	34.0	18.0	65.7	9.3	1.3	5.1
619.0	Goodyear	0.7	29.0	10.0	55.5	3.0	3.5	12.5
626.0	Litchfield Park	2.2	31.0	16.0	56.7	5.9	6.7	15.0
648.0	Mesa	1.2	28.0	12.0	68.6	5.8	3.9	10.1
651.0	Peoria	0.8	34.0	17.0	38.5	2.2	3.9	12.2
656.0	Peoria	4.0	45.0	22.0	52.5	8.4	5.8	12.2
657.0	Peoria	3.8	41.0	20.0	59.4	9.4	4.1	9.5
668.0	Peoria	0.8	34.0	17.0	43.4	3.4	7.3	22.5
670.0	Phoenix	0.7	30.0	8.0	43.2	0.7	3.6	11.0
676.0	Phoenix	1.5	30.0	14.0	59.6	5.5	4.0	11.7
685.0	Phoenix	0.7	31.0	10.0	45.4	1.6	4.9	7.2
686.0	Phoenix	3.8	37.0	19.0	78.5	13.8	4.8	12.2
691.0	Phoenix	1.3	29.0	14.0	57.7	5.0	4.3	10.4
703.0	Phoenix	0.5	27.0	9.0	51.0	1.8	2.8	5.9
717.0	Queen Creek	2.0	28.0	11.0	60.1	4.0	4.2	14.9
718.0	Scottsdale	1.3	35.0	18.0	37.3	2.2	5.2	12.5
733.0	Surprise	2.8	36.0	17.0	50.7	5.3	0.8	5.0
735.0	Surprise	4.6	33.0	14.0	50.3	3.9	3.0	5.6
738.0	Surprise	1.3	25.0	10.0	50.0	1.9	0.2	2.1
739.0	Surprise	1.3	30.0	16.0	45.8	3.5	1.7	2.2
746.0	Tempe	0.1	26.0	8.0	43.9	0.6	5.8	14.1
4.0	Gilbert	4.5	38.0	23.0	68.0	13.2	2.3	11.8
73.0	Phoenix	6.0	45.0	27.0	56.0	11.7	0.7	5.6
112.0	Phoenix	3.7	37.0	19.0	63.0	9.5	2.2	9.1
167.0	Glendale	2.2	43.0	24.0	47.0	7.1	1.2	8.2
303.0	Chandler	3.5	31.0	18.0	61.0	7.7	0.8	6.5
370.0	Mesa	5.1	49.0	28.0	42.0	6.6	4.0	11.6
443.0	Phoenix	4.8	35.0	19.0	55.0	7.1	3.8	11.9
140.0	Phoenix	4.5	42.0	27.0	69.0	16.3	0.8	7.4
198.0	Cave Creek	3.5	37.0	18.0	30.0	0.3	0.7	3.5
216.0	Tolleson	7.7	38.0	20.0	92.0	18.5	1.5	8.3
232.0	Tolleson	7.3	42.0	23.0	83.0	18.9	0.7	4.5
281.0	Mesa	5.6	41.0	22.0	74.0	15.1	3.8	14.9
331.0	Gilbert	5.2	41.0	25.0	58.0	11.2	1.3	8.1
341.0	Gilbert	5.6	42.0	26.0	67.0	15.0	0.5	4.6
404.0	Peoria	6.4	58.0	37.0	53.0	15.5	0.3	2.7
47.0	Gilbert	3.7	41.0	27.0	51.0	9.4	0.1	3.5

90.0	Phoenix	3.8	36.0	21.0	58.0	8.9	2.0	6.6
147.0	Tempe	4.0	31.0	17.0	59.0	6.8	1.3	6.7
375.0	Mesa	3.2	38.0	20.0	57.0	8.4	2.8	8.6
391.0	Paradise Valley	3.8	40.0	23.0	61.0	11.2	4.6	7.0
468.0	Sun City	5.4	44.0	25.0	55.0	10.4	1.3	5.0
66.0	Phoenix	1.8	30.0	8.0	53.0	1.9	1.3	7.3
111.0	Gilbert	5.4	38.0	22.0	60.0	10.2	0.1	3.5
164.0	Phoenix	5.8	43.0	27.0	83.0	21.9	4.5	15.6
294.0	Buckeye	6.3	41.0	23.0	92.0	21.7	6.0	15.1
296.0	Buckeye	3.5	35.0	16.0	64.0	8.0	3.7	12.0
334.0	Gilbert	4.0	38.0	22.0	51.0	7.4	2.2	11.3
431.0	Phoenix	4.5	35.0	18.0	75.0	11.8	3.5	11.0
458.0	Apache Junction	3.3	35.0	18.0	46.0	4.4	5.1	11.8
149.0	Mesa	3.6	34.0	18.0	65.0	9.1	4.8	10.5
528.0	Chandler	3.6	43.0	23.0	50.0	7.8	4.5	18.6
121.0	Glendale	4.6	34.0	20.0	57.0	7.9	3.5	5.4
197.0	Peoria	5.4	45.0	21.0	77.0	16.3	7.7	18.4
213.0	Peoria	4.8	37.0	19.0	56.0	7.6	7.3	19.1
264.0	Chandler	4.1	37.0	19.0	45.0	4.6	5.6	16.3
312.0	Chandler	5.1	39.0	20.0	45.0	5.0	5.2	14.5
339.0	Chandler	2.6	31.0	14.0	32.0	0.2	5.6	17.4
352.0	Glendale	3.9	37.0	19.0	65.0	10.1	6.4	19.6
383.0	Mesa	3.2	37.0	21.0	49.0	6.3	3.7	13.8
27.0	Phoenix	5.0	36.0	19.0	70.0	11.3	3.8	12.2
40.0	Phoenix	5.1	40.0	22.0	70.0	13.6	4.0	10.0
188.0	Phoenix	3.2	38.0	21.0	57.0	8.8	3.2	11.4
357.0	Glendale	6.3	33.0	20.0	86.0	15.5	3.8	14.0
448.0	Phoenix	2.8	38.0	22.0	53.0	8.0	5.4	13.8
3.0	Glendale	5.8	39.0	21.0	58.0	9.2	1.8	4.2
18.0	Phoenix	3.7	38.0	19.0	50.0	6.0	5.4	13.2
99.0	Phoenix	4.7	38.0	23.0	55.0	9.0	5.8	22.4
214.0	Mesa	4.1	39.0	22.0	57.0	9.3	6.3	21.2
313.0	Chandler	4.5	35.0	20.0	54.0	7.2	3.5	10.2
415.0	Phoenix	2.8	34.0	18.0	64.0	8.9	4.0	11.2
442.0	Phoenix	3.4	33.0	17.0	63.0	8.0	4.5	13.5
16.0	Phoenix	5.5	39.0	24.0	58.0	10.5	3.3	8.3
39.0	Phoenix	4.2	45.0	27.0	39.0	5.0	3.6	11.7
236.0	Tolleson	3.8	33.0	16.0	70.0	9.1	0.3	2.7
325.0	Gilbert	4.6	36.0	21.0	46.0	5.4	3.6	11.5
420.0	Phoenix	5.9	40.0	19.0	55.0	7.6	0.8	3.6



475.0	Surprise	5.2	43.0	26.0	70.0	16.3	4.6	11.4
479.0	Surprise	3.5	33.0	17.0	65.0	8.5	5.4	16.2
486.0	Tempe	4.3	38.0	21.0	69.0	12.4	4.8	10.6
63.0	Phoenix	0.9	40.1	12.8	40.1	1.7	4.1	8.6
98.0	Mesa	4.0	40.0	21.0	73.0	14.0	5.1	9.0
122.0	Phoenix	2.3	40.1	12.8	40.1	1.7	2.6	4.5
185.0	Phoenix	3.8	34.0	15.0	75.0	9.8	3.9	12.4
204.0	Glendale	4.0	35.0	14.0	69.0	8.1	3.2	10.3
205.0	Phoenix	4.6	41.0	23.0	80.0	17.7	5.0	13.3
267.0	Gilbert	4.5	44.0	28.0	56.0	12.0	5.1	15.4
285.0	Gilbert	3.7	36.0	20.0	86.0	16.3	3.2	12.0
412.0	Phoenix	5.3	34.0	18.0	68.0	9.9	6.3	17.2
439.0	Phoenix	4.8	35.0	19.0	81.0	14.0	2.8	11.7
554.0	Avondale	1.8	31.0	14.0	53.3	4.4	5.8	12.2
566.0	Chandler	0.6	35.0	18.0	49.4	5.3	3.7	9.5
570.0	Chandler	4.5	29.0	13.0	70.4	6.8	4.7	12.7
579.0	Gilbert	1.2	34.0	19.0	47.8	5.1	4.1	12.5
580.0	Gilbert	0.6	34.0	18.0	25.4	0.0	4.5	10.8
584.0	Gilbert	4.1	35.0	22.0	49.2	6.6	2.8	11.5
590.0	Gilbert	8.9	47.0	31.0	63.0	16.7	3.4	10.7
603.0	Glendale	3.4	33.0	14.0	73.2	8.6	5.5	13.9
606.0	Glendale	3.4	40.0	20.0	55.8	8.2	4.2	10.5
608.0	Glendale	0.9	38.0	19.0	31.8	0.9	3.8	11.2
612.0	Glendale	2.8	32.0	13.0	62.3	5.8	4.6	9.7
649.0	Mesa	2.3	30.0	16.0	50.3	4.4	5.9	10.5
671.0	Phoenix	2.3	35.0	17.0	56.7	6.7	5.2	18.2
690.0	Phoenix	2.4	42.0	23.0	47.4	6.8	3.5	11.1
696.0	Phoenix	1.9	33.0	18.0	58.2	7.3	4.3	14.5
710.0	Phoenix	9.6	58.0	39.0	59.2	19.8	0.9	5.1
730.0	Surprise	1.1	31.0	10.0	49.7	2.3	4.0	15.3
62.0	Glendale	3.1	40.0	20.0	54.0	7.7	2.3	5.1
64.0	Phoenix	7.3	50.0	30.0	74.0	21.6	3.8	11.3
104.0	Phoenix	4.9	33.0	16.0	88.0	13.1	4.0	9.7
209.0	Peoria	4.5	38.0	21.0	61.0	10.0	4.6	18.4
217.0	Scottsdale	4.5	42.0	24.0	73.0	16.1	4.5	15.7
235.0	Phoenix	5.3	39.0	23.0	73.0	15.0	3.7	17.2
467.0	Mesa	5.0	37.0	20.0	79.0	14.5	5.3	12.2
30.0	Chandler	5.1	37.0	19.0	36.0	2.1	4.8	15.4
68.0	Phoenix	5.4	39.0	22.0	80.0	16.6	1.8	7.5
70.0	Phoenix	4.3	42.0	24.0	77.0	17.5	0.6	8.9

71.0	Phoenix	6.0	41.0	22.0	91.0	20.6	4.5	9.2
139.0	Gilbert	3.9	41.0	24.0	49.0	7.6	1.2	9.1
252.0	Mesa	5.5	39.0	24.0	64.0	12.5	0.6	4.6
282.0	Gilbert	4.7	36.0	22.0	36.0	2.7	4.1	10.8
438.0	Phoenix	5.6	41.0	26.0	86.0	21.8	8.9	19.5
447.0	Phoenix	5.7	36.0	23.0	66.0	12.2	3.4	10.2
11.0	Glendale	6.6	44.0	28.0	74.0	19.2	3.4	11.2
41.0	Phoenix	6.0	47.0	30.0	64.0	16.6	0.9	6.0
45.0	Phoenix	5.5	45.0	29.0	69.0	17.9	2.8	8.1
85.0	Phoenix	4.7	38.0	20.0	68.0	11.6	2.3	8.0
272.0	Phoenix	4.3	43.0	23.0	60.0	11.2	2.3	9.6
278.0	Chandler	4.2	37.0	20.0	54.0	7.4	2.4	10.9
359.0	Goodyear	5.2	43.0	26.0	71.0	16.7	1.9	10.5
385.0	Mesa	4.0	40.0	23.0	69.0	13.8	9.6	23.1
387.0	Mesa	5.3	47.0	30.0	56.0	13.1	1.1	5.0
26.0	Phoenix	5.9	40.0	22.0	73.0	14.6	3.1	10.8
53.0	Phoenix	4.5	47.0	29.0	41.0	6.4	7.3	22.2
65.0	Phoenix	3.8	34.0	17.0	69.0	9.6	4.9	14.1
74.0	Mesa	5.7	38.0	20.0	64.0	10.4	4.5	12.8
91.0	Phoenix	5.4	50.0	25.0	53.0	10.2	4.5	17.5
150.0	Phoenix	4.4	39.0	19.0	55.0	7.5	5.3	16.8
324.0	Gilbert	7.9	43.0	26.0	60.0	12.6	5.0	15.8
378.0	Mesa	4.7	34.0	19.0	61.0	8.6	5.1	6.8
539.0	Sun Lakes	3.8	31.0	13.0	78.0	8.6	5.4	17.6
10.0	Phoenix	4.2	40.0	22.0	80.0	16.8	4.3	18.5
56.0	Phoenix	4.1	34.0	16.0	82.0	12.0	6.0	20.0
146.0	Glendale	4.1	36.0	18.0	78.0	12.8	3.9	11.8
355.0	Glendale	4.9	39.0	22.0	70.0	13.4	5.5	15.4
141.0	Phoenix	5.9	42.0	23.0	70.0	14.5	4.7	7.9
172.0	Glendale	4.7	43.0	25.0	64.0	13.6	5.6	22.4
228.0	Fountain Hills	4.2	42.0	22.0	52.0	8.0	5.7	15.2
250.0	Cave Creek	4.4	39.0	23.0	60.0	10.7	6.6	20.7
290.0	Avondale	5.0	42.0	25.0	62.0	12.7	6.0	19.2
372.0	Mesa	5.4	42.0	24.0	41.0	4.9	5.5	20.0
72.0	Phoenix	4.0	36.0	20.0	68.0	11.2	4.7	13.6
83.0	Chandler	3.9	38.0	22.0	52.0	7.7	4.3	13.8
373.0	Mesa	5.3	44.0	26.0	67.0	15.4	4.2	10.8
8.0	Phoenix	3.2	34.0	17.0	67.0	9.1	5.2	18.5
92.0	Phoenix	4.8	41.0	21.0	71.0	13.5	4.0	15.9
132.0	Chandler	3.0	36.0	18.0	53.0	6.3	5.3	16.8

316.0	Chandler	7.1	47.0	28.0	66.0	16.5	5.9	16.1
345.0	Gilbert	5.1	37.0	22.0	62.0	10.6	4.5	11.9
426.0	Phoenix	3.6	36.0	20.0	77.0	13.8	3.8	11.7
32.0	Phoenix	5.2	60.0	38.0	52.3	15.6	5.7	12.8
34.0	Highley	6.6	53.0	35.0	71.0	23.5	5.4	13.3
169.0	Glendale	3.9	37.0	20.0	61.0	9.4	4.4	10.5
251.0	Phoenix	1.2	29.9	9.6	50.9	2.2	7.9	15.6
271.0	Chandler	3.3	40.0	22.0	46.0	5.9	4.7	11.6
337.0	Gilbert	3.8	41.0	24.0	54.0	9.4	3.8	10.1
368.0	Litchfield Park	6.0	42.0	26.0	60.0	12.5	4.2	17.6
369.0	Mesa	3.3	36.0	18.0	78.0	12.8	4.1	13.1
400.0	Peoria	5.6	46.0	28.0	72.0	18.8	4.1	14.0
424.0	Phoenix	5.9	43.0	24.0	68.0	14.5	4.9	15.4
33.0	Chandler	3.8	38.0	20.0	71.0	12.4	5.9	16.1
100.0	Phoenix	4.3	35.0	18.0	88.0	15.1	4.7	16.0
245.0	Chandler	3.9	38.0	22.0	55.0	8.6	4.2	11.4
323.0	Gilbert	8.4	57.0	39.0	70.0	25.9	4.4	13.8
367.0	Mesa	4.5	42.0	16.0	60.0	8.0	5.0	15.5
377.0	Mesa	3.3	41.0	22.0	57.0	9.6	5.4	9.8
416.0	Phoenix	5.5	34.0	14.0	78.0	9.8	4.0	13.6
455.0	Phoenix	4.2	38.0	20.0	68.0	11.6	3.9	11.4
488.0	Tempe	4.0	40.0	23.0	67.0	13.2	5.3	17.4
550.0	Avondale	1.2	32.0	13.0	79.4	9.0	3.2	11.4
572.0	Chandler	2.0	30.0	15.0	48.7	3.7	4.8	14.9
585.0	Gilbert	5.1	48.0	31.0	60.3	15.6	3.0	9.5
597.0	Glendale	3.8	42.0	21.0	57.0	9.2	7.1	18.5
607.0	Glendale	3.8	42.0	23.0	62.5	12.0	5.1	13.6
621.0	Goodyear	0.8	33.0	8.0	43.4	0.8	3.6	15.4
624.0	Goodyear	2.1	33.0	11.0	78.0	7.7	5.2	19.9
635.0	Mesa	0.7	33.0	10.0	44.8	1.6	6.6	24.9
652.0	Peoria	1.0	34.0	16.0	50.0	4.7	3.9	12.2
660.0	Peoria	3.8	36.0	20.0	63.5	10.0	1.2	4.9
693.0	Phoenix	2.2	34.0	14.0	65.2	7.1	3.3	10.1
747.0	Tempe	0.7	38.0	16.0	35.5	1.3	3.8	13.0
44.0	Phoenix	5.5	44.0	25.0	61.0	12.6	6.0	15.6
154.0	Glendale	3.6	33.0	14.0	84.0	10.8	3.3	14.0
333.0	Gilbert	4.1	41.0	25.0	61.0	12.2	5.6	20.2
15.0	Gilbert	4.3	35.0	21.0	60.0	9.3	5.9	16.3
208.0	Peoria	3.7	44.0	24.0	63.0	12.9	3.8	14.2
243.0	Buckeye	3.5	40.0	20.0	57.0	8.6	4.3	15.8

254.0	Tempe	4.5	40.0	23.0	73.0	15.1	3.9	12.1
287.0	Maricopa	4.6	42.0	28.0	35.0	3.6	8.4	27.3
307.0	Chandler	3.0	35.0	20.0	75.0	13.0	4.5	9.6
365.0	Maricopa	3.1	35.0	19.0	75.0	12.4	3.3	12.5
384.0	Mesa	3.5	35.0	19.0	83.0	14.5	5.5	10.9
414.0	Phoenix	5.1	39.0	24.0	73.0	15.5	4.2	13.6
532.0	Peoria	4.2	33.0	17.0	76.0	11.0	4.0	15.4
96.0	Tempe	3.6	37.0	16.0	74.0	10.8	1.2	10.3
247.0	Chandler	3.7	37.0	19.0	57.0	7.9	2.0	7.3
338.0	Gilbert	6.4	49.0	31.0	81.0	25.1	5.1	18.7
398.0	Peoria	4.6	42.0	21.0	68.0	12.8	3.8	12.0
444.0	Phoenix	3.3	36.0	20.0	58.0	8.4	3.8	14.4
483.0	Tempe	5.2	42.0	24.0	53.0	9.1	0.8	3.5
484.0	Tempe	4.6	42.0	25.0	75.0	17.4	2.1	8.6
6.0	Phoenix	4.6	36.0	18.0	83.0	14.1	0.7	4.5
118.0	Phoenix	4.6	37.0	20.0	89.0	17.4	1.0	8.0
176.0	Scottsdale	4.2	40.0	21.0	63.0	10.9	3.8	12.7
295.0	Buckeye	3.6	35.0	18.0	71.0	10.8	2.2	9.1
360.0	Goodyear	5.3	43.0	25.0	74.0	17.2	0.3	4.5
433.0	Phoenix	6.0	39.0	20.0	88.0	17.6	0.7	5.7
59.0	Phoenix	4.6	40.0	21.0	58.0	9.3	5.5	15.3
79.0	Tempe	4.1	40.0	23.0	68.0	13.5	3.6	11.8
105.0	Phoenix	4.7	42.0	27.0	60.0	12.9	4.1	15.3
196.0	Phoenix	4.5	36.0	19.0	90.0	16.7	4.3	12.6
249.0	Cave Creek	3.3	47.0	31.0	39.0	6.0	3.7	15.1
269.0	Mesa	4.7	39.0	23.0	67.0	13.0	3.5	11.4
306.0	Chandler	4.2	41.0	23.0	54.0	9.0	4.5	16.8
405.0	Phoenix	4.1	43.0	26.0	70.0	16.3	4.6	9.8
450.0	Phoenix	5.2	46.0	30.0	79.0	22.9	3.0	15.0
35.0	Phoenix	3.7	33.0	18.0	75.0	11.4	3.1	14.3
152.0	New River	5.2	46.0	30.0	60.0	14.8	3.5	15.8
351.0	Glendale	5.9	41.0	22.0	86.0	19.0	5.1	17.5
417.0	Phoenix	4.6	40.0	22.0	67.0	12.6	4.2	12.9
2.0	Gilbert	6.4	45.0	27.0	70.0	17.2	3.6	11.8
67.0	Phoenix	4.5	40.0	21.0	76.0	14.9	3.7	10.8
179.0	Glendale	4.1	36.0	17.0	78.0	12.2	6.4	25.1
207.0	Phoenix	4.3	39.0	19.0	84.0	15.8	4.6	14.3
263.0	Chandler	5.9	47.0	30.0	69.0	18.8	3.3	11.6
288.0	Phoenix	5.2	40.0	20.0	61.0	9.8	5.2	12.7
350.0	Glendale	4.3	39.0	21.0	85.0	17.5	4.6	18.8

411.0	Phoenix	6.6	52.0	31.0	62.0	16.9	4.6	14.9
491.0	Tolleson	6.0	40.0	19.0	78.0	14.3	4.6	17.8
504.0	Gilbert	5.6	39.0	23.0	61.0	11.1	4.2	13.2
514.0	Gilbert	5.6	39.0	23.0	61.0	11.1	3.6	12.8
101.0	Desert Hills	6.8	40.0	21.0	85.0	17.7	5.3	18.5
115.0	Phoenix	6.4	46.0	33.0	90.0	29.9	6.0	17.6
116.0	Phoenix	5.1	41.0	25.0	59.0	11.5	4.6	12.2
151.0	Phoenix	4.6	39.0	21.0	87.0	18.1	4.1	15.6
262.0	Phoenix	3.5	32.0	14.0	78.0	9.4	4.7	16.2
291.0	Goodyear	5.1	43.0	25.0	73.0	16.9	4.5	17.1
386.0	Mesa	7.3	46.0	31.0	78.0	23.1	3.3	12.1
451.0	Laveen	3.9	33.0	17.0	89.0	14.1	4.7	15.4
166.0	Phoenix	4.7	37.0	19.0	87.0	16.1	4.2	12.4
301.0	Cave Creek	3.7	31.0	13.0	61.0	5.4	4.1	18.2
362.0	Goodyear	5.8	41.0	23.0	82.0	18.3	5.2	23.7
409.0	Phoenix	6.0	40.0	22.0	82.0	17.4	3.7	13.5
422.0	Phoenix	6.5	40.0	21.0	77.0	15.2	5.2	18.0
38.0	Phoenix	5.7	43.0	26.0	71.0	16.7	5.9	18.9
109.0	Phoenix	4.8	38.0	18.0	85.0	15.1	4.6	14.7
131.0	Phoenix	5.0	40.0	25.0	75.0	17.0	6.4	18.9
201.0	Phoenix	5.4	44.0	24.0	90.0	22.6	4.5	16.0
268.0	Gilbert	5.4	48.0	32.0	60.0	15.9	4.1	13.3
493.0	Tolleson	6.0	52.0	32.0	80.0	26.0	4.3	16.0
593.0	Gilbert	7.3	46.0	31.0	51.0	11.2	5.9	20.7
614.0	Glendale	1.6	26.0	12.0	62.9	4.6	5.2	12.2
630.0	Maricopa County	5.8	35.0	19.0	62.4	9.1	4.3	17.9
661.0	Peoria	2.3	43.0	22.0	56.2	9.5	6.6	19.2
663.0	Peoria	5.3	42.0	23.0	66.0	13.1	6.0	14.8
688.0	Phoenix	5.0	37.0	12.0	93.5	12.4	5.6	14.0
695.0	Phoenix	5.8	42.0	25.0	61.9	12.7	5.6	14.0
751.0	Tempe	2.5	37.0	21.0	49.9	6.6	6.8	17.9
120.0	Desert Hills	6.4	46.0	27.0	74.0	19.0	6.4	29.7
219.0	Scottsdale	4.1	46.0	25.0	67.0	15.2	5.1	14.8
343.0	Gilbert	7.3	48.0	28.0	79.0	22.1	4.6	18.3
496.0	Chandler	3.9	35.0	17.0	62.0	8.0	3.5	10.9
225.0	Tolleson	6.3	51.0	30.0	96.0	31.8	5.1	18.3
482.0	Tempe	6.5	45.0	26.0	77.0	19.4	7.3	24.2
490.0	Tempe	3.7	38.0	20.0	84.0	16.2	3.9	15.1
19.0	Phoenix	6.4	39.0	20.0	88.0	17.6	4.7	16.5
348.0	Gilbert	6.7	51.0	33.0	57.0	15.3	3.7	7.9

487.0	Tempe	5.4	44.0	28.0	83.0	22.8	5.8	18.9
276.0	Tolleson	8.3	51.0	29.0	97.0	31.4	6.0	18.0
127.0	Mesa	5.6	63.0	36.0	60.0	19.6	6.5	16.2
193.0	Scottsdale	4.3	42.0	23.0	76.0	16.5	5.7	18.5
212.0	Mesa	4.2	42.0	25.0	55.0	10.2	4.8	15.3
289.0	Apache Junction	4.9	42.0	21.0	59.0	9.9	5.0	18.8
327.0	Gilbert	4.8	39.0	24.0	52.0	8.5	5.4	21.6
330.0	Gilbert	3.9	45.0	26.0	53.0	10.1	5.4	19.2
531.0	Mesa	3.4	40.0	19.0	45.0	4.7	6.0	25.6
29.0	Phoenix	6.0	41.0	23.0	83.0	18.7	7.3	15.8
89.0	Chandler	6.0	51.0	30.0	72.0	20.8	1.6	7.5
93.0	Phoenix	4.0	40.0	21.0	89.0	18.9	5.8	11.9
332.0	Gilbert	6.4	47.0	28.0	68.0	17.3	2.3	12.4
24.0	Phoenix	4.7	39.0	22.0	74.0	14.7	5.3	15.2
191.0	Glendale	5.0	33.0	15.0	85.0	11.8	5.0	11.2
238.0	Phoenix	5.9	44.0	25.0	81.0	20.0	5.8	15.5
326.0	Gilbert	6.1	50.0	33.0	75.0	23.8	2.5	10.5
421.0	Avondale	3.3	27.0	13.0	61.0	4.9	6.4	20.0
260.0	Phoenix	6.4	43.0	22.0	77.0	16.5	4.1	16.8
361.0	Goodyear	5.7	42.0	24.0	82.0	19.3	7.3	22.1
406.0	Phoenix	4.7	39.0	21.0	82.0	16.5	3.9	10.5
187.0	Phoenix	3.5	35.0	17.0	77.0	11.7	6.3	28.8
266.0	Desert Hills	5.3	47.0	28.0	86.0	24.8	6.5	20.0
309.0	Chandler	8.6	61.0	41.0	74.0	30.2	3.7	16.8
340.0	Gilbert	6.3	46.0	30.0	76.0	21.6	6.4	17.6
344.0	Gilbert	4.3	40.0	21.0	57.0	9.0	6.7	18.8
511.0	Gilbert	3.7	31.0	17.0	49.0	4.6	5.4	23.2
175.0	Glendale	4.7	39.0	19.0	71.0	12.1	8.3	28.1
342.0	Gilbert	6.3	55.0	37.0	65.0	21.8	5.6	21.6
565.0	Chandler	5.1	31.0	12.0	85.4	9.2	4.3	17.5
568.0	Chandler	5.5	40.0	22.0	79.0	16.5	4.2	13.8
600.0	Glendale	5.9	38.0	19.0	72.4	12.3	4.9	12.4
615.0	Glendale	3.8	47.0	28.0	62.4	15.0	4.8	12.5
687.0	Phoenix	1.9	41.0	19.0	56.0	8.0	3.9	13.8
31.0	Mesa	4.7	43.0	24.0	88.0	21.6	3.4	8.6
177.0	Phoenix	5.4	37.0	17.0	87.0	14.7	6.0	19.1
292.0	Avondale	7.2	46.0	30.0	85.0	25.5	6.0	21.6
346.0	Gilbert	4.4	36.0	17.0	85.0	13.9	4.0	18.7
161.0	Goodyear	7.5	49.0	32.0	74.0	22.5	6.4	19.0
230.0	Tolleson	5.7	48.0	28.0	91.0	27.1	4.7	16.3

273.0	Chandler	5.0	41.0	26.0	52.0	9.4	5.0	12.8
328.0	Gilbert	4.5	43.0	25.0	70.0	15.8	5.9	20.3
364.0	Litchfield Park	3.8	30.0	9.6	58.7	3.4	6.1	24.8
366.0	Gila Bend	3.4	37.0	17.0	72.0	10.8	3.3	7.9
434.0	Phoenix	4.2	44.0	20.0	58.0	9.4	6.4	16.9
310.0	Chandler	4.0	42.0	22.0	65.0	12.3	5.7	19.7
184.0	Glendale	3.9	40.0	20.0	92.0	19.1	4.7	17.2
540.0	Sun Lakes	0.5	32.0	16.0	46.0	3.6	3.5	13.1
14.0	Peoria	6.5	49.0	32.0	81.0	25.8	5.3	24.1
113.0	Phoenix	3.8	32.0	14.0	71.0	8.0	8.6	30.3
125.0	Phoenix	6.9	49.0	24.0	85.0	22.1	6.3	22.8
224.0	Tolleson	8.2	54.0	33.0	84.0	29.1	4.3	12.0
314.0	Chandler	5.6	44.0	25.0	60.0	12.3	3.7	8.3
336.0	Gilbert	4.3	41.0	24.0	80.0	18.3	4.7	13.5
492.0	Phoenix	8.6	50.0	28.0	96.0	29.8	6.3	24.1
46.0	Fountain Hills	4.0	50.0	26.0	48.0	8.5	5.1	10.2
279.0	Chandler	4.3	36.0	17.0	79.0	12.4	5.5	17.4
466.0	Mesa	11.7	48.0	32.0	87.0	28.3	5.9	13.8
270.0	Chandler	4.6	46.0	31.0	63.0	16.5	3.8	17.5
60.0	Mesa	7.4	71.0	49.0	72.0	35.4	1.9	10.6
320.0	Fountain Hills	8.5	61.0	41.0	73.0	29.6	4.7	21.1
625.0	Laveen	5.2	48.0	27.0	95.2	28.1	5.4	14.8
633.0	Mesa	5.5	49.0	31.0	80.5	24.9	7.2	25.5
634.0	Mesa	5.5	49.0	31.0	80.5	24.9	4.4	14.5
707.0	Phoenix	4.7	46.0	23.0	69.2	14.9	7.5	23.7
720.0	Scottsdale	3.8	45.0	27.0	67.2	16.1	5.7	25.5
459.0	Queen Creek	5.5	37.0	18.0	86.0	15.1	5.0	13.5
86.0	Phoenix	5.7	48.0	30.0	88.0	27.3	4.5	17.5
226.0	Phoenix	4.2	40.0	22.0	86.0	18.7	3.8	5.6
408.0	Phoenix	5.7	48.0	27.0	86.0	24.3	3.4	12.2
440.0	Phoenix	7.0	40.0	21.0	89.0	18.9	4.2	11.6
533.0	Peoria	4.8	33.0	14.0	88.0	11.7	4.0	14.3
305.0	Chandler	4.6	34.8	11.4	84.3	9.5	3.9	18.4
103.0	Cave Creek	8.3	56.0	34.0	72.0	24.0	0.5	7.4
395.0	Peoria	4.8	47.0	29.0	62.0	15.3	6.5	25.9
114.0	Phoenix	6.3	36.0	20.0	91.0	17.7	3.8	9.9
182.0	Phoenix	4.7	37.2	14.4	81.4	11.6	6.9	20.4
192.0	Phoenix	5.5	37.2	14.4	81.4	11.6	8.2	27.7
221.0	Tolleson	6.4	48.0	27.0	90.0	26.0	5.6	15.0
374.0	Mesa	3.9	38.0	20.0	70.0	12.2	4.3	19.2

489.0	Tempe	7.7	43.0	25.0	85.0	21.3	8.6	26.9
435.0	Phoenix	3.2	45.0	26.0	50.0	9.0	4.0	12.5
524.0	Chandler	3.3	34.0	17.0	49.0	4.8	4.3	13.4
222.0	Phoenix	4.4	38.0	20.0	80.0	15.1	11.7	27.8
322.0	Fountain Hills	6.6	48.0	23.0	72.0	16.3	4.6	19.5
436.0	Phoenix	6.1	69.0	42.0	62.0	24.4	7.4	35.3
353.0	Glendale	3.9	38.0	17.0	87.0	14.9	8.5	29.9
419.0	Phoenix	3.8	60.0	37.0	34.0	4.8	5.2	25.7
502.0	Gilbert	5.3	36.0	20.0	62.0	9.6	5.5	25.0
277.0	Phoenix	4.9	38.0	20.0	90.0	18.0	5.5	25.0
347.0	Gilbert	7.5	58.0	40.0	86.0	36.1	4.7	15.9
445.0	Phoenix	8.7	53.0	33.0	92.0	32.8	3.8	18.1
677.0	Phoenix	5.3	48.0	25.0	91.7	25.1	5.5	15.5
428.0	Phoenix	7.2	44.0	22.0	98.0	23.8	5.7	26.4
381.0	Mesa	4.9	59.0	31.0	69.0	21.4	4.2	18.9
477.0	Surprise	4.5	30.7	12.9	84.3	9.6	5.7	23.2
171.0	Phoenix	3.4	32.0	15.0	85.0	11.5	7.0	18.7
190.0	Glendale	5.5	45.0	27.0	66.0	15.6	4.8	12.3
94.0	Desert Hills	8.6	56.0	33.0	76.0	25.5	4.6	9.6
239.0	Chandler	10.1	55.0	25.5	97.4	29.9	8.3	24.5
244.0	Chandler	7.1	48.5	25.2	67.3	15.8	4.8	18.0
202.0	Phoenix	3.1	26.9	9.3	73.5	4.8	6.3	18.2
501.0	Gilbert	4.8	41.0	25.0	78.0	18.3	4.7	11.7
503.0	Gilbert	4.1	46.0	26.0	63.0	14.1	5.5	11.7
242.0	Phoenix	9.3	71.0	39.0	85.0	38.1	6.4	24.3
241.0	Phoenix	10.4	74.0	44.0	82.0	40.2	3.9	14.0
200.0	Phoenix	5.6	34.4	15.7	84.5	12.5	7.7	21.3
529.0	Glendale	5.4	48.0	20.0	67.0	12.9	3.2	13.0
544.0	Glendale	5.4	48.0	20.0	67.0	12.9	3.3	8.3
199.0	Phoenix	4.9	35.6	14.7	87.9	12.8	4.4	16.0
203.0	Phoenix	4.1	42.7	17.0	77.2	13.4	6.6	16.6
576.0	Fountain Hills	7.6	59.0	31.0	80.0	26.9	6.1	26.0
321.0	Fountain Hills	8.4	68.0	40.0	92.0	42.5	3.9	14.8
223.0	Tolleson	7.6	42.0	18.6	96.2	19.8	3.8	12.6
672.0	Phoenix	25.6	132.0	105.0	89.9	107.4	5.3	12.4
500.0	Gilbert	5.1	45.0	28.0	83.0	23.0	4.9	18.0
508.0	Gilbert	4.5	31.0	16.0	53.0	5.1	7.5	34.4
510.0	Gilbert	6.5	45.0	28.0	66.0	16.2	8.7	30.4
522.0	Scottsdale	7.1	50.0	32.0	62.0	17.1	5.3	22.9
525.0	Chandler	2.7	31.0	14.0	48.0	3.3	7.2	21.6



526.0	Chandler	2.9	34.0	16.0	43.0	3.0	4.9	21.4
534.0	Peoria	4.1	40.0	22.0	60.0	10.4	4.5	10.9
537.0	Litchfield Park	2.8	51.0	18.0	74.0	14.7	3.4	12.8
598.0	Glendale	0.3	43.0	19.0	32.2	0.9	5.5	17.8
618.0	Goodyear	2.6	34.0	17.0	73.9	10.7	8.6	25.1
628.0	Maricopa County	2.5	39.0	14.0	55.7	5.7	10.1	24.8
632.0	Maricopa County	2.9	47.0	27.0	27.2	0.2	7.1	17.0
669.0	Phoenix	8.6	55.0	31.0	64.7	18.6	3.1	6.8
727.0	Surprise	1.5	26.0	11.0	47.1	1.9	4.8	19.5
728.0	Surprise	1.5	26.0	11.0	47.1	1.9	4.1	16.4
	Anthem	8.6	48.0	27.0	88.7	25.4	9.3	33.2
	San Antonio	14.1	67.0	43.0	88.5	42.2	10.4	36.1
	Colorado	18.7	65.0	42.0	99.1	47.7	5.6	13.3
							5.4	13.4
							5.4	13.4
							4.9	12.9
							4.1	13.1
							7.6	24.8
							8.4	36.8
							7.6	17.9
							25.6	94.4
							5.1	23.2
							4.5	8.5
							6.5	18.5
							7.1	19.8
							2.7	6.7
							2.9	6.9
							4.1	13.2
							2.8	13.3
							0.1	2.5
							0.3	6.1
							2.6	12.6
							2.5	7.8
							2.9	7.3
							8.6	20.1
							1.5	5.2
							1.5	5.2
							1.1	2.5
							8.6	24.0
							14.1	38.1

| 18.7 41.6